SSD

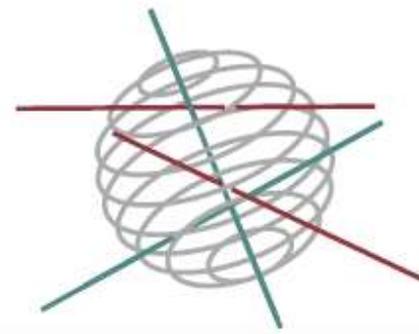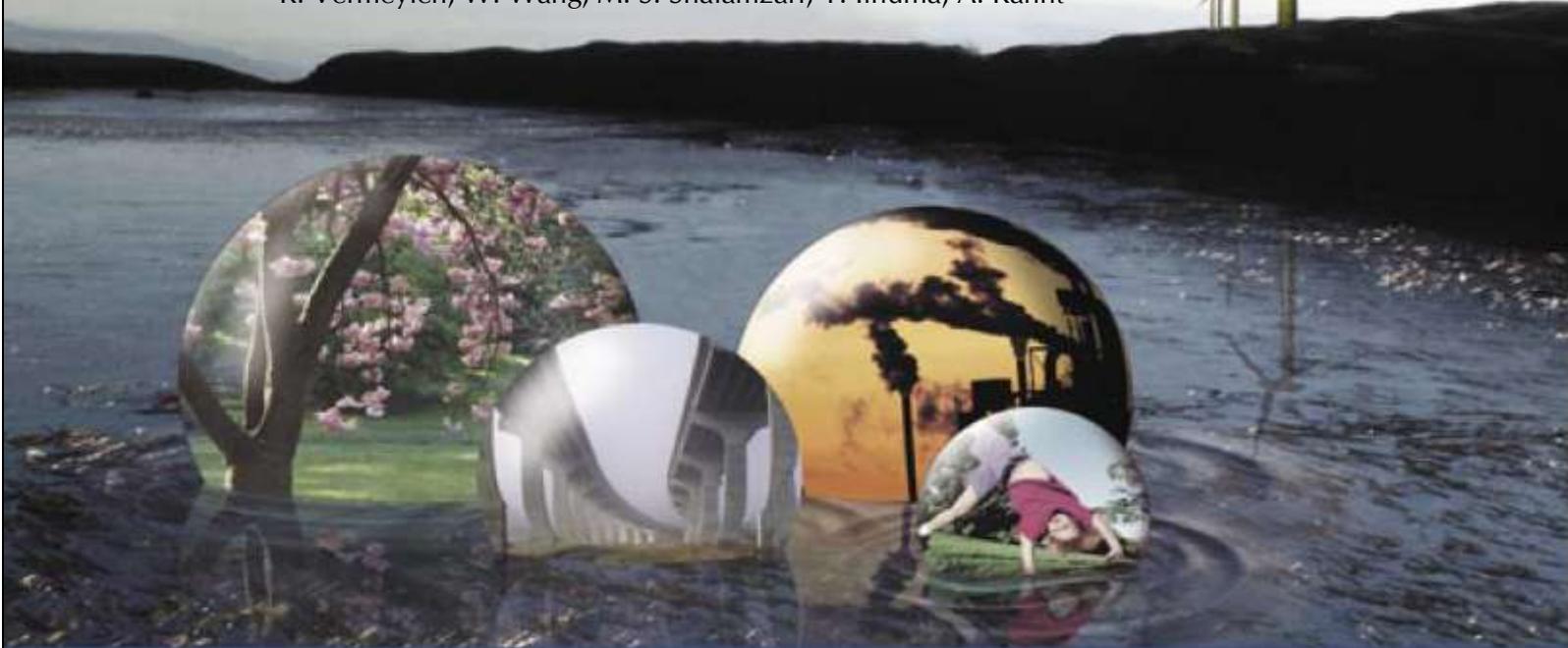## SCIENCE FOR A SUSTAINABLE DEVELOPMENT

**Biogenic Influences on Oxidants and Secondary Aerosols:
Theoretical, laboratory and modelling investigations**

"BIOSOA"

J.-F. Müller, S. Compernolle, K. Ceulemans, T. Stavrakou,
J. Peeters, S. V. Nguyen, M. Claeys, W. Maenhaut,
R. Vermeylen, W. Wang, M. S. Shalamzari, Y. Iinuma, A. Kahnt

ENERGY
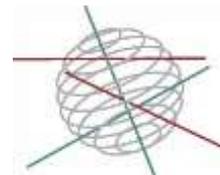
TRANSPORT AND MOBILITY

AGRO-FOOD

HEALTH AND ENVIRONMENT

CLIMATE

BIODIVERSITY

ATMOSPHERE AND TERRESTRIAL AND MARINE ECOSYSTEMS

TRANSVERSAL ACTIONS

.be

Climate

FINAL REPORT

**Biogenic Influences on Oxidants and Secondary Aerosols:
Theoretical, laboratory and modelling investigations**

"BIOSOA"

Promotors
Jean-François Müller (BIRA-IASB, Brussels)
Shaun Carl and Jozef Peeters (K.U. Leuven, Heverlee-Leuven)
Magda Claeys (Universiteit Antwerpen)
Yoshiteru Iinuma and Hartmut Herrmann (TROPOS Leipzig, Germany)

Authors
J.-F. Müller, S. Compernolle, K. Ceulemans, T. Stavrakou (BIRA-IASB)
J. Peeters, S. V. Nguyen (K.U. Leuven)
M. Claeys, W. Maenhaut, A. Kahnt, R. Vermeylen, W. Wang, M. S.
Shalamzari (Universiteit Antwerpen)
Y. Iinuma (TROPOS)

TABLE OF CONTENT

ANNEX 1: COPY OF THE PUBLICATIONS
ANNEX 2: MINUTES OF THE FOLLOW-UP COMMITTEE MEETINGS

Acronyms, abbreviations and units

BOREAM	Biogenic compounds Oxidation and RElated Aerosol formation
BVOC	biogenic volatile organic compound
CESAM	Chambre Expérimentale de Simulation Atmosphérique Multiphasique
CAO	campholenic aldehyde ozonolysis
EI	electron ionisation
EIC	extracted ion chromatogram
EPA	Environmental Protection Agency
ESI	electrospray ionisation
EVAPORATION	Estimation of VApour Pressure, Accounting for Temperature, Intramolecular, and Non-additivity effects
DBAA	dibutylammonium acetate
DNPH	dinitrophenylhydrazone
FTIR	Fourier transform infra-red
GC	gas chromatography
GROMHE	GROup contribution Method for Henry's law Estimate
HLC	Henry's law constant
HPALD	hydroperoxy-aldehyde
IMAGES	Intermediate Model for the Annual and Global Evolution of Species
IP	ion-pairing
KPP	Kinetic PreProcessor
LC	liquid chromatography
LIM	Leuven Isoprene Mechanism
LISA	Laboratoire Interuniversitaire des Systèmes Atmosphériques
MBTCA	3-methyl-1,2,3-butanetricarboxylic acid
MS	Mass spectrometry
MW	molecular weight
NOx	mixture of NO and NO_2
OA	organic aerosol
OS	organosulfate
PM2.5	particulate matter with an aerodynamic diameter $\leq$ 2.5 μm
QC	Quantum Chemical
PEOE	Partial Equalization of Orbital Electronegativity
RH	relative humidity
RRKM-ME	Rice-Ramsperger-Kessel-Marcus rate theory combined with master equation analyses
SAR	Structure-Activity Relationship
SMPS	scanning mobility particle sizer
SOA	secondary organic aerosol
TROPOS	Institut für TROPOSspherische Chemie (Leipzig, Germany)
VOC	volatile organic compound

SUMMARY

Context

Terrestrial vegetation releases vast quantities of volatile organic compounds (VOCs) to the atmosphere, of the order of 1 billion tons each year. Although of natural origin, biogenic VOCs (BVOCs) are central to our understanding of the role played by human activities in climate change and air quality issues. Most importantly,

- they influence the oxidizing capacity of the atmosphere and therefore the abundance of e.g. the greenhouse gas methane, air quality compounds (e.g. carcinogenic benzene) and chemicals contributing to stratospheric ozone depletion (e.g. hydrochlorofluorocarbons);
- in polluted areas, they participate to summertime "ozone smog" episodes, i.e. to the build-up of noxious pollutants, primarily ozone, due to the catalytic action of nitrogen oxides of anthropogenic origin; and
- they are a source of Secondary Organic Aerosol (SOA) which makes up a substantial fraction of fine aerosols (i.e. particulate matter or PM).

Aerosols play a central role in climate through direct radiative effects and through their influence on clouds. Along with ground-level ozone, fine aerosols are a major component of smog. They have acute adverse effects on human health, e.g. on the respiratory and cardiovascular systems; over Europe, they were estimated to cause ~200,000 premature deaths per year. Regulation measures are tightening as a growing body of scientific evidence suggests that there is no safe level of exposure to ozone or PM. Although anthropogenic emissions of ozone precursors have decreased since the 1990s, exposure to ground-level ozone has not declined substantially, and the number of premature deaths due to ground level ozone worldwide is expected to quadruple by 2030. This trend has also negative consequences for crop yields and for natural ecosystems and their ability to take up atmospheric carbon dioxide.

Although crucial to these issues, the effects of BVOCs remain poorly quantified, as illustrated by the outstanding difficulty in explaining the high observed OH levels in forested environments or the strong apparent influence of anthropogenic activities on the organic aerosol abundance. A better understanding of the processes involved is required in order to assess the effect of regulatory measures aiming at the mitigation of air pollution and climate change, in particular at the European level and in the framework of global climate negotiations.

Objectives

Our objectives were a better understanding and quantification of the role of BVOCs, in particular with respect to the formation of oxidants and aerosols, by means of

laboratory, theoretical and modelling investigations of the chemical degradation and aerosol formation potential of important BVOCs. Our specific objectives were:

(1) to assess the impact of isoprene emissions on the budget of oxidants, based on concerted theoretical and modelling efforts;

(2) to gain insights into the chemical pathways leading to key chemical constituents of SOA, termed "tracers", from the photooxidation of isoprene and selected monoterpenes; and

(3) to provide an improved model evaluation of the impact of BVOC emissions on organic aerosols.

Science results

The oxidation of isoprene (P1 & P2)

Prompted by observations of unexpectedly high OH radical concentrations above forests, we investigated the OH-initiated oxidation of isoprene using the highest levels of theory applicable, in order to rationalize the efficient HOx radical regeneration that clearly occurs and cannot be explained by traditional mechanisms. In our previous work (e.g. Peeters et al., 2009), we showed the existence of new reactions of isoprene peroxy radicals, leading to substantial HOx recycling. These findings were confirmed by laboratory experiments although differences with theory were also pointed out by the Caltech group. In BIOSOA, we considerably upgraded and extended our theoretical results, leading to the updated chemical mechanism "Leuven Isoprene Mechanism" LIM1 (Peeters et al. 2014). Our improved estimation of the key reaction rates is shown to be consistent with experimental data obtained at Caltech. The subsequent chemistry was also greatly extended and found to lead to ample OH recycling and to chemical compounds detected in the laboratory. The overall OH recycling predicted by LIM1 is in quantitative agreement with recent detailed chamber investigations at FZ Jülich. Modelling indicates that at the global scale, about 30% of the isoprene peroxys react via isomerisation routes.

We used satellite observations and a global model to better quantify the sources of formic acid. Its global source is found to be 2-3 times larger than the known sources, with a large contribution from the degradation of BVOCs, in particular of terpenoids emitted by coniferous trees. These conclusions are confirmed by comparisons with independent measurements. Formic acid is estimated to account for 60-80% of rain water acidity over remote forests. The results are published in Nature Geoscience.

Using available laboratory data, we demonstrated the previously unsuspected importance of photolysis for isoprene-derived carbonyl nitrates, an important organic nitrate component over vegetated areas. The photolysis sink of key carbonyl nitrates is estimated to be between ~3 and 20 times higher than their sink due to reaction with OH in atmospheric conditions.

The global budget of organic nitrates was investigated. The sources of small alkyl nitrates were constrained using airborne observations. Most importantly, the nitrate yield from the $CH_3O_2 + NO$ reaction was found to be much lower (by a factor > 40) than a recent laboratory determination. Comparisons of model results with total organic nitrate measurements show an excellent performance in isoprene-rich areas.

Formation pathways to key SOA markers (P3 & P4)

New insight has been obtained on pathways leading to the formation of the SOA markers 2-methyltetrols from isoprene. According to the literature, they can either be explained by acid-catalysed hydrolysis of C_5-epoxydiols or further photo-oxidation of C_5-alkene diols. It is shown that C_5-alkene diols serve as precursors for the 2-methyltetrols under low-NO$_x$ conditions, but their involvement is ruled out in the formation of the C_5-alkene triols. In addition, it is demonstrated that isoprene and C_5-alkene diols result in C_5-mono- and -diacids, which have retained the isoprene skeleton and as such may serve as suitable isoprene SOA markers. Furthermore, evidence is presented for a minor pathway to 2-methylglyceric acid.

Several potential tracers for **α-pinene** SOA ageing have been tentatively identified. Their formation has been explained by OH-initiated hydroxylation and fragmentation, and hydrolysis. SOA ageing can thus be regarded as a complex process involving different types of chemical reactions resulting in an array of products with different molecular weights (MWs) and polarities.

An **α**-pinene SOA marker (MW 188) abundantly present in ambient aerosol has been identified as the 2-hydroxyterpenylic acid 2R,3R diastereoisomer. Based on a time-resolved α-pinene oxidation experiment it was concluded that this compound is not a suitable marker for aged α-pinene SOA as previously suggested, but should be regarded as a higher-generation product of the α-pinene oxidation cascade.

Several organosulfates that contribute to PM acidity and are formed by interaction of biogenic SOA with sulfuric acid have been identified. Detailed interpretation of LC/MS data led to the structural characterisation of polar organosulfates related to SOA from isoprene and green leaf volatiles, 2-*E*-pentenal, 3-*Z*-hexenal, and 2-*E*-hexenal. Novel sources for polar organosulfates have been identified as methyl vinyl ketone, a major oxidation product of isoprene, and 2-*E*-pentenal, a photolysis product of 3-Z-hexenal. Possible formation pathways have been suggested.

Organic aerosol modelling (P1)

The vapour pressure estimation method EVAPORATION has been completed and validated. It will provide a more reliable description of partitioning of organic molecules to SOA. Several methods for estimating Henry's law constants were evaluated against literature data as well as against newly derived data based on measurements for related

properties. The combination of EVAPORATION with a method for activity coefficients (AIOMFAC) was found to perform best among the different methods.

The representation of SOA ageing in the BOREAM model for α-pinene has been greatly improved by increasing the number of compounds (to ~91000) with the help of an automatic mechanism generation tool. This model was evaluated against a wide range of laboratory data. It appears that the photolysis rates of SOA compounds are strongly underestimated and require a revision of photolysis parameters.

Finally, the evaluation of our global model against OA measurements revealed (i) the existence of a large missing source over polluted areas, in line with previous model-based analyses, and (ii) an overestimation over biogenically-influenced regions. The model performance was improved by adding a new OA source proportional to the anthropogenic primary OA source, and decreasing the biogenic SOA source in low-NOx environments. The biosphere is therefore only a moderate source of OA in absence of anthropogenic influence.

Contribution in a context of scientific support to a sustainable development policy
Environmental policy should be based on accurate information regarding the respective roles of natural and anthropogenic emissions on the abundance of air pollutants. BIOSOA has contributed to answer the following questions:

What is the impact of BVOCs on the oxidizing capacity of the atmosphere?
BVOCs were traditionally believed to deplete hydroxyl radical (OH) concentrations and to reduce the oxidizing capacity of the atmosphere. Recent field campaigns as well as our own previous theoretical work have shown that the oxidation of isoprene, the single-most important BVOC, regenerates OH, and that the overall impact of isoprene on the oxidizing capacity of the atmosphere is weak. Our work, confirmed experimentally by other groups, provides an extensive assessment as to how this regeneration proceeds. This finding will affect model estimates of how anthropogenic activities influence key pollutants like ozone and the climate gas methane.

What is the impact of BVOCs on acid rain?
Our model investigation revealed that BVOC oxidation is the largest source of formic acid worldwide, which is itself a large, even often dominant, source of cloud and rain acidity. It is important however to stress that the consequence of this acidity for ecosystems is limited owing to the assimilation of simple organic acids by the biota.

How much do BVOCs contribute to atmospheric aerosol?
Secondary organic aerosol (SOA) is a major component of fine aerosols over continents. Our work provided new insights on the processes leading to SOA formation, which will

allow improved estimations for the role of BVOCs as a source of aerosols. Although biogenic SOA is by far the largest component of organic aerosol, its formation appears to be strongly enhanced by anthropogenic pollution, due to complex interactions which BIOSOA research contributed to elucidate.

In conclusion, contrary to long-held beliefs, and as rationalized by this work, BVOC emissions have a relatively limited influence on the oxidizing capacity, in particular at remote locations (e.g. rainforests). Deforestation is therefore not expected to increase the self-cleansing property of the atmosphere and to mitigate pollutant build-up. On the other hand, BVOCs are a substantial source of organic aerosol with far-reaching effects on climate and air quality. The complex interaction of these emissions with anthropogenic emissions warrants further investigation.

Key words : Biogenic volatile organic compounds (BVOC); air quality; atmospheric composition ; climate change; aerosols ; smog; hydroxyl radical; tropospheric ozone ; oxidative capacity of the atmosphere ; chemical mechanisms

1. INTRODUCTION

Due to their very large emissions ($\sim$1000 Tg/year globally), biogenic volatile organic compounds (BVOCs) released by vegetation exert multiple influences on the atmospheric composition and climate. Their photochemical oxidation affects the oxidising capacity of the atmosphere through its impact on the concentrations of oxidants (chiefly the hydroxyl radical OH) and is a source of secondary organic aerosol (SOA). In the presence of nitrogen oxides, the oxidation of BVOCs generates ozone, a greenhouse gas which also plays a prominent role in photochemical smog episodes. SOA is a major component of ambient fine mode aerosol, which affects climate, degrades visibility and causes adverse health effects (Hallquist et al., 2009). It follows that any policy aiming at mitigating the impact of anthropogenic emissions on air quality and the climate must take into consideration the complex role of BVOCs. A better understanding of BVOC oxidation and biogenic SOA formation and ageing is needed in order to assess the role of the biosphere in climate regulation.

In this project, laboratory, theoretical and modelling investigations were conducted with the aim to better understand and quantify the role of biogenic hydrocarbons, in particular with respect to the formation of ozone and aerosols and the oxidation capacity of the atmosphere. This project aimed to provide a better scientific basis for decision-making (especially at an international level) with regard to anthropogenic emissions of pollutants like the nitrogen oxides, volatile organic compounds and fine particulate matter. Our specific objectives were the following:

(1) to assess the impact of isoprene emissions on the composition of the troposphere, based on concerted theoretical and modelling efforts;

(2) to gain insights into the chemical pathways leading to key chemical constituents of SOA, termed "tracers", from the photooxidation of isoprene and selected monoterpenes;

(3) to develop analytical methodology that allows to quantify the contributions of individual BVOCs to the organic aerosol;

(4) to evaluate the impact of BVOC emissions on organic aerosols.

Isoprene gas-phase oxidation mechanism

In previous work, partner P2 at KULeuven proposed and theoretically quantified a novel mechanism for the oxidation of the dominant biogenic compound isoprene (LIM0). The mechanism features new, major HO_x-radical regenerating pathways (Peeters et al., 2009; Peeters and Müller, 2010; Nguyen et al., 2010) that are believed to explain the unexpectedly high hydroxyl concentrations measured in several recent campaigns over areas with high isoprene emissions in the tropical and temperate zones (e.g. Lelieveld et al., 2008; Ren et al., 2008; Hofzumahaus et al., 2009). The key new

pathways in LIM0 are allyl-resonance-enhanced unimolecular dissociation and isomerisation reactions of the initial isoprene hydroxy-peroxy radicals that can outrun the traditional peroxy radical reactions with NO and HO_2 radicals in all atmospheric conditions, except in polluted urban/industrialised areas, and that mainly result in highly photolabile hydroperoxy-methyl-butenals (HPALDs) with yields of 30 - 80%. These HPALDs were argued to photolyse quickly and to result, with the subsequent chemistry, in the generation of additional OH and HO_2 radicals; a consistent body of evidence could also be construed from recent observations in the literature supporting this mechanism (Peeters and Müller, 2010). Global modelling studies demonstrated the large potential impact of the new chemistry on the oxidising capacity of the atmosphere over continents (Stavrakou et al., 2010; Archibald et al., 2010); in comparison to existing isoprene oxidation models, LIM0 was found to entail 50 - 300% higher hydroxyl concentrations over forested areas, while leaving surface ozone nearly unchanged.

Through its large impact on OH, the LIM0 chemistry influences the lifetime and therefore the abundance of the greenhouse gas methane, but also organic aerosol abundances and properties, due to the key role of OH in the formation and ageing of atmospheric SOA. It thus appears that the theory-based LIM0 mechanism represented a major step towards a better understanding of the role of isoprene. However, the subsequent chemistry following the photooxidation of the newly proposed dominant first-generation HPALDs products is still largely unknown or speculative.

A prime objective of the present research proposal is therefore the further theory-based development of the OH-initiated isoprene oxidation mechanism, applying high-level methodologies and box-modelling validation by confrontation against available chamber data. Besides the impact of the new mechanism on HOx regeneration, attention will be given to the formation yields of key oxygenated intermediates involved in SOA formation (e.g. glyoxal and methylglyoxal) and major products for which satellite datasets are available (e.g. formaldehyde). Such observational databases have been widely used in combination with atmospheric models to infer constraints on BVOC emissions based on the inverse modelling technique (Palmer et al., 2006; Stavrakou et al., 2009a,b).

SOA formation and ageing

It is generally accepted that semi-volatile organic compounds, produced in the atmospheric oxidation of anthropogenic and biogenic volatile organic compounds, contribute to the growth of atmospheric aerosol. However, this process is still only partially understood, although considerable efforts have been undertaken to obtain insights into this phenomenon. The formidable complexity of the gas-phase oxidation mechanisms for large BVOCs (e.g. α-pinene), in addition to the important but poorly quantified role of particle-phase reactions, probably explains why the formation

pathways to several key products observed in smog chamber experiments or in ambient SOA remain unclear. In such context, to palliate the lack of mechanistic understanding, attempts to quantify global SOA formation from terpenoid compounds have relied on highly parameterised schemes such as the two-product model (Odum et al., 1996), with parameters fitted from smog chamber experiments. However, this approach ignores the dynamical nature of SOA formation and the large differences existing between laboratory setups and the atmosphere, as illustrated by e.g. the generally higher O/C ratios observed in ambient aerosols compared to SOA obtained in smog chambers (Jimenez et al., 2009). It has become evident that, once in the atmosphere, secondary organic aerosol (SOA) is not inert. Photochemical ageing of SOA, primarily due to OH radical oxidation (often leading to more functionalised, less volatile species) and photolysis (generally producing more volatile compounds) has a strong influence on the concentrations and hydrophilic properties of atmospheric SOA and contribute to its cloud effect.

Besides the traditional SOA formation pathway, according to which gas-phase oxidation products either nucleate or condense on existing organic aerosol, there is strong evidence from model, laboratory and field studies that the uptake of water-soluble organics by cloud droplets, followed by oligomerisation and/or oxidation, leads to the formation of low-volatility products that remain to a large extent in the particle phase upon droplet evaporation (e.g. Carlton et al., 2007, Lim et al., 2010). This sequence of processes represents a significant additional source of SOA to the global atmosphere. Whereas acid formation is the dominant pathway to SOA in cloud droplets, oligomerisation plays a dominant role in aqueous aerosols and also in evaporating cloud droplets (Tan et al., 2009; Loeffler et al., 2006). The formation of SOA through the uptake of small dicarbonyls by aqueous aerosols and cloud droplets has been estimated in global models using very simplified parameterisations (Fu et al., 2008; Stavrakou et al., 2009c). Large uncertainties are associated to the global budget of water-soluble SOA precursors (e.g. glyoxal, see Stavrakou et al., 2009b), the representation of their aqueous-phase chemistry, and the fate of the carboxylic acids. Fixed values are generally used in models for the gas/particle ratios of carboxylic acids (e.g. Lim et al., 2005), ignoring their dependence on aerosol abundance and thermodynamic properties (vapour pressure, Henry's Law constant). The estimation of those properties is very uncertain due to lack of direct experimental determination, and relies on estimation methods based on a relatively limited dataset of experimental values. Furthermore, experimental data are mostly available for monofunctional compounds, whereas SOA is mostly made of polyfunctional compounds.

Molecular characterisation of SOA

Characterisation of BVOC oxidation products at the molecular level in atmospheric aerosols allows to gain insights into aerosol sources (i.e. BVOCs such as isoprene, monoterpenes, green leaf volatiles) and oxidation pathways. Common terms to denote analytically accessible organic compounds that provide this valuable information in a complex ambient aerosol matrix are "tracer", or "marker" or "indicator" compound. Molecular characterisation of unknown biogenic SOA markers is an analytically challenging and complex task, in which partners P3 and P4 have gained a unique expertise during the last fifteen years, mainly by resorting to combined chromatographic/mass spectrometric approaches. Noteworthy examples are the discovery of the 2-methyltetrols as markers for isoprene SOA (Claeys et al., 2004) and the structural characterisation of the tricarboxylic acid 3-methyl-1,2,3-tricarboxylic acid as a marker for aged biogenic SOA (Szmigielski et al., 2007) and of the lactone-containing α-pinene SOA marker terpenylic acid (Claeys et al., 2009).

Objectives of the current project were to obtain a more complete insight into the photo-oxidation of isoprene under low-NO_x ($NO + NO_2$) conditions, the atmospheric oxidation of α-pinene resulting in terpenylic acid and aged products, and the formation of polar organosulfates from isoprene and other BVOCs, i.e. unsaturated C_5 and C_6 aldehydes.

As to the formation of isoprene SOA, the underlying chemistries are not fully understood. Major SOA tracers from isoprene photo-oxidation are the diastereoisomeric 2-methyltetrols (2-methylthreitol and 2-methylerythritol), the isomeric C_5-alkene triols [2-methyl-1,3,4-trihydroxy-1-butene (cis and trans) and 3-methyl-2,3,4-trihydroxy-1-butene], and 2-methylglyceric acid. The 2-methyltetrols and the C_5-alkene triols were first discovered in fine aerosol from the Amazon forest (Claeys et al., 2004a; Wang et al., 2005), whereas 2-methylglyceric acid was first reported in fine aerosol from K-puszta, Hungary (Claeys et al., 2004b). Two mechanistic pathways have been suggested to explain the formation of the 2-methyltetrols through photo-oxidation of isoprene under low-NO_x conditions (Kleindienst et al., 2009; Paulot et al., 2009b). Key intermediates in the first pathway are the C_5-alkene diols, whereas those in the second one are the C_5-epoxydiols. Here, we have evaluated whether the C_5-alkene diols, which are known to be formed in the ambient atmosphere, can serve as precursors for the 2-methyltetrols, C_5-alkene triols and other tracers under low-NO_x conditions.

In regard to the atmospheric oxidation of **α-pinene**, it is becoming increasingly recognised that the resulting SOA is a very complex and dynamic mixture containing products with a different chemical nature and physicochemical properties that are dependent on chemical evolution or ageing processes (Kroll et al., 2008, 2011; Jimenez et al., 2009). In the current project a study has been performed on the chemical

characterisation of major products that are formed upon formation of α-pinene ozonolysis SOA and subsequent ageing through OH-initiated reactions in the absence of NO_x. These conditions are relevant to pristine forests such as the Amazonian rainforest, where NO/HO_2 and NO/RO_2 ratios are very low (Lelieveld et al., 2008). In addition, the molecular structures of MW 188 oxidation (aged) products of terpenylic acid, which as terpenylic acid also show significant atmospheric concentrations (Claeys et al., 2009; Gómez-González et al., 2012), have been examined in detail.

Organosulfates are potential marker compounds for SOA formation occurring under acidic conditions by particle-phase reactions with sulfuric acid (Surratt et al., 2007b), formed by oxidation of sulfur dioxide, which is mainly from anthropogenic origin in continental regions of the globe. More specifically, they are formed by reaction of epoxy-containing compounds, which are formed in the gas phase (e.g. epoxydiols), with sulfuric acid in the particle phase (Surratt et al., 2010), or alternatively, by reactive uptake of unsaturated compounds in the particle phase and reaction with the sulfate radical anion (Rudzinski et al., 2009). Unlike isoprene very little was known about SOA formation from green leaf volatiles such as unsaturated C_5 and C_6 aldehydes at the start of this project. These volatiles are released by plants when they are wounded (e.g. grass cutting, animal grazing, storms) or attacked by insects (for a reviews, see Holopainen et al., 2004, and Scala et al., 2013). The most abundant isoprene-related organosulfates (OSs) in ambient fine aerosol from forested sites during summer are sulfate esters of the 2-methyltetrols. Similar to the polar OSs related to SOA from the photo-oxidation of isoprene, those originating from the photo-oxidation of unsaturated aldehydes may also be hydrophilic and substantially contribute to the total SOA budget. Polar OSs are of climatic interest due to their capability to enhance the hydrophilic properties of the aerosol, and, hence, their cloud-forming properties (Facchini et al., 1999).

As in previous research on the molecular characterisation of biogenic SOA tracers, we resort to off-line organic chemical analysis using chromatographic techniques [i.e. gas chromatography (GC) coupled to electron ionisation MS or liquid chromatography (LC)] coupled to electrospray ionisation MS, as well as advanced mass spectrometric techniques including multidimensional (MS^n) and high-resolution MS.

2. METHODOLOGY AND RESULTS

WP1. The novel isoprene oxidation mechanism LIM1

Theory-based development of detailed isoprene oxidation-mechanism

The theoretical development of the isoprene oxidation mechanism relies on 1° high-level quantum-chemical characterisation and 2° subsequent theoretical-kinetics quantification of reactions that are expected to be significant. Such methodologies were applied by us during the past 15 years, e.g. for the construction of the oxidation mechanisms of α-pinene (Peeters et al., 2001; Fantechi et al., 2002) incorporated in the BOREAM model (Ceulemans et al. 2010; Ceulemans et al., 2012), and allowed the identification and quantification of non-traditional reactions of alkoxy and peroxy radicals (Vereecken et al., 2004; Hermans et al. 2005; Vereecken et al., 2007), with the novel isoprene hydroxy-peroxy radical isomerisations as a prime example.

In this work, much higher-quality quantum chemical DFT and ab initio methods are brought to bear. The new-generation, powerful DFT functional M06-2X with large 6-311++G(3df,2p) basis set, further designated simply as M06-2X, is used for potential energy surface (PES) constructions. This functional is far superior to B3LYP used in our earlier studies (Peeters et al., 2009), as, among others, it accounts properly for London dispersion effects found to be of critical importance in the hydrogen-bonded structures of interest here. Besides geometry optimisations, M06-2X is used to calculate multi-conformer partition functions. For rate-determining reaction steps, geometries of the lowest-energy conformers of reactants and transition states (TS) are optimised using the proven Quadratic Configuration Interaction method, QCISD/6-311G(d,p), and single-point energies are computed using the high-performance but costly Coupled Cluster method with very large basis set, CCSD(T)/aug-cc-PVTZ. This combination, further denoted as CC//QC, is the most accurate method presently feasible for the molecules of interest. The calculations were carried out with the Gaussian 09 program suite and Molpro 2012.1 program.

On basis of the quantum computations, advanced theoretical kinetics calculations are performed to obtain temperature- (and pressure-) dependent rate coefficients and branching ratios, using mainly Multi-Conformer Transition State Theory (MC-TST), or RRKM theory and Exact Stochastic Model- based Master Equation analysis for chemically activated reactions. In the MC-TST approach (Vereecken and Peeters, 2003), applied here among others for the key 1,6-H shift isomerisations of the Z-δ-OH-isoprenyl-peroxy radicals, all local potential energy minima of a reactant or transition state (TS) separated by high enough conformational (internal rotation) barriers, of >2 kcal/mol at 300 K, are considered as separate "states", each contributing to the total

partition function weighted by the Boltzmann factor $\exp(-\varepsilon i/k_B T)$. For the crucial peroxy radicals of interest (the Z-δ-OH-isoprenyl- and β-OH-isoprenylperoxys), some 20 to 29 relevant conformers are found, and 5 to 7 for the transition states. M06-2X is used for the geometry optimisations of the conformers and for computing their relative energies εi with respect to the lowest-lying conformer, as well as for all the data needed to evaluate their partition functions, i.e. vibration frequencies, rotation parameters, and zero-point vibration energies (ZPVE). Note that all relative energies or barrier heights mentioned in the article always include the Δ(ZPVE). It is important to note that the presently obtained multi-conformer partition functions and their ratios differ in many instances considerably, often by a factor of 3 to 7, from our earlier results at the B3LYP level (Peeters et al., 2009), mainly because the latter does not take into account London dispersion effects. Tunneling factors for the crucial H shifts in isoprene-derived peroxys are calculated in the asymmetric Eckart-barrier approximation, which was recently shown to quite well match the high-level small curvature tunneling (SCT) factors calculated for 1,4- and 1,5-H shifts in n-pentylperoxy radicals for temperatures around 300 K (Zhang and Dibble, 2011) .

As a second major predictive tool, quantitative Structure-Activity Relationships (SARs) are applied, such as SARs for site-specific OH-addition to (poly)alkenes, decomposition of substituted alkoxy radicals, and H-shifts in such radicals (Peeters et al., 2004, 2007; Vereecken and Peeters, 2009, 2010).

Kinetics of the reactions of the hydroxy-isoprenylperoxy radicals: Results
Figures 1 and 2 present an overview of formation and removal reactions of the hydroxy-isoprenylperoxy radicals that determine the concentration fractions of the specific peroxy-isomers undergoing the newly proposed unimolecular reactions. The contributions of these unimolecular reactions to overall isoprene chemistry depend on the fractional populations of these specific isomers as well as on their isomer-specific rates. The peroxy radicals are formed by addition of hydroxyl radicals to isoprene, followed by addition of O_2. OH radicals can add to each of the four unsaturated C-atoms of isoprene, labelled as shown below:
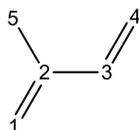
Owing to the conjugated diene structure of isoprene, the initial OH-adducts to the two terminal carbons, denoted in Figures 1 and 2 as OH-Adduct I and OH-Adduct II are resonance-stabilised allylic radicals, e.g. for the OH-Adducts I:

$$HOCH_2\text{-}C^\bullet(CH_3)\text{-}CH=CH_2 \leftrightarrow HOCH_2\text{-}C(CH_3)=CH\text{-}CH_2^\bullet$$

Figure 1. LIM1 reaction scheme of OH-initiated oxidation of isoprene under low-NO conditions for initial HOCH$_2$C(CH$_3$)CHCH$_2$ hydroxy-isoprenyl adducts (Case I). Rate constants shown are at 298.

which also explains why they dominate by far over the much less stable OH-adducts to the two central carbons (Peeters et al., 1994, 2007; Park et al., 2004). It also follows that O$_2$ can add to both the major OH-adducts either in β- or in δ- position, resulting in β-OH-isoprenylperoxys and in Z- as well as E-δ-OH-isoprenylperoxys. The peroxys resulting from OH-Adduct I and OH-Adduct II and their subsequent chemistry are displayed separately in Figures 1 and 2, respectively. The three peroxy isomers for each case are denoted in these Figures and below as β-OH-peroxy, Z-OH-peroxy and E-OH-peroxy (followed by I or II when necessary).

The allyl-resonance stabilisation of 12 - 14 kcal mol^{-1} of the initial OH-Adducts I and II is lost upon O$_2$-addition, such that the stability of the resulting allylperoxys is expected to be only of the order of 20 kcal/mol. For this reason, the β-OH- and δ-OH-peroxys from isoprene are thermally unstable at tropospheric temperatures, and their redissociation must therefore be expected when the peroxy lifetime is long enough, as

in near-pristine low-NO environments, such that the β-OH- and δ-OH-peroxys may actually interconvert and even tend to a thermal equilibrium ratio.
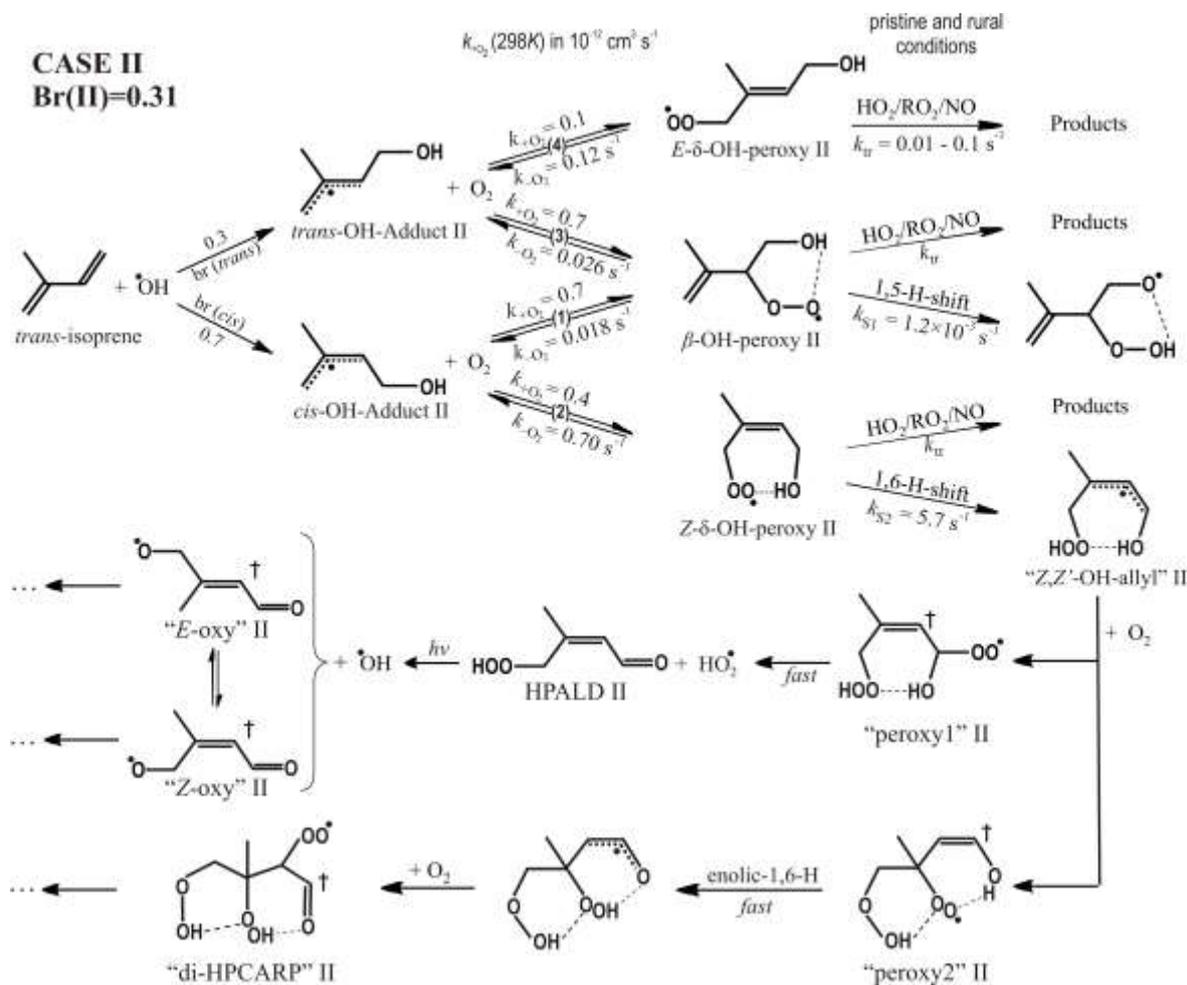

Figure 2. LIM1 reaction scheme of OH-initiated oxidation of isoprene under low-NO conditions for initial $CH_2C(CH_3)CHCH_2OH$ hydroxy-isoprenyl adducts (Case II). Rate constants shown are at 298 K.

Other peroxy removal reactions influencing the population fractions are the proposed unimolecular H-migration reactions, also displayed in Figures 1 and 2. Obviously, one needs also to consider the "traditional" peroxy radical reactions with NO and with HO_2 and RO_2 radicals. For the reactions with NO, a rate coefficient $k_{NO} = 9 \times 10^{-12}$ cm^3 s^{-1} at 298 K is generally adopted as for regular alkylperoxys; the products are mainly NO_2 together with the corresponding oxy radicals, $RO_2 + NO \rightarrow RO + NO_2$, the RO giving rise to the bulk of the 1st-generation isoprene oxidation products at high NO levels, but also about 8.5% nitrates, $RO_2 + NO \rightarrow RONO_2$ (Orlando and Tyndall, 2012). The reactions of the isoprene peroxys with HO_2, with measured overall rate coefficient $k_{HO2} = 1.7$ 10^{-11} cm^3 s^{-1} at 298 K (Boyd et al., 2003), are believed to produce mainly hydroperoxides, $RO_2 + HO_2 \rightarrow ROOH + O_2$, but recent results indicate also some 6 to

12% formation of O_2 + OH + RO (Paulot et al. 2009b; Liu et al., 2013). Mutual or cross reactions of the isoprene-peroxys, with weighted average rate coefficient around $k_{RO2} \approx 2 \times 10^{-12}$ cm^3 s^{-1} (Jenkin et al., 1998) are generally thought to be minor under atmospheric conditions. The total pseudo-first order isoprene-peroxy removal rate by the traditional reactions combined in pristine or remote regions is mostly in the range of k_{tr} = 0.02 to 0.05 s^{-1}. The rates of the other peroxy removal and interconversion reactions and their formation reactions are addressed in the following subsections.

Addition of OH to isoprene

Four OH-adducts can be formed, including for about 7% OH-adducts to the two inner carbons atoms (Lei and Zhang, 2001) of which the chemistry is not considered further in this work, and 93 % adducts to the two outer carbons: OH-Adduct I and OH-Adduct II (see Figure 1 and 2). For the latter two, following and concurring with Park et al. (2004) we adopt branching fractions of 62 % and 31%, respectively, to best reproduce the well-established experimental product distribution at high NO. These values are compatible with and close to the averages of two independent theoretical approaches within their expected uncertainties of several % (Peeters et al., 1994; Peeters et al., 2007; Greenwald et al. 2007). Both the OH-Adducts I and II can be formed as either cis- or trans- allylic structures: their high initial internal energies of some 36-39 kcal mol^{-1}, which includes a few kcal mol^{-1} thermal energy, allow for prompt cis-trans interconversion, over barriers computed to be only 14-15 kcal mol^{-1} (Peeters et al. 2009), before they are fully collisionally stabilized. An RRKM-master equation analysis revealed that OH-Adducts I collisionally stabilize as $\approx$ 50% trans and $\approx$ 50% cis, whereas the OH-Adducts II end up as $\approx$ 30% trans- and 70% cis-OH-Adducts II (see Figures 1 and 2) (Peeters et al. 2009), in excellent agreement with earlier predictions by Dibble (2002). The addition of O_2 in β position to the OH-Adducts I and II allows for near-free internal rotation of the -CH=CH2 or -C(CH3)=CH2 moieties in the β peroxys, merging the contributions from cis- and trans- OH-isoprene radicals; however, O_2-addition to the δ-carbon leads to distinct E- or Z- substituted alkene frames (see Figures 1 and 2).

It must be stressed that the β-OH- $\rightleftharpoons$ δ-OH-peroxy interconversion above does not occur between peroxys from different initial OH-adducts. The peroxy pool from the OH-Adducts I remains strictly separated from the pool derived from OH-Adducts II since the initial OH-adducts are far too stable to redissociate. For the peroxy chemistries and subsequent processes, we therefore consider below always two distinct cases: Case I for the chemistry resulting from the OH-Adducts I (Figure 1); and Case II for that from the OH-Adducts II (Figure 2).

Addition of O₂ to hydroxy-isoprene adducts: rate and initial branching ratios

The rate coefficients for the various site-specific O_2-additions, leading to the six different peroxys (see Figures 1 and 2), are obtained from the overall O_2-addition rate k_{+O2}^{bulk}, in combination with the branching to the OH-adducts, above, and with the 1st-generation oxidation-product distribution as measured in laboratory experiments at very high NO, on which there is a consensus within a few percent (Park et al., 2004; IUPAC). At very high NO, the isoprene peroxys react immediately with NO, producing MVK, MACR and other compounds via well understood mechanisms. In this way, the relative formation rates of the six isoprene peroxys of interest can be retrieved with good precision. The values adopted differ somewhat from these reported previously (Peeters et al., 2009), because the expected products from the minor, central adducts are now included in the analysis. Remarkably, the overall k_{+O2}^{bulk} is not well known. In our earlier paper we used the value of 2.3×10^{-12} cm³ s⁻¹ reported by Park et al. (2004), though with a large uncertainty of $\pm 2 \times 10^{-12}$ cm³ s⁻¹. In this work, we adopted the more recent value of (1.0 +1.7/-0.5)$\times 10^{-12}$ cm³ s⁻¹ determined by Ghosh et al. (2010) for O_2 addition to the major OH-Adduct I, a value consistent with the range (2.3 $\pm$ 2.0)$\times 10^{-12}$ cm³ s⁻¹ of the above mentioned study. It turns out that at low NO (< 100 ppt) the product distribution deriving from OH-Adduct I shows little sensitivity to k_{+O2}^{bulk}, while it affects the product yields from OH-Adduct II in a minor way. The rate coefficients derived in this way for the isomer-specific O_2-addition rates k_{+O2} are shown on Figures 1 and 2. Note that the precise initial branching to the E-δ-OH-peroxys is of only marginal importance for this work, since under the low-NO conditions of interest, these isomers are shown below to be in near-equilibrium with the majority β-OH-peroxy isomers anyway.

Redissociation and interconversion of the OH-isoprenylperoxy radicals

To quantify the fractions of the six peroxys, the required rates of their redissociation by O_2 loss, k_{-O2}, can be evaluated from the k_{+O2} above via the thermal equilibrium constants, $K_{eq} = k_{+O2} / k_{-O2}$. Note that the OH-adducts should be fully thermalized when adding O_2, since they will have suffered some ~ 1000 collisions before that. The K_{eq} are evaluated theoretically using a multi-conformer quantum-statistical approach:

$$K_{eq} = \frac{\sum Q_{peroxy}}{Q_{O_2} \times \sum Q_{OH\text{-}Adduct}} \times e^{-\frac{\Delta E}{k_B T}} \tag{1}$$

in which Q_{O2} is the partition function of O_2; $\sum Q_{peroxy}$ and $\sum Q_{OH\text{-}Adduct}$ are the multi-conformer partition function of the considered peroxy isomer and OH-Adduct isomer, respectively; ΔE is the energy difference between the lowest-energy conformers of peroxy and OH-Adduct + O_2; and k_B is the Boltzmann constant. The relative energies of the lowest-lying conformers of the key β-OH- and Z-δ-OH-peroxys and of their OH-Adduct precursors, needed for the critical energy difference ΔE in the exponent of

equation (1), were computed at the high-performance CC//QC level of theory. It should be noted that to reduce the computational cost by a factor of ≈ 10, the CC//QC energies for the lowest conformer were computed for each structure involved (molecule, radical or transition state) with the methyl substituent replaced by an H atom, and including separately the effect of the methyl substituent computed for each structure at the M06-2X level. It was duly verified for a few structures that the accuracy loss of this procedure was only ≈ 0.15 kcal mol^{-1}. The energy separations ε_i of the various conformers relative to the lowest, and all other parameters required for the multi-conformer partition functions were computed at the M06-2X level. For each of the crucial β-OH- and Z-δ-OH-peroxy radicals of interest, about 25 relevant conformers had to be taken into account, versus 4 to 5 for the allylic OH-Adducts. For the less important trans-OH-adducts and the E-δ-OH-peroxys the ΔE were computed at the M06-2X level. In each of the two peroxy pools, the β-OH-peroxy isomers are the most stable, mainly because of the 4 to 5 kcal mol^{-1} strong internal hydrogen bond, while the Z-δ-OH-peroxy isomers which feature an only weak H-bond, are less stable by 2.22 (Case I) and 2.54 (Case II) kcal mol^{-1}; worth noting, these crucial CC//QC computed differences are supported by the M06-2X values being both only 0.19 kcal mol^{-1} higher. The less important E-δ-OH-peroxys, lacking an H-bond, are highest in energy but are looser and therefore have somewhat higher partition functions. The CC//QC computed O_2-addition energies ΔE for the various reactions of interest, which can be obtained from these data, are only about 20 to 24 kcal mol^{-1} as expected, and therefore low enough for substantial re-dissociation of the peroxys. The K_{eq}, evaluated over the temperature range of interest, 280-320 K, show strong dependences on temperature T, as expected.

The T-dependent expressions $K_{eq}(T)$ and $k_{-O2}(T)$ are listed in TABLE I. The k_{-O2} (298 K) values are in the range of 0.02 to 5 s^{-1}, higher than or comparable to the rates of their removal by NO/HO$_2$/RO$_2$ in near-pristine conditions. The highest redissociation rates are found for the Z- and E- δ-OH-peroxys, in particular for Case I, with k_{-O2} (298 K) approaching 5 s^{-1}. Both the E- and Z-δ-OH-peroxy isomers in each separate pool (Case I; Case II) may then tend to thermal equilibration with the majority β-OH-peroxys, but, as made clear in a next subsection, full equilibration, within 5%, of

$$\beta\text{-OH-peroxy} \rightleftharpoons Z\text{-}\delta\text{-OH-peroxy} \qquad\qquad (Ra)$$

is only possible for the Case I peroxys, and then only at temperatures T $\geq$ 310K, while for the Case II peroxys, these equilibria are far from attained. Abbreviating K_{eq} a $\equiv \{[Z\text{-}\delta]/[\beta]\}_{eq}$ for potential equilibrium (Ra) as $K_{eq}(Z\text{-}\delta/\beta)$, and K_{eq} b $\equiv \{[E\text{-}\delta]/[\beta]\}_{eq}$ for potential equilibrium

$$\beta\text{-OH-peroxy} \rightleftharpoons E\text{-}\delta\text{-OH-peroxy} \qquad\qquad (Rb)$$

as $K_{eq}(E\text{-}\delta/\beta)$, we find for Case I: $K_{eq}(Z\text{-}\delta/\beta)(I) = 0.0133$ and $K_{eq}(E\text{-}\delta/\beta)(I) = 0.0158$ at 298 K, such that the β-OH-peroxys would make up $\geq 97\%$ of a potential peroxy equilibrium

population. The K_{eq} data for the Case II peroxys are quite similar, but the actual steady-state $\{[Z\text{-}\delta]/[\beta]\}$ ratio at low NO is far below the equilibrium value.

It can be noted that the present $\{[Z\text{-}\delta]/[\beta]\}_{eq}$ values are about 4 times lower than the preliminary values of about 0.06 in our earlier proof-of-concept communication (Peeters et al., 2009). The major reason is that the multi-conformer partition function ratio of the Z-δ-OH- and β-OH-peroxy isomers computed at the superior M06-2X level is much lower than obtained with the B3LYP functional that neglects London dispersion and hence substantially underestimates several low-vibration frequencies of the Z-δ-OH-peroxy conformers and moreover predicts too small energy separations between the lower Z-δ-OH-peroxy conformers.

1,6-H shift of the Z-δ-OH-peroxys and 1,5-H shift of the β-OH-peroxys

The rate coefficients k(Z-δ 1,6-H) of the 1,6-H shift in the Z-δ-OH-peroxys and k(β 1,5-H) of the 1,5-H shift in the β-OH-peroxys are evaluated using multi-conformer transition state theory, MC-TST (Vereecken and Peeters, 2003), e.g.:

$$k(\text{Z-}\delta\ 1,6\text{-H})(T) = \kappa(T)\frac{k_B T}{h}\frac{\Sigma Q^{\neq}_{TS}}{\Sigma Q_{Z\text{-}\delta\text{-}OH\text{-peroxy}}}\times e^{-\frac{E_0}{k_B T}} \qquad (2)$$

in which h is Planck's constant and k_B Boltzmann's constant; $\Sigma Q^{\neq}_{TS\ 1,6\text{-H}}$ and $\Sigma Q_{Z\text{-}\delta\text{-}OH\text{-peroxy}}$ are the multi-conformer partition functions of the TS for the 1,6-H shift and of the Z-δ-OH-peroxy considered, respectively, evaluated as above, with each individual Q_i weighted by the relative thermal population $\exp(-\varepsilon_i/k_B T)$; $E_0(1,6\text{-H})$ is the energy barrier or difference between the energies of the lowest conformers of TS and peroxy radical, respectively, both computed at the high CC//QC level of theory; $\kappa(T)$ is the average tunnelling factor, obtained by weighting the individual κ_i by the individual partition functions Q_i of the TS conformers, i.e.: $\kappa = \Sigma(\kappa_i \times Q^{\neq}_i)/\Sigma Q^{\neq}_i$. For Case I only two TS conformers and For Case II three TS conformers were taken into account, the contribution of all higher conformers being minor.

The barrier height values for the 1,6-H shifts thus found are $E_0(1,6\text{-H})$ = 19.62 and 18.11 kcal mol^{-1} for Cases I and II, respectively. The about 1.5 kcal/mol lower barrier for Case II, found systematically at all levels of theory, is due to the stabilizing effect of the methyl-group on that carbon in the allylic product. A schematic PES for the 1,6-H shift, Case I, through the lowest TS conformer, is depicted in Figure 3. Worth noting, the CC//QC barriers above are supported by the 19.46 and 17.95 kcal mol^{-1} values computed at M06-2X level, but they are significantly higher than the lower-level CBS-APNO results of our earlier communication (2009). However, the higher barriers are compensated by the M06-2X-based multi-conformer partition functions of the Z-OH-peroxy reactants being substantially lower than the earlier, lower-level B3LYP-based data, as already implied above. Another important difference are the tunnelling factors,

which were earlier evaluated in a unidimensional zero-curvature (ZCT) WKB-approximation. As recently pointed out by Zhang and Dibble (2011), ZCT underestimates tunnelling in 1,4-H and 1,5-H shifts in C5-peroxy radicals by factors 3 to 4 compared to the much more reliable small-curvature SCT results, which, on the other hand, these authors found to be fairly well reproduced by the asymmetric Eckart barrier approximation. Therefore, we presently adopt the Eckart approximation.

The scaled imaginary frequencies of the two lowest conformers of TS(Z-δ 1,6-H)(I) for example, computed at M06-2X using an ultra-fine grid, are 1735.45 and 1820.53 cm-1, while the reverse barriers were taken equal to the forward barriers in order to account for the allyl-resonance-induced widening of the barrier starting at ≈ 15 kcal mol^{-1} below the top, as discussed below and illustrated in Figure 3. The resulting tunnelling factors κ_i(298 K) of 102 and 161 are indeed around 4 times higher than the ZCT values (Peeters et al. 2009). It follows that the 1,6-H shifts occur for >99% by H atom tunnelling. Finally, the fall-off factors at 1 atm, calculated using the standard RRKM approach, are found to be $\geq$ 0.99 at all relevant temperatures.
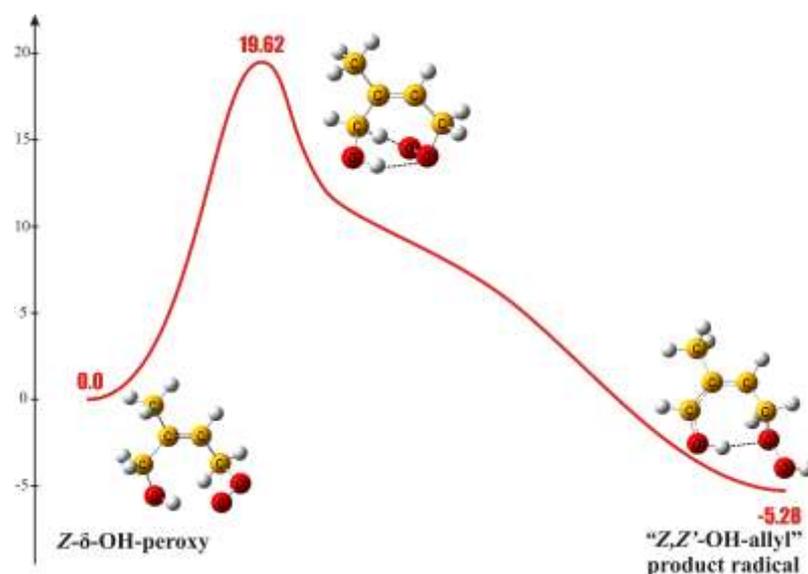

Figure 3. Potential energy surface (PES) of 1,6-H shift isomerisation of most stable conformer of Z-δ-OH-peroxy radical, Z-HOCH2-C(CH3)=CH-CH2OO•. Energies at CCSD(T)/aug-cc-PVTZ // QCISD/6-311G(d,p) level of theory, including ZPVE at M06-2X/311++G(3df,2p) level. Reactant, transition state and product are hydrogen-bonded.

The rate coefficients at 280, 285, 298, 315 and 320 K can be fitted within 0.25% by the T-dependent expressions listed in TABLE I. In these expressions, the exponential functions featuring T^{-3} express the strongly curved negative T-dependence of the tunnelling factors. The rate coefficient values at 298 K are k(Z-δ 1,6-H)(I)(298) = 0.52 s^{-1} and k(Z-δ 1,6-H)(II)(298) = 5.72 s^{-1}, respectively. These values are not too different from our earlier results, but, as explained above, the accord is rather fortuitous.

TABLE I. Expressions of the equilibrium constants and rates involving the OH-adducts and peroxy radicals, T = 280-320 K. Notations as in Figures 1 and 2. ci = *cis*-OH-Adduct; tr = *trans*-OH-Adduct; β = β-OH-peroxy; Z-δ = Z-δ-OH-peroxy; E-δ = E-δ-OH-peroxy.

CASE I: OH-isoprenyl Adduct I, $HOCH_2C^•(CH_3)CH=CH_2$,   62%

IA. *cis*-OH-isoprenyl Adduct,   br(*cis*) = 0.5

Reversible reaction: *cis*-OH-Adduct I + O_2 ⇌ β-OH-peroxy I

$$K_{eq}(ci+O_2 \leftrightarrow \beta) = 3.481 \times 10^{-28} \times \exp(11322/T) \text{ cm}^3$$
$$k(ci+O_2 \rightarrow \beta) = 0.60 \times 10^{-12} \text{ cm}^3 \text{ s}^{-1} \text{ (independent of T)}$$
$$k(\beta \rightarrow O_2+ci) = 1.724 \times 10^{15} \times \exp(-11322/T) \text{ s}^{-1}$$

Reversible reaction: *cis*-OH-Adduct I + O2 ⇌ Z-δ-OH-peroxy I

$$K_{eq}(ci+O_2 \leftrightarrow Z\text{-}\delta) = 6.712 \times 10^{-28} \times \exp(9837.6/T) \text{ cm}^3$$
$$k(ci+O_2 \rightarrow Z\text{-}\delta) = 0.70 \times 10^{-12} \text{ cm}^3 \text{ s-1 (independent of T)}$$
$$k(Z\text{-}\delta \rightarrow O_2+ci) = 1.043 \times 10^{15} \times \exp(-9837.6/T) \text{ s-1}$$

Interconversion β-OH-peroxy I ⇌ Z-δ-OH-peroxy I (via O_2-loss and re-addition, above)

$$K_{eq}(\beta \leftrightarrow Z\text{-}\delta) = 1.928 \times \exp(-1483.9/T)$$

1,6-H shift: Z-δ-OH-peroxy I →hydroxy-hydroperoxy-allylic product radical I

$$k(Z\text{-}\delta \text{ 1,6-H}) = 3.556 \times 10^{10} \times \exp(-8590.8/T) \times \exp(1.0265 E+8/T3) \text{ s}^{-1}$$

1,5-H shift: β-OH-peroxy →OH + MVK + CH_2O

$$k(1,5\text{-H}) = 1.038 \times 10^{11} \times \exp(-9746.4/T) \text{ s}^{-1}$$

IB. *trans*-OH-isoprenyl Adduct,   br(*trans*) = 0.5

Reversible reaction: *trans*-OH-Adduct I + O_2 ⇌ β-OH-peroxy I

$$K_{eq}(tr+O_2 \leftrightarrow \beta) \approx 3.5 \times 10^{-28} \times \exp(10743/T) \text{ cm}^3$$
$$k(tr+O_2 \rightarrow \beta) = 0.60 \times 10^{-12} \text{ cm}^3 \text{ s}^{-1} \text{ (independent of T)}$$
$$k(\beta \rightarrow tr+O_2) \approx 1.71 \times 10^{15} \times \exp(-10743/T) \text{ s}^{-1}$$

Indirect interconversion β-OH-peroxy I ⇌ E-δ-OH-peroxy I

$$K_{eq}(\beta \leftrightarrow E\text{-}\delta) \leq 25 \times \exp(-2195/T) \quad \text{approximate}$$

Reversible reaction: *trans*-OH-Adduct I + O_2 ⇌ E-δ-OH-peroxy I

Equilibrium constant $K_{eq}(tr+O_2 \leftrightarrow E\text{-}\delta) = K_{eq}(tr+O_2 \leftrightarrow \beta) \times K_{eq}(\beta \leftrightarrow E\text{-}\delta)$

$$K_{eq}(tr+O_2 \leftrightarrow E\text{-}\delta) \leq 8.75 \times 10^{-27} \times \exp(8548/T) \text{ cm}^3$$
$$k(tr+O_2 \rightarrow E\text{-}\delta) = 0.5 \times 10^{-12} \times \exp(-480/T) \text{ cm}^3 \text{ s}^{-1}$$
$$k(E\text{-}\delta \rightarrow O_2+tr) \geq 5.714 \times 10^{13} \times \exp(-9028/T) \text{ s}^{-1}$$

Case II: OH-isoprenyl Adduct II, $CH_2=C(CH_3)C^•HCH_2OH$,   31%

IIA. *cis*-OH-isoprenyl Adduct II,   br(*cis*) = 0.7

Reversible reaction: cis-OH-Adduct II + O_2 ⇌ β-OH-peroxy II

$$K_{eq}(ci+O_2 \leftrightarrow \beta) \quad = 3.331 \times 10^{-28} \times exp(11705/T) \ cm^3$$

$$k(ci+O_2 \rightarrow \beta) \quad = 0.70 \times 10^{-12} \ cm^3 \ s^{-1} \ (independent \ of \ T)$$

$$k(\beta \rightarrow O_2+ci) \quad = 2.1013 \times 10^{15} \times exp(-11705/T) \ s^{-1}$$

Reversible reaction: cis-OH-Adduct II + O_2 ⇌ Z-δ-OH-peroxy II

$$K_{eq}(ci+O_2 \leftrightarrow Z\text{-}\delta) = 6.538 \times 10^{-28} \times exp(10254/T) \ cm^3$$

$$k(ci+O_2 \rightarrow Z\text{-}\delta) \quad = 0.40 \times 10^{-12} \ cm^3 \ s^{-1} \ (independent \ of \ T)$$

$$k(Z\text{-}\delta \rightarrow O_2+ci) \quad = 6.118 \times 10^{14} \times exp(-10254/T) \ s^{-1}$$

Indirect interconversion β-OH-peroxy II ⇌ Z-δ-OH-peroxy II (via O_2-loss and re-addition)

$$K_{eq}(\beta \leftrightarrow Z\text{-}\delta) \quad = 1.963 \times exp(-1450.9/T)$$

1,6-H shift Z-δ-OH-peroxy II →hydroxy-hydroperoxy-allylic product radical II

$$k(Z\text{-}\delta \ 1,6\text{-H}) \quad = 1.070 \times 10^{11} \times exp(-8174.3/T) \times exp(1.000 E+8/T^3) \ s^{-1}$$

1,5-H shift β-OH-peroxy II →OH + MACR + CH_2O

$$k(\beta \ 1,5\text{-H}) \quad = 1.877 \times 10^{11} \times exp(-9751.7/T) \ s^{-1}$$

IIB. *trans*-OH-isoprenyl Adduct II, br(*trans*) = 0.30

Reversible reaction: *trans*-OH-Adduct II + O_2 ⇌ β-OH-peroxy II

$$K_{eq}(tr+O_2 \leftrightarrow \beta) \quad \approx 3.333 \times 10^{-28} \times exp(11569/T) \ cm^3$$

$$k(tr+O_2 \rightarrow \beta) \quad = 0.70 \times 10^{-12} \ cm^3 \ s^{-1} \ (independent \ of \ T)$$

$$k(\beta \rightarrow tr+O_2) \quad \approx 2.10 \times 10^{15} \times exp(-11569/T) \ s^{-1}$$

Indirect interconversion β-OH-peroxy II ⇌ E-δ-OH-peroxy II

$$K_{eq}(\beta \leftrightarrow E\text{-}\delta) \quad \approx 35.33 \times exp(-2065/T) \ approximate$$

Reversible reaction: *trans*-OH-Adduct II + O_2 ⇌ E-δ-OH-peroxy II

Equilibrium constant $K_{eq}(tr+O_2 \leftrightarrow E\text{-}\delta) = K_{eq}(tr+O_2 \leftrightarrow \beta) \times K_{eq}(\beta \leftrightarrow E\text{-}\delta)$

$$K_{eq}(tr+O_2 \leftrightarrow E\text{-}\delta) \approx 1.178 \ 10^{-26} \times exp(9504/T) \ cm^3$$

$$k(tr+O_2 \rightarrow E\text{-}\delta) \quad = 0.5 \times 10^{-12} \times exp(-480/T) \ cm^3 \ s^{-1}$$

$$k(E\text{-}\delta \rightarrow O_2+tr) \quad \approx 4.25 \times 10^{13} \times exp(-9984/T) \ s^{-1}$$

Note that Taraborrelli et al. (2012) reported theoretical rates $k(Z\text{-}\delta \ 1,6\text{-H})$ that are 2.5-3 times lower than our results, computing (relative) single-point energy barriers at the high CCSD(T)/aug-cc-pVTZ level but on B3LYP-optimized geometries and adopting B3LYP-based partition functions as used in our earlier papers. The lower rates are explained by the neglect of London dispersion in B3LYP causing the relative energy of the lowest TS to be too high by about 1.3 kcal/mol compared to M06-2X; in our computations, the H-bonded TS contributes as much as the other TS conformers combined to the total 1,6-H shift rate.

At this stage, it is necessary to strongly emphasise that the $k(Z\text{-}\delta \ 1,6\text{-H})$ values, of order 1 s^{-1}, are the rate constants for the elementary reactions of the Z-δ-OH peroxys, and, contrary to what was erroneously implied in two recent reviews (Orlando and Tyndall, 2012; Pilling, 2013), not the "bulk rate coefficient" for isomerisation of the pool

of isoprene-peroxys, as measured by Crounse et al. (2011). In fact, these two quantities differ by orders of magnitude.

An important difference compared to our earlier results is that at our present levels of theory, the lowest of the two contributing TS conformers for the 1,6-H shift of Case I conserves the H-bond throughout the reaction, leading directly to the most stable, H-bonded Z,Z'-conformer of the allylic product radical, as shown in Figure 3. Similarly for Case II, one of the lowest TS conformers conserves the H-bond. The other contributing TS conformer(s) for Cases I and II are connected to open, i.e. non-H-bonded product radicals, with the OH group pointing outwards. However, these nascent products are formed with an internal energy of some 21 kcal mol^{-1} (including 4 kcal mol^{-1} thermal energy but accounting for the tunnelling occurring on average about 3 kcal mol^{-1} below the barrier top). Of this total, about 14 kcal mol^{-1} is owed to allyl-resonance stabilization, which however can become active only after the H atom has quasi-completely migrated such that a half-occupied p orbital (together with three sp2 bonding orbitals) develops on carbon 1, which can then align and overlap with the two existing p orbitals of the $>C_2=C_3<$ double bond. The associated potential energy decrease appears as vibration energy of the allyl mode, i.e. simultaneous asymmetric stretching of the bent C_1-C_2-C_3 frame and counter-rotation about the two C-C axes. The so dynamically induced internal rotation of the $HOC_1\overset{\bullet}{H}$ moiety about C_1-C_2 should allow the hot product radical to overcome the 12 to 13 kcal mol^{-1} barrier leading to the 5 kcal mol^{-1} more stable H-bonded Z,Z'- product isomer displayed in Figure 3 for Case I. As discussed in detail in a next section, this is relevant for the subsequent fates of the allylic product radicals of the 1,6-H shifts. It is useful to already add here that because of the allyl character, the product radicals feature two radical sites and hence one expects subsequent formation of two different peroxy radicals, in similar quantities.

Our best-level CC//QC results for the barriers of the concerted 1,5-H shifts in the β-OH-peroxys are 21.29 for Case I and 21.03 kcal mol^{-1} for Case II, with the M06-2X results of 21.68 and 21.42, respectively, even somewhat higher. These data are significantly higher that our earlier, lower-level CBS-APNO and B3LYP values. In the partition function ratios, 3 (Case I) and 2 (Case II) contributing TS conformers and ca. 25 conformers of the β-OH-peroxys are accounted for. The tunnelling factor, in the asymmetric-Eckart approximation, is small, only around 3 at 298 K, because of the low imaginary frequencies and the rapid widening of the barrier from ca. 4 kcal mol^{-1} below the top down, both due to the concerted nature of the reaction that results in OH + CH_2O + MVK for Case I and in OH + CH_2O + MACR for Case II, without stable intermediate (Peeters et al., 2009). The isomer-specific rate coefficients for the 1,5-H shifts of the β-OH-peroxys computed for the 280-320 K range, can be represented within 0.25% by the expressions given in TABLE I, with values at 298 K of 6.5×10^{-4} and 1.15×10^{-3} s^{-1} for Case I and Case II, respectively. These rates are substantially lower than

our earlier results, and about 1.5 to 2 times higher than the theoretical predictions of da Silva et al. (2010) based on computed energy barriers taken as the average of two composite methods (G3SX and CBS-QB3), although with a reported possible error of 2 kcal mol^{-1}, amounting to an error factor of 25 on the rates.

The present rate coefficient results are about 20 times smaller than the combined rates of the traditional peroxy reactions in relevant conditions, meaning that the 1,5-H shifts of the β-OH-peroxys are quasi-negligible —except at the highest relevant temperatures —in agreement with experimental findings of Crounse et al. (2011). Our average k(1,5-H) result of about 2×10^{-3} s^{-1} at 305 K suggests that the 1,5-H shifts of the β-OH-peroxys could have contributed only in a minor way to the about 50% OH regeneration observed in the recent chamber study of Fuchs et al. (2013) at this temperature, given the peroxy removal rate around 0.035 s^{-1} by the traditional reactions in their conditions.

Steady-state population fractions and bulk peroxy isomerisation rate
The empirical bulk peroxy isomerisation rate, designated as k(bulk 1,6-H), is defined as the volumic rate of the 1,6-H shifts of the Z-δ-OH-peroxys divided by the total concentration of all hydroxy-isoprenyl peroxys. It can be seen that k(bulk 1,6-H) is equal to the isomer-specific rate k(Z-δ 1,6-H) multiplied by the steady-state fraction f(Z-δ), or rather the sum for the two cases weighted by their branching fraction (Br = 0.62 for Case I, 0.31 for Case II):

k(bulk 1,6-H) = Br(I) × f(Z-δ)(I) × k(Z-δ 1,6-H)(I) + Br(II) × f(Z-δ)(II) × k(Z-δ 1,6-H)(II)

(3)

The condition for full equilibrations such as β-OH-peroxy ⇌ Z-δ-OH-peroxy (Ra) is essentially that the redissociation rates of each of the two peroxy isomers involved are much higher than their removal rates by all the other reactions together.

The rate coefficients (TABLE I) show that the above condition is not generally met for the relevant temperatures of ca. 280 - 305 K and k_{tr} range 0.01 - 0.1 s^{-1}, i.e. for low and moderate NO levels. (Only the less important analogous equilibrium (Rb) for Case I is always established within a few percent). The departures from equilibrium and reduced analytical expressions for the real, steady-state peroxy population fractions could be derived that give the fractions f(Z-δ) and hence also the bulk rates k(bulk 1,6-H) with a precision better than $\pm 2\%$ over the relevant T and k_{tr} ranges above. Also, the rigorous population fractions as well as bulk rates k(bulk 1,6-H) and the yields of the various 1st-generation products (see Figure 4) as functions of k_{tr} and of T have been obtained by box-modelling on the full, explicit mechanism.

For Case I, the steady-state [Z-δ]/[β] ratio and f(Z-δ) fraction in the relevant k_{tr} range are considerably higher than the equilibrium values and increase substantially as k_{tr} becomes higher, in particular at lower T; the departures from equilibrium remain

below 5% throughout this k_{tr} range only for $T \geq 310$ K. The reason for this behaviour is that firstly at lower temperatures the Z-δ-OH- and β-OH-peroxys redissociate (far) too slowly to ensure equilibration such that the [Z-δ]/[β] ratio is determined to a larger extent by their (near-unity) initial formation ratio (see Figure 1) and their respective rates of irreversible removal; secondly, at higher k_{tr} the absolute concentrations of the β-OH-peroxys and E-δ-OH-peroxy that are removed almost solely by the traditional reactions will decrease substantially, whereas [Z-δ-OH-peroxy] will be much less affected since k(Z-δ 1,6-H) is much larger than k_{tr} in the considered range. For Case II, the high k(Z-δ 1,6-H)(II) values of order 1 - 10 s^{-1} preclude the establishment of the equilibrium at any relevant T and k_{tr}, such that the [Z-δ]/[β] ratio is mostly only 0.1 - 0.5 times the {[Z-δ]/[β]}$_{eq}$ value, but showing a strong increase with k_{tr} for the same reason as in Case I. As an example, at $T = 298$ K and $k_{tr} = 0.025$ s^{-1}, one has f(Z-δ)(I) $= 1.35 \times 10^{-2}$ and f(Z-δ)(II) $= 2.72 \times 10^{-3}$, such that the k(bulk 1,6H) are two to three orders of magnitude smaller than the isomer-specific rate coefficients k(Z-δ 1,6-H).

It should be remarked that the steady-state f(Z-δ) and therefore the k(bulk 1,6H) depend indirectly on the choice of k_{+O2}^{bulk}, because the k_{-O2} as derived above are simultaneously proportional to k_{+O2}^{bulk}, and higher k_{-O2} values should bring the [Z-δ]/[β] ratios closer to equilibrium. Note that the steady-state f(Z-δ) fractions for Case I are about 3 to 6 times lower, and those for Case II more than an order of magnitude lower than found earlier (Peeters et al., 2009), mainly because of the presently computed lower partition function ratio of the Z-δ-OH- and β-OH-peroxy isomers and slower redissociations of both isomers. Mainly for that reason, the present k(bulk 1,6-H) values too are about an order of magnitude lower than the original estimates.

Based on the present set of rate coefficients, both the f(Z-δ) and the bulk isomerisation rate k(bulk 1,6-H) show an increase with k_{tr}. k(bulk 1,6-H) increases nearly linearly with the isoprene-peroxy sink rate by the traditional reactions k_{tr}:

k(bulk 1,6-H)(I) $= 9.5 \times 10^7$ s^{-1} $\times$ exp(-7009/T) + 1.79×10^{-7} $\times$ exp(3722.5/T) $\times$ k_{tr} (4a)

k(bulk 1,6-H)(II) $= 3.8 \times 10^{13}$ $\times$ exp(-10745/T) s^{-1} + 5.82×10^{-2} $\times$ exp(476.3/T) $\times$ k_{tr} (4b)

with k(bulk 1,6-H)(total) $= 0.62$ k(bulk 1,6-H)(I) $+ 0.31$ k(bulk 1,6-H)(II). For example, at 295 K, the bulk rate increases from 0.006 to 0.017 s^{-1} between $k_{tr} = 0.01$ s^{-1} and 0.1 s^{-1}. The nearly-perfect linear increase with k_{tr} over the relevant T and k_{tr} ranges can be exploited for the implementation of the 1,6 H-shift reactions in large-scale models, by splitting the isomerisation into a constant-rate unimolecular component and pseudo-bimolecular reactions with HO$_2$, NO and RO$_2$ accounting for the dependence of the bulk rate on k_{tr}.

The overall uncertainty on the derived k(bulk 1,6-H) is estimated based on the probable errors on the six parameters affecting k(Z-δ 1,6-H) and f(Z-δ). The first two are the barrier height of the 1,6-H shift and the ΔE between the Z-δ-OH- and β-OH-peroxys; as objective estimates available for the expected errors on the ΔE, we adopted the

differences, of 0.16 and 0.19 kcal mol^{-1}, respectively, between the values computed at the independent high-quality CC//QC and M06-2X levels used in this work. Further, we assumed a factor 1.5 error on the tunnelling factor; a factor of 1.3 each for the MC-partition function ratios for the 1,6-H shift and the $\{[Z\text{-}\delta]/[\beta]\}_{eq}$ equilibrium constant; and a factor 1.3 error on the calculated departures from that equilibrium. Error propagation thus yields an overall uncertainty estimate on k(bulk 1,6-H) of a factor $\approx$ 2, or +100%/-50%. The estimated uncertainty of a factor $\sim$2 on the bulk rate coefficient is considerably smaller than the reported uncertainty of a factor 5 to 10 on just the isomer-specific 1,6-H shift rates of the Z-δ-OH-peroxys in our earlier work (Nguyen et al., 2010).

Pathways following isoprene-peroxy isomerisation by 1,6-H shift

The allylic product radicals of the 1,6-H shifts, expected to be formed predominantly as the more stable, H-bonded, cyclic Z,Z'- conformers (see Figure 3) should arise with a nascent internal energy of around 25 kcal mol^{-1}. In principle, some chemically activated reactions might occur promptly. We have thoroughly examined some 10 possible reactions, but found their barriers to be too high to be of major importance —except for the internal rotation of the initially "open" product conformers to yield the more stable H-bonded ones discussed above. The most likely decomposition reactions are (i) elimination of H_2O to form an oxy radical $O=CH\text{-}C(CH_3)=CH\text{-}CH_2O^\bullet$; (ii) concerted elimination of OH to yield a hydroxy-methyl-butenal $O=CH\text{-}C(CH_3)=CH\text{-}CH_2OH$; (iii) concerted expulsion of an OH to form an epoxide; and (iv) the elimination of H_2O_2 giving an $O=CH\text{-}C(CH_3)=CH\text{-}C^\bullet H_2$ allylic radical. At the sufficiently high and reliable levels of theory M06-2X and/or CC//QC, the barriers for the three first, most favourable reactions are found to be around 17 kcal mol^{-1} or higher; which is too high for these reactions to outrun collisional stabilisation. We estimate that the various prompt reactions contribute no more than some 10% together, and possibly much less.

After collisional stabilisation, the allylic product radicals should add O_2 to form two different allylperoxys, the "1st peroxy" and "2nd peroxy", as depicted in the detailed subsequent PES for Case I in Figure 5. O_2 addition should show a slight preference for allylic carbon 2 with its higher spin density of 0.58 vs 0.42 for carbon 1. It has been ascertained that both additions can occur without any significant barrier, owing to the simultaneous formation of H-bonds. The "1st peroxy" rapidly yields a strongly H-bonded complex of HO_2 and a carbonyl over a barrier of 12.5 kcal mol^{-1}, followed by decomposition of the complex into free HO_2 and Z-1-hydroperoxy-2/3-methyl-but-2-enal (Z-HPALD), requiring 12.0 kcal mol^{-1}. The first step, through a very rigid TS, is rate controlling and may occur promptly given the $\approx$ 25 kcal mol^{-1} nascent internal energy of "1st peroxy". In any case, its overall decomposition into HO_2 + Z-HPALD will be much faster than the re-dissociation of this allylperoxy radical.
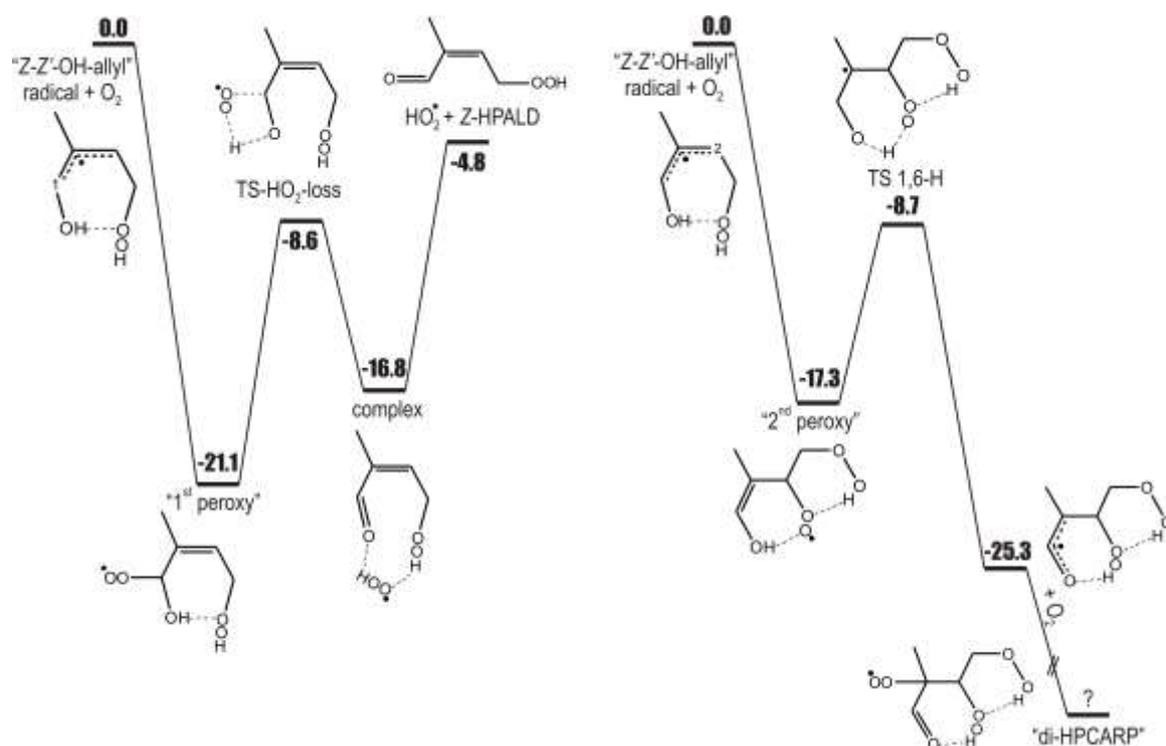
Figure 5. Potential energy surface (PES) of O_2 addition to Z,Z' OH-allylic product of 1,6-H shift isomerisation (Case I, see Figure 3) forming a 1st peroxy and 2nd peroxy, and subsequent chemistry; M06-2X/311 + +G(3df,2p) level of theory (including ZPVE).

The "2nd peroxy", somewhat less stable than the first, undergoes a fast enolic 1,6-H shift over an unusually low barrier of only 8.6 kcal mol^{-1} similar to the shift we discovered for the 1st-generation production of hydroxy-acetone and glycolaldehyde in isoprene oxidation at high NO (Peeters and Nguyen, 2012). Here too, the reaction will be prompt, and outrun the re-dissociation of the "2nd peroxy" by orders of magnitude. However, we do not exclude that some 10 or 20% of the products of the 1,6-H shifts arise as "open" Z,E'-conformers with the OH pointing outwards; these cannot undergo the enolic 1,6-H shift and their sole fate should be redissociation and hence finally conversion to the "1st peroxy" isomers that can still rapidly yield HPALDs plus HO$_2$. This is why we adopt here effective branchings to the two peroxys of 0.5 : 0.5, despite the somewhat higher spin density on allylic carbon 2. The doubly-H-bonded, vinoxy-stabilized product radical from the 1,6-H shift of the "2nd peroxy", with nascent internal energy of about 28 kcal mol^{-1}, might undergo several possible prompt unimolecular reactions, including concerted OH expulsion and epoxide formation, but all have been found to face too high barriers ($\geq$ 18 kcal mol^{-1}, partly on account of the lost vinoxy resonance in the TS's) to compete with collisional stabilisation. Therefore, it should instead rapidly add another O_2 —a third already —to form a di-hydroperoxy-carbonyl-peroxy radical (di-HPCARP), which keeps the double H-bond, and should arise with a

nascent internal energy of some 20 - 25 kcal mol^{-1}, which is insufficient for important prompt reactions, such that the di-HPCARP should collisionally thermalize before reacting.

Fate of HPALDs: fast photolysis and reaction with OH

In the earlier work (Peeters et al., 2009; Peeters and Müller, 2010) we proposed fast photolysis of the Z-4-hydroperoxy-2/3-methyl-but-2-enals (HPALDs) into OH and oxy radicals (O=CH-C(CH$_3$)=CH-CH$_2$O$^{\bullet}$ in Case I and O=CH-CH=C(CH$_3$)-CH$_2$O$^{\bullet}$ in Case II), assuming similar absorption cross sections as for the analogous α,β-enones MVK and MACR, but —very different from the latter —with near-unit quantum yield (QY), and hence J-values of order 5×10^{-4} s^{-1}. The high-QY mechanism proposed was an avoided crossing of the excited S1 state of the O=C-C=C enone chromophore (or its triplet counterpart T1) with the repulsive excited S2 state of the -OOH hydroperoxide chromophore (or its triplet counterpart T2). The fast photolysis of HPALDs into OH with near-unit QY has since then been confirmed experimentally by Wolfe et al. (2012) for a HPALD proxy, E-4-hydroxyperoxy-hex-2-enal.

A detailed theoretical investigation is in progress on the intricate photo-physical and molecular mechanism of the Z-HPALD photolysis process and the subsequent chemistry. A detailed discussion of the findings so far is beyond the scope of this report, but some conclusions having direct bearing on the potential of the co-product oxy radical, above, to re-generate additional hydroxyl radicals should be outlined here. First, though we have theoretically located a transition state for an avoided crossing as proposed, we have now identified an unexpected but much faster mechanism to OH + oxy radical, while still another mechanism could also become competitive in particular at higher excitation energies; these two dominant pathways have still to be kinetically quantified. Secondly, of prime importance, the dynamics of both these faster mechanisms are such that the oxy radical, co-product of OH, will be formed with a very high internal energy of some 35 - 40 kcal mol^{-1}, much higher than expected for the originally assumed photolysis mechanism, such that the chemical fate of these oxy co-products will be quite different from that originally proposed (Peeters et al., 2009; Peeters and Müller, 2010). Thirdly, the oxy radicals can be formed either as the E- or the ca 3 kcal mol^{-1} less stable Z-conformers, which we found can readily interconvert via an unusual, newly proposed mechanism (Nguyen and Peeters, 2015), through a nearly-iso-energetic oxyranyl intermediate, over CC//QC-computed energy barriers of only 5 to 8 kcal mol^{-1}:
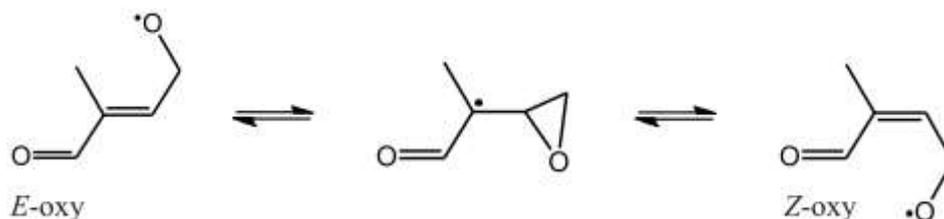
As a result, two prompt, chemically activated pathways are open for these oxy radicals, shown below for Case I: a nearly barrierless 1,5-H shift of the aldehyde hydrogen in the Z-oxy, exothermal for 17 kcal mol^{-1}, possible for both Cases I and II; and a 1,5-H shift of a methyl-hydrogen in the E-oxy of Case I facing a CC//QC-computed barrier of 8.86 kcal mol^{-1} and exothermal for 19 kcal mol^{-1}:
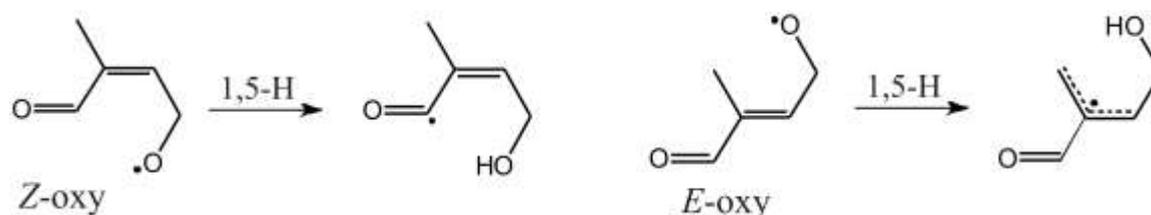
The expected subsequent chemistry still needs to be fully characterized and kinetically quantified. The relative energies and barrier heights mentioned below, are computed at the M06-2X level. The nascent acyl radical from the prompt aldehyde-H shift in the Z-oxy contains already over 50 kcal mol^{-1} internal energy, enough to promptly overcome the 23 kcal mol^{-1} barrier for CO loss and so form a vinyl-type radical, which can rapidly interconvert from a Z- to an E-conformer over a low barrier of $\leq$ 5 kcal mol^{-1} (Case I) resulting in their thermal equilibration with Z- / E- ratio governed mainly by the relative stabilities. Fast O$_2$ addition should then give rise to two chemically activated vinylperoxy conformers with nascent internal energies of about 45 kcal mol^{-1}, but with very different subsequent fates. A fast and dominant 1,5-H shift over a barrier of only 16.5 kcal mol^{-1} is open to the Z-vinylperoxy conformer, whereas the E-counterpart can only undergo "traditional" reactions with NO, HO$_2$, RO$_2$ or NO$_2$. The H-shift in the Z-vinylperoxy forms an unstable 1-hydroperoxy-1-methyl-3-OH-allyl radical that spontaneously expels OH (Vereecken et al., 2004), to form a strongly H-bond-stabilized ketone-enol —which can be termed hydroxy-vinylmethylketone —and is the more stable tautomer of the β-diketone formylacetone, similar to the homologous ketone-enol tautomer of acetylacetone. Again by analogy with acetylacetone, it should photolyze quickly into OH and a (strongly resonance-stabilized) radical (Yoon et al., 1999) at a rate that can be estimated at about (2 - 3) $\times$ 10^{-4} s^{-1} for an overhead sun using the known absorption cross sections for the (allowed) π,π^* transition of acetylacetone and assuming a quantum yield of unity. However, this ketone-enol is expected to react also very quickly by OH-addition (Peeters et al. 2007), with a rate coefficient close to 1$\times$10^{-10} cm^3 s^{-1}. The net OH budget of the Z-oxy chemistry is therefore uncertain, and may be decided by the subsequent chemistry of the (unknown) photo-product radical and of the

OH-adducts, as well as by the further "traditional" chemistry of the E-vinylperoxy conformer, all still to be explored in detail. Most interestingly, reaction of this E-vinylperoxy with NO_2 is expected to quickly yield an hydroxy-carbonylnitrate, a process that to our knowledge is newly characterized here:

E-vinylperoxy   vinylperoxy-nitrate   hydroxy-carbonyl-nitrate
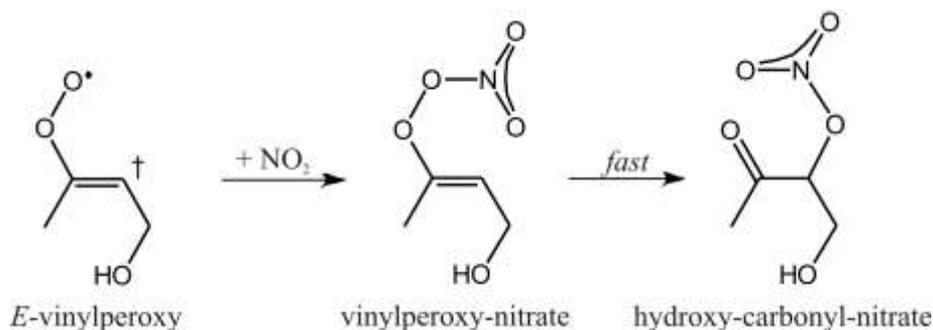
The radical-radical combination of a vinylperoxy with NO_2 forms a vinylperoxynitrate. While alkylperoxynitrates, which are stable for only around 20 kcal mol^{-1}, are known to merely redissociate within a fraction of a second, a preliminary investigation revealed that the vinylperoxynitrate proxy $H_2C=CHOONO_2$ should readily isomerise over a barrier estimated between 11 and 16 kcal mol^{-1} through a fairly loose TS directly to a carbonyl-nitrate that is ca. 63 kcal mol^{-1} more stable. This newly predicted pathway may contribute substantially to nitrate formation from isoprene. Interestingly, the hydroxy-carbonyl-nitrates expected here are precisely also formed in the oxidation of isoprene at high NO (Paulot et al. 2009a) and that we argued to undergo rapid photolysis (Müller et al., 2014; see below).

For Case I, the chemistry following the low-barrier 1,5-H shift of a methyl-hydrogen in the E-oxy from HPALD photolysis shows greater potential for OH-recycling. The three or four probable reaction sequences that can be envisaged are expected to result in the net regeneration of 2 up to 4 hydroxyl radicals. These pathways too need to be further examined theoretically in future work.

Concerning the reactions of the HPALDs with OH, we refer to a previous paper (Peeters and Müller, 2010). Nearly all channels are predicted to regenerate OH, including a major route yielding an unsaturated peracid-aldehyde (PACALD), and estimating a total rate coefficient of about 5×10^{-11} cm^3 s^{-1}, as experimentally confirmed by Wolfe et al. (2012). The subsequent chemistry of PACALDs was discussed earlier (Peeters and Müller, 2010), while the other major products are largely hydroperoxy-carbonyls, of which the generic fate will be addressed briefly below, together with that of similar compounds resulting from the di-HPCARPs.

Similar to the oxy radical photoproducts from HPALDs, the subsequent chemistry of the di-HPCARP radicals still needs to be further elucidated and also quantified kinetically; these investigations are ongoing. It can however be expected that the thermalized di-HPCARPs undergo mainly three competitive reactions at low NO levels,

all three displayed in Figure 6 for Case I: (i) a 1,4-H shift of the aldehyde-H to the peroxy function, known for similar cases to face a barrier around 20 - 21 kcal mol^{-1} and therefore to have a rate of order 0.1 s^{-1} (Asatryan et al., 2010); (ii) the traditional reactions with NO and (iii) with HO$_2$.
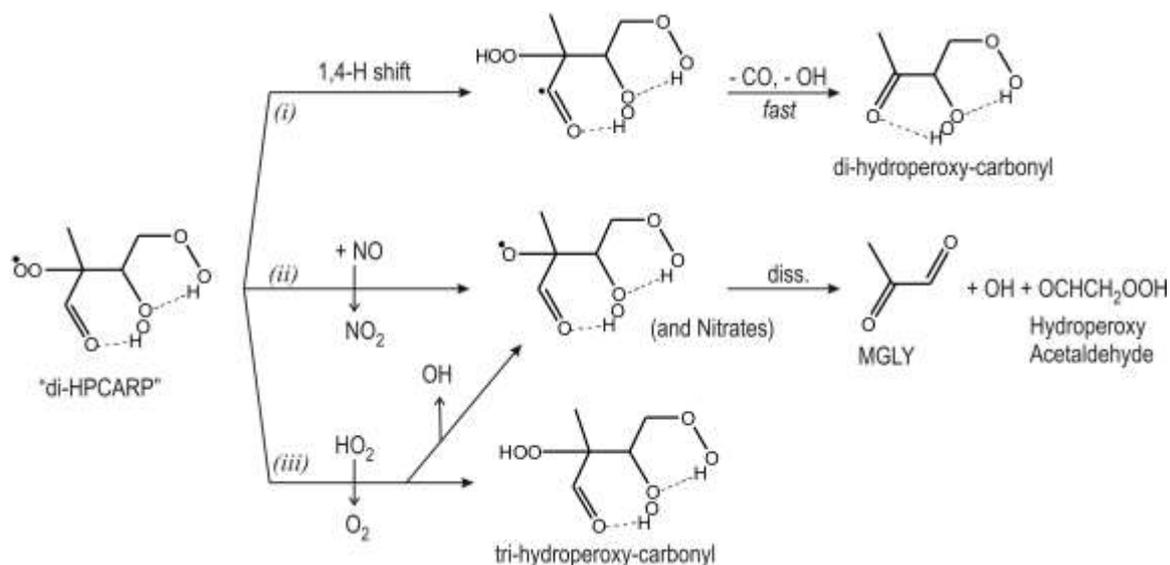

Figure 6. Expected subsequent chemistry of di-hydroperoxy-carbonyl-peroxy radicals (di-HPCARP) resulting from 2nd peroxy (Case I, see Figure 5).

The 1,4-H shift (i) results in a chemically activated acyl radical with internal energy 22 - 25 kcal mol^{-1} that promptly eliminates CO, over a barrier of $\leq$ 7 kcal mol^{-1} (Méreau et al., 2001), after which the unstable α-hydroperoxy-alkyl will spontaneously expel OH (Vereecken et al. 2004) to form a di-hydroperoxy-carbonyl compound. Two other possible H-shifts, of the α-hydroperoxy-hydrogens, will result in OH and di-hydroperoxy-di-carbonyls. Reaction (ii) of di-HPCARP with NO will yield (besides nitrates) an oxy radical that dissociates over a negligible barrier (Peeters et al., 2004; Vereecken and Peeters, 2009) into methylglyoxal and another unstable α-hydroperoxy-alkyl that breaks up immediately in OH and hydroperoxy-acetaldehyde. Finally, a fraction of the reaction (iii) of the α-carbonyl-peroxy di-HPCARP with HO$_2$ should yield OH and the same oxy radical as produced in the NO reaction (Hasson et al., 2004), while another, likely larger fraction yields a tri-hydroperoxy-carbonyl. Important to note is that Crounse et al. (2012) observed hydroperoxy-acetaldehyde and its hydroperoxy-acetone counterpart from the Case II-sequence in yields about 25% of the HPALDs, whereas in the oxidation of fully deuterated isoprene these products were found in yields comparable to the (deuterated) HPALDs, rationalized by the much lower tunnelling factor of D- compared to H atoms in the competing 1,4-D/H shifts (i). Since reaction (iii) is expected to yield also another product besides hydroperoxy-acetaldehyde or -acetone, these observations indicate that the di-HPCARP/HPALD branching ratio

following the Z-δ-OH-peroxy 1,6-H shifts is at least equal to and likely even larger than the 0.5 : 0.5 adopted above.

Importantly, several of the di-HPCARP reactions can regenerate OH, and all produce hydroperoxy-carbonyls. The latter compounds can react in mainly two ways: 1° reactions with OH, in particular abstractions of α-hydroperoxy-H's or of aldehyde-H's from the α-hydroperoxy-aldehydes, which are both expected to directly recycle OH; and 2° photolysis, which for α-hydroperoxy-carbonyls should lead to OH re-generation with a high quantum yield. Indeed, as will be detailed in follow-up work, high-level M06-2X and CC//QC computations show that excited triplet α-hydroperoxy-carbonyls, resulting from fast intersystem crossing of the initially excited singlet states upon ≈ 315-340 nm absorption (Leu et al., 1998), decompose within picoseconds over a barrier of only 3.5 - 4.5 kcal mol^{-1} into an acyl radical and an unstable α-hydroperoxyalkyl radical that spontaneously expels OH to form a carbonyl, whereas the concerted H-shift and triplet O_2 elimination via a Norrish II mechanism is an order of magnitude slower. Again, the net budget of OH from hydroperoxy-carbonyls will be decided by the competition of their photolysis and OH reactions and subsequent chemistry, all still to be fully elucidated and quantified.

Theoretical yields. Comparison with laboratory measurements

As seen on Figure 4, the LIM1-predicted 1,6 H-shift yield is found to range between 15% and 50% in typical non-urban atmospheric conditions, whereas the 1,5 H-shift yield is very low. A reduced version of LIM1 has been implemented in the global chemistry model IMAGES (Stavrakou et al., 2010). The isoprene oxidation mechanism at high-NOx is based on Stavrakou et al. (2010, 2012). The traditional reaction products of the δ-hydroxy-peroxy radicals from isoprene are omitted, since their yields are negligible in relevant atmospheric conditions. The 1,6 isomerisation reactions are accounted for through bulk reactions of the isoprene peroxys with rates which are linearly dependent on their traditional sink rate (k_{tr}), as described above. The formation of di-hydroperoxy carbonyl peroxy radicals (see below) is not considered here, since their subsequent chemistry remains to be elucidated. For a similar reason, the further photochemistry of HPALD is highly simplified, as in Stavrakou et al. (2010). This representation is sufficient for the purpose of estimating the isomerisation yields. The global and annually averaged yields of the 1,6 and 1,5 H-shifts are estimated to be 28% and 2.3%, respectively. The uncertainty on k(bulk 1,6-H), above, translates into a relative error on the global 1,6-H yield of +54%/-40%, which brackets this yield between 17 and 43%.

We evaluate the theoretical yields using an explicit chemical model against the measured formation rates of HPALD and other stable products in the low-NOx isoprene oxidation experiments of Crounse et al. (2011). As discussed above, HPALD formation is only one of the two major possible pathways following the 1,6 H-shift, with an

estimated branching fraction of 50%. The radical source in the experiments was provided by CH_3ONO photolysis using black lights.
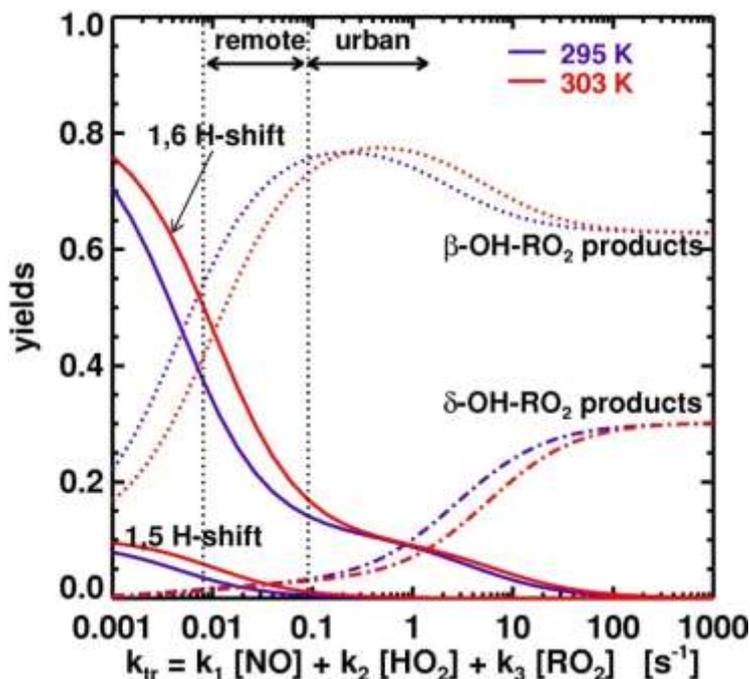

Figure 4. Isomerisation (1,6 and 1,5 H-shift) yields in the oxidation of isoprene by OH at 295 and 303 K, and yields of traditional (β-OH-RO2 and δOH-RO2) peroxy reaction products, as functions of the traditional sink rate (k_{tr}) of isoprene peroxys.

The photolysis rates are calculated from the lamp spectrum and the reported photolysis rate of NO_2 (2.8×10^{-5} s^{-1}) (Crounse et al., 2011). The product J(CH_3ONO) × [CH_3ONO] is estimated from the balance between HOx production and HOx removal which is obtained from the reported production rates of hydroperoxides and nitrates, i.e. 2 × (P(H_2O_2) + P(ISOPOOH)) + P(ISOPNO2). As seen on TABLE II, a reasonable agreement is found between the measured and simulated product formation rates at three different temperatures. LIM1 appears to overestimate the measured HPALD formation rate by an almost constant factor (~ 1.8). This discrepancy is compatible with the combined experimental and theoretical uncertainties. Moreover, we find that experimental peroxy isomerization yields from new laboratory results at long RO2 lifetimes (Crounse et al., to be published 2015) differ by only $\sim$ 25% from our theoretical predictions. The observed steep increase in HPALD between 295 and 318 K (factor of 4), well reproduced by LIM1, is primarily due to the temperature dependence of the peroxy dissociation rates: indeed, model results obtained when ignoring peroxy dissociation reactions show very little dependence of HPALD formation on temperature (TABLE II), in spite of the strong temperature dependence of the isomerisation rates of Z-δ-OH-peroxys. Since isomerisation is by far the dominant sink reaction of those Z-δ-OH-peroxys at the low-NO conditions of the experiments, the main limiting factor to

HPALD formation is the formation rate of the Z-δ-OH-peroxys. This rate is constant when neglecting peroxy dissociation, but it increases with temperature in LIM1 due to the conversion of β-OH- to Z-δ-OH-peroxys. In conclusion, the Caltech measurements appear to validate not only the formation of HPALD, but even more —and quasi-quantitatively —the importance of the O_2-elimination reactions of the hydroxyperoxys resulting in their rapid interconversion under low-NO conditions.

TABLE II. Observed and LIM1 production rates (ppt/min) of products in the experiments of Crounse et al. (2011). Model results ignoring peroxy interconversion are shown in parentheses.

	MVK + MACR		ISOPNO2		ISOPOOH		HPALD	
	obs.	LIM1	**obs.**	LIM1	**obs.**	LIM1	**obs.**	LIM1
Exp. # 1 (295.2 K)	**7.53**	6.77 (6.38)	**0.53**	0.56 (0.62)	**4.27**	4.13 (4.10)	**1.02**	1.85 (1.83)
Exp. # 2 (310.2 K)	**5.31**	6.96 (8.01)	**0.36**	0.47 (0.66)	**3.78**	3.94 (4.43)	**2.78**	4.78 (2.21)
Exp. # 3 (318.2 K)	**4.76**	7.31 (10.1)	**0.16**	0.39 (0.68)	**3.10**	3.62 (4.66)	**4.06**	7.47 (2.62)

Summary: novel features and impact of LIM1

The quantum-chemical and statistical-kinetics based rate coefficients of the isoprene-peroxy redissociation and isomerisation reactions have been upgraded using much higher levels of theory.

- The peroxy redissociations are shown to be fast enough to allow major interconversion at low NO, although full equilibration is not attained in relevant atmospheric conditions. The very low steady-state fractions of the Z-δ-OH-peroxy radicals lead to bulk-peroxy isomerisation rates that are over two orders of magnitude lower than the isomerisation rates of the Z-δ-OH-peroxys. The experimental HPALD yield data at varying *T* of Crounse et al. (2011) support unequivocally substantial peroxy interconversion as predicted.

- The calculated isomer-specific rates of the 1,6-H shifts of the Z-δ-OH peroxys are of the order of 1 s^{-1}, whereas the bulk peroxy rates are of the order of 0.01 s^{-1} or less. The bulk isomerisation rate increases substantially with increasing rate k_{tr} of the traditional peroxy reactions, as increasing k_{tr} reduces the concentration of the β-OH-peroxy radicals but has much less influence on [Z-δ-OH].

- The concerted 1,5-H shifts of the β-OH-peroxys are very slow, ∼0.001 s^{-1}, in accord with Crounse et al. (2011). It follows that the observed OH regeneration in the recent study of Fuchs et al. (2013) resulted mainly from the 1,6-H shift of the Z-δ-OH-peroxys. Further detailed studies (Hofzumahaus et al., to be published, 2015) show that LIM1 is quantitatively compatible with these chamber measurements.

- The HPALD yields are consistent with experimental results (Crounse et al., 2011), taking into account the additional 1,6 H-shift pathway besides HPALD production. This pathway leads to di-hydroperoxy-carbonylperoxy radicals expected to react in several ways, one of which should produce hydroperoxy-acetone and hydroperoxy-acetaldehyde, both observed by Crounse et al. (2012).

- Global modelling predicts that on average ~30% of the emitted isoprene reacts via isomerisation routes, which, considering the expected secondary OH regeneration, would put hydroxyl recycling at a considerably higher percentage.

Fast photolysis of carbonyl nitrates from isoprene

The formation of organic nitrates is an important process by which nitrogen oxides are kept in the form of reservoirs which can be transported over relatively long distances. Their subsequent removal can either release NOx, in which case the whole process is NOx-neutral, or it can result in a net NOx sink (by e.g. deposition or conversion to HNO_3). Clearly, the fate of organic nitrates is crucial to determine the overall impact of their formation. Isoprene oxidation is the largest source of organic nitrates in the atmosphere, due to the combination of large isoprene emissions with the sizable organic nitrate yield in the oxidation of isoprene by OH and NO_3, of the order of 10 and 80%, respectively (Kwan et al., 2012; Paulot et al., 2009a). Among the organic nitrates, carbonyl nitrates are an important class. Previous studies considered their photolysis as a relatively slow process. In most cases, their absorption cross sections and quantum yields were assumed to be low and reaction with OH was considered to be the dominant sink.

However, published laboratory studies on the absorption cross sections (Barnes et al., 1993) and photolysis rates (Suarez-Bertoa et al., 2012) of nitrooxy ketones suggest that the presence of the nitrate group (i) greatly enhances the absorption cross sections, and (ii) facilitates dissociation such that the photolysis quantum yield is of the order of unity. Furthermore, NO_2 is likely dissociated in the photolysis process. On this basis, we have provided new recommendations for estimating the cross sections and photolysis rates of carbonyl nitrates. The absorption cross sections of an α-nitrooxy aldehyde (na) are estimated as

$S_{na} = (S_n + S_a) \times r_{nk}$,

where S_n and S_a are measured cross sections of structurally similar monofunctional species (nitrate and aldehyde), and r_{nk} is an enhancement ratio for a nitrooxy ketone most similar to na, defined as

$r_{nk} = S_{nk} / (S_n + S_k)$,

with S_n and S_k the cross sections of monofunctional compounds (nitrate and ketone) similar to nk, and S_{nk} the measured cross sections of the nitrooxy ketone. The updated photorates are substantially higher than those used in previous modelling studies, with

important implications for the budget of nitrogen oxides (and therefore ozone) in the troposphere.

The fast photolysis of carbonyl nitrates was validated by box model simulations of a photooxidation experiment under high-NOx conditions (Paulot et al., 2009a). The OH- and O_3-reaction rates of the hydroxynitrates were obtained from Lee et al. (2014). The OH-reaction rates of carbonyl nitrates were obtained from the Structure-Activity Relationships of either Neeb (2000) or the MCMv3.2 (Saunders et al., 2003), which are both found to reproduce measured OH-reaction rates for nitrooxy ketones (Suarez-Bertoa et al., 2012) within their experimental uncertainties.

The results for ethanal nitrate are shown on Figure 7. Its fast decay after ∼2 hours is strong indication that its photolysis rate is very fast, corroborating our assumptions of enhanced cross sections and near-unit quantum yield.
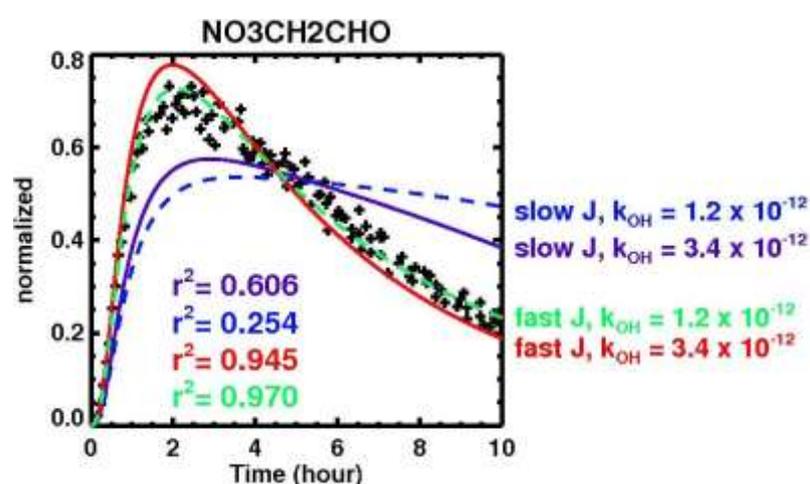

Figure 7. Calculated (lines) and observed (crosses) ethanal nitrate mixing ratios in Paulot et al. (2009b). OH-reaction rates are obtained from either MCMv32 (full lines) or Neeb (2000) (dashed). Indigo/blue: MCM photorates; green/red: fast photolysis as proposed in this work.

Fast photolysis is confirmed also for the major secondary carbonyl nitrates ($CH_3COCH(ONO_2)CH_2OH$ and isomers). Optimal agreement is obtained when the photorates are further enhanced (factor of two) due to the presence of OH group in β position, as suggested by the cross section data of Messaadia et al. (2012).

These results have significant atmospheric implications: the photorates of carbonyl nitrates from isoprene are estimated to be typically 3-20 times higher than their sink due to reaction with OH. Moreover, photolysis is especially effective in depleting the organic nitrate pool, as it is expected to release NO_2.

Distribution and budget of organic nitrates: the contribution of isoprene
The budget and distribution of organic nitrates has been investigated in a global modelling study. A reduced isoprene oxidation mechanism based on LIM1 and the

above recommendations has been constructed and validated by box model comparisons with the explicit mechanism. The formation of organic nitrates due to many other NMVOCs has been also incorporated in the model. The temperature and pressure dependence of the nitrate yield in $RO_2 + NO$ reactions (Arey et al., 2001) has been implemented. The oceanic emissions of small alkyl nitrates were adjusted based on aircraft measurements over the Pacific (PEM-Tropics A and B). The yield of methylnitrate from the reaction of CH_3O_2 with NO was derived from comparisons with measurements during the campaign INTEX-A conducted over the United States. The value derived in this way (1.8×10^{-4} at surface conditions) is considerably lower than the value (0.01) determined in a recent laboratory study (Butkovskaya et al., 2012) but is broadly consistent with the value inferred from stratospheric measurements by Flocke et al. (1998). Despite this very low yield, methylnitrate is found to be the most abundant individual organic nitrate in the atmosphere, representing $\sim 34\%$ of the total burden of alkyl nitrates ($\Sigma(RONO_2)$).

The total alkyl nitrate mixing ratios measured during the INTEX-A campaign were used to validate the model (Figure 8). Isoprene oxidation is the dominant precursor over land, especially below 40°N. The model performs very well, especially where isoprene is abundant. The relationship between total organic nitrate and formaldehyde over isoprene-rich areas is also very well reproduced by the model. However, the large contribution of lumped anthropogenic $C_{>3}$ organic nitrates (17% of the global chemical production, 31% of the global burden) emphasizes the need for a more detailed representation of anthropogenic NMVOC precursors.
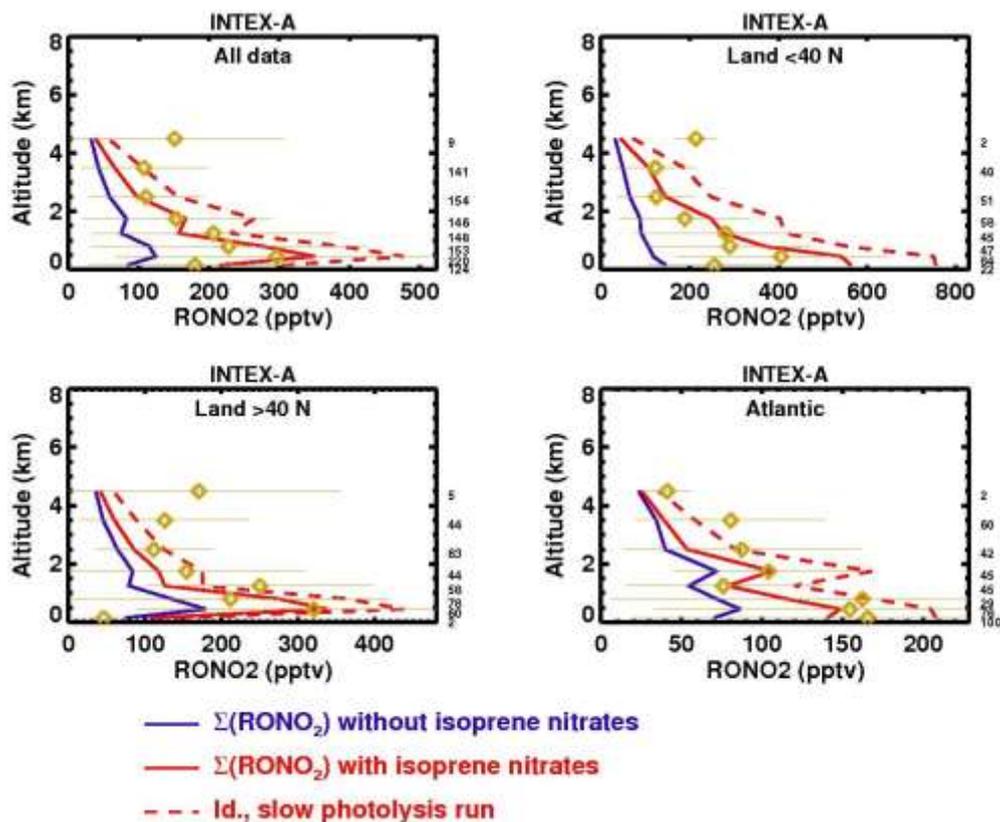
Figure 8. Simulated vs observed mixing ratios of organic nitrates during INTEX-A. The number of measurements per altitude bin is indicated at the right of each plot. Dashed line: simulation using carbonyl nitrate photolysis parameters of the MCMv3.2. Blue : contribution of non-isoprene organic nitrates.

Impact of biogenic VOCs on formic acid and on precipitation acidity

The oxidation of biogenic VOCs is a large source of formic acid, a compound consistently underestimated by models (Paulot et al., 2011) despite its importance for rain water acidity in remote continental areas. We have used recently acquired satellite observations of HCOOH (Razavi et al., 2011) in order to quantify the sources by means of the inverse modelling technique for which partner P1 has acquired a broad expertise (e.g., Stavrakou et al., 2009a,b). For that purpose, the direct emissions of formic acid and its known photochemical formation pathways have been included in the IMAGES model, and an extensive compilation of in situ measurements has been realized, including in situ HCOOH concentrations in air and in rain water, aircraft mission data as well as vertically integrated columns (FTIR).

Based on IASI data, the global annual source of HCOOH is inferred to be ca. 100-120 Tg, about 2-3 times the magnitude of known sources. The biogenic contribution is estimated to be ∼90%. Comparisons of the model results with FTIR total columns, ground-based measurements in air and in rain water, and aircraft measurements lend support to the strong biogenic source inferred from the inversion. The distribution of the inferred missing source inferred (Figure 9) implies a large

contribution from the degradation of BVOCs and suggests that terpenoids emitted by coniferous trees generate substantial amounts of HCOOH. Should the entire missing source be attributed to monoterpenes, a molar yield of 200% HCOOH in their oxidation would be required; however, other BVOCs might also contribute.
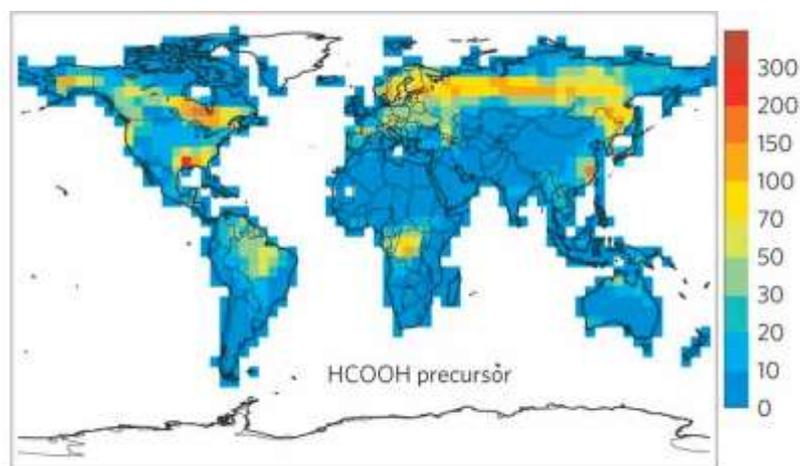

Figure 9. Emissions of HCOOH precursor (μg C m^{-2} s^{-1}) inferred by inverse modelling of satellite HCOOH data (July 2009). Our results imply that formic acid accounts for as much as 60-80% of rain water acidity in remote environments (Stavrakou et al., 2012).

WP2. SOA model development

Vapour pressure estimation method

To describe the gas/aerosol partitioning of an organic molecule, its vapour pressure is a central property which is however not experimentally known for most compounds. We developed the estimation method EVAPORATION (Estimation of VApour Pressure of ORganics, Accounting for Temperature, Intramolecular, and Non-additivity effects) designed specifically for functionalised organic molecules. Data of about 800 molecules were collected and the parameters of EVAPORATION were fitted to this extensive database. For some functionalised acids, we first had to develop a method to estimate their fusion property, to convert sublimation data to liquid vapour pressure data (Compernolle et al., 2011a). The exceptional behaviour shown by functionalised diacids according to recent data (Booth et al., 2010) led us to introduce a counter-intuitive correction term, not without noting, however, that it could be due to an experimental artefact.

The vapour pressure method EVAPORATION has been completed and published (Compernolle, 2011b), as well as a fusion property estimation method (Compernolle et al, 2011a). EVAPORATION has lower error margins compared to previously published methods (see e.g. Pankow and Asher, 2008; Nannoolal et al., 2008). The method has also been deployed as a web-application (see Valorisation). EVAPORATION has already

been applied by Zuend and Seinfeld (2012) to model **α-pinene** oxidation experiments, with good results. New experimental data from Huisman et al. (2013) on multifunctional acids confirmed the performance of EVAPORATION, provided the counter-intuitive correction factor was dropped.

EVAPORATION was also –with assistance from BIRA-IASB- implemented by Dr. William Carter for use in his (still preliminary) updated SAPRC Mechanism Generation System (http://mechgen.cert.ucr.edu:8000/). Moreover, the method has also been assessed together with other vapour pressure estimation methods by O'Meara et al. (2014), and it was found that within its scope, EVAPORATION gave among the best results for vapour pressure estimation and SOA loading estimation.

Henry's Law Constants

Henry's law constant (HLC) describes the partitioning of a compound between the gas phase and an aqueous, highly dilute solution. In the atmosphere, such dilute solutions are found in cloud droplets. Aqueous aerosols are another example where liquid water is important, but in this case the solvent must be regarded as multicomponent, with significant inorganic and/or organic contributions. As for vapour pressure, often no measured HLC value is available for relevant compounds (especially polyfunctional ones), and one has to resort to estimation methods.

Literature data on polyfunctional compounds is very limited, making difficult to properly evaluate estimation methods. Therefore, we derived additional HLC values from literature data for other properties (solubility, vapour pressure, water activity, and others), by employing thermodynamic relationships (see Figure 10).
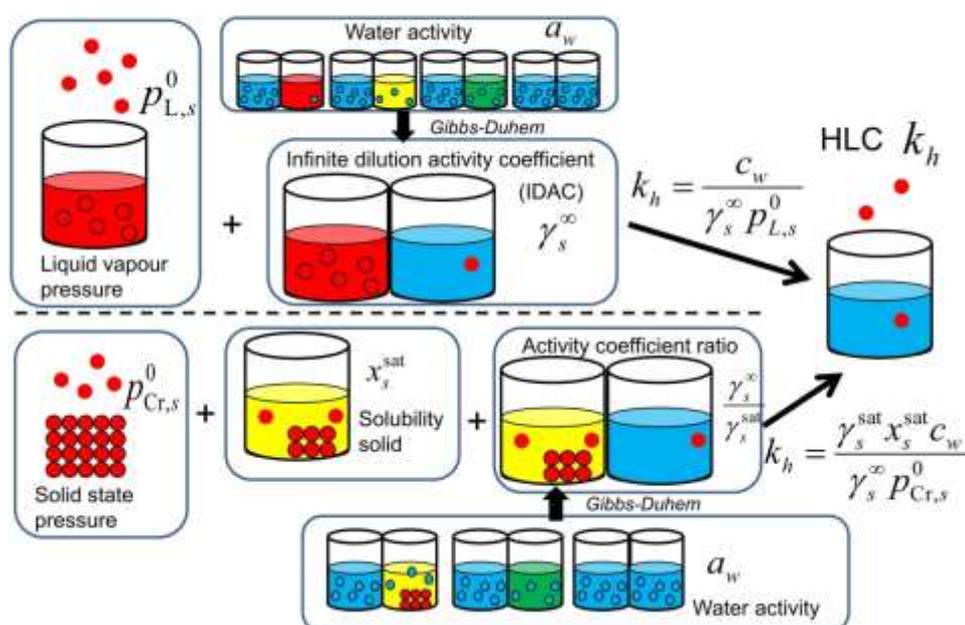

Figure 10. Derivation of HLC values from other data.

Using this approach, HLC data was derived for diacids and functionalized polyacids (Compernolle, 2014a) and for polyols (Compernolle, 2014b). Following our request, these data were added by Dr. Rolf Sander to version 3.99 of his comprehensive compilation of HLC data (Sander, 2014). For polyols, a detailed uncertainty analysis of the HLC values was performed, and it was concluded that the use of high-temperature vapour pressures is a major source of uncertainty in the derived HLC values. Regarding air-droplet partitioning, diacids, hydroxyl-polyacids, and polyols with three or more hydroxyl groups are expected to be completely in the aqueous phase, while for diols this is case-dependent. Partitioning simulations to a wet ammonium sulphate particle (with vanishing organic component) (Figure 11) revealed that polyols with four or more hydroxyl groups and the longer diacids are partially or completely in the particulate phase, depending on the RH. The shorter diacids (oxalic and malonic) and the hydroxyl polyacids are completely in the particulate phase, due to a higher acid dissociation constant and/or a high HLC.

Using literature as well as these newly derived data, an assessment of different HLC estimation methods was performed. Both direct and indirect (combination of vapour pressure estimation and infinite dilute activity coefficient (IDAC) estimation) methods were tested. An overview of the methods is given in TABLE III. The indirect estimation method EVAPORATION + AIOMFAC is found to be the most promising (TABLE IV). A few modifications were applied to AIOMFAC (hereafter referred to as AIOMFAC (m)), leading to better results for monofunctional acids, nitrates, peroxy acyl nitrates and dicarbonyls.
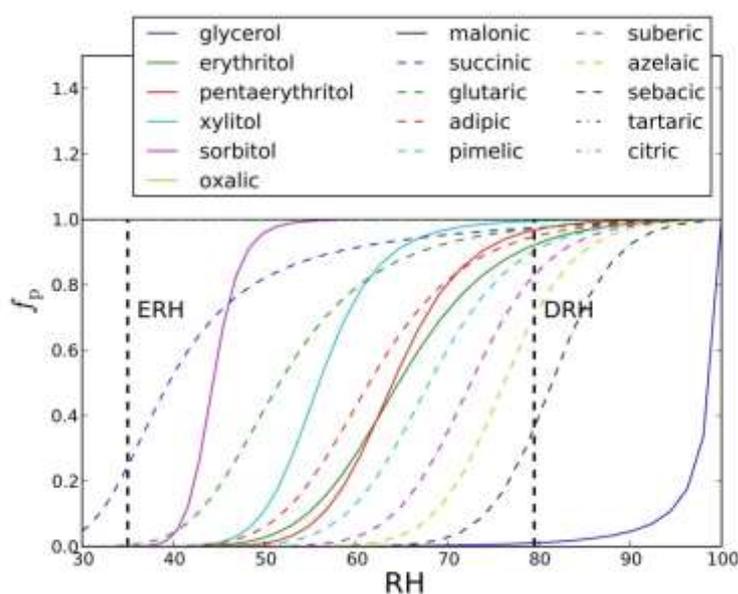

Figure 11. Simulated partitioning of polyols, diacids and hydroxyl polyacids to an ammonium sulphate particle under varying relative humidity.

TABLE III. Overview of the methods used to estimate HLC. Note that vapour pressure estimation methods and IDAC estimation methods can be combined to give HLC.

method	abbr.	property
GROMHE	grom	k_h
Cabani	Cab	k_h
EVAPORATION	evap	p_0^L
Nannoolal	Nan	p_0^L
UNIFAC-Hansen	Hansen	γ
AIOMFAC	aiom	γ
AIOMFAC(m)	aiom(m)	γ
UNIFAC-Raatikainen	Raat	γ
UNIFAC-Dortmund	dort	γ
AQUAFAC-Jain	aqua	γ^{∞}

The EVAPORATION+AIOMFAC(m) method was then used to estimate HLC values and corresponding enthalpies for the organic compounds calculated in the global CTM IMAGES, in order to improve the estimation of gas-wet partitioning for soluble compounds undergoing washout and rainout.

TABLE IV. Comparison of several HLC estimation methods to experiment. Numbers are standard deviations and marked with colors (green: SD < 0.5, orange: 0.5 < SD < 1.0, red: SD > 1.0). Asterisks denote molecule classes which cannot be handled by all methods. In the 'filtered**' class, these classes are not included, such that all methods can be compared.

scope	# data points	grom	ev/Han	ev/aiom	ev/aiom(m)	ev/Raat	ev/dort	ev/aqua
all	216	0.90	0.80	0.70	0.58	1.69	nan†	0.87
filtered**	161	1.01	0.80	0.67	0.54	1.81	1.09	0.96
mono-aldehydes	26	0.26	0.47	0.47	0.64	0.88	0.55	0.45
mono-ketones	19	0.17	0.44	0.44	0.44	0.72	0.35	0.67
mono-ethers	11	0.55	0.60	0.60	0.60	0.40	0.30	0.83
mono-esters	14	0.05	0.24	0.24	0.24	0.53	0.20	0.28
mono-formates	5	0.04	0.20	0.20	0.20	0.20	0.13	0.37
mono-alcohols	26	0.20	0.55	0.42	0.42	1.23	0.36	0.79
mono-acids	14	0.40	0.38	0.60	0.29	0.55	0.38	0.34
mono-nitrates*	20	0.21	0.78	0.78	0.43	1.17	nan	0.22
mono-pans*	7	0.32	1.29	1.29	0.90	1.53	nan	0.19
mono-per*	5	0.09	0.28	0.25	0.32	1.50	nan	0.16
dicarbonyls	5	1.05	2.41	2.41	0.69	2.41	2.42	2.51
diols	18	0.45	0.87	0.52	0.52	2.03	1.12	0.71
diacids	12	1.70	0.95	0.51	0.51	0.52	1.31	0.54
polyols	9	1.47	1.03	0.57	0.57	6.15	2.89	2.56
func. diacids	2	6.73	2.83	2.14	2.14	0.85	3.72	1.48
others*	23	0.70	0.67	0.60	0.81	1.23	nan	0.83

scope	# data points	Cab	Nan/Han	Nan/aiom	Nan/aiom(m)	Nan/Raat	Nan/dort	Nan/aqua
all	216	nan	1.28	1.20	1.27	1.99	nan	1.52
filtered**	161	3.50	0.91	0.74	0.75	2.05	1.06	1.28
mono-aldehydes	26	0.32	0.51	0.51	0.51	0.88	0.53	0.54
mono-ketones	19	0.10	0.46	0.46	0.46	0.70	0.35	0.73
mono-ethers	11	0.27	0.57	0.57	0.57	0.44	0.30	0.80
mono-esters	14	0.07	0.28	0.28	0.28	0.51	0.23	0.37
mono-formates	5	0.17	0.14	0.14	0.14	0.22	0.08	0.30
mono-alcohols	26	0.10	0.66	0.49	0.49	1.02	0.48	0.97
mono-acids	14	0.34	0.46	0.36	0.54	0.38	0.46	0.57
mono-nitrates*	20	nan	0.87	0.87	0.51	1.26	nan	0.21
mono-pans*	7	nan	2.76	2.76	3.16	2.54	nan	3.92
mono-per*	5	nan	3.35	3.42	3.51	2.20	nan	3.56
dicarbonyls	5	2.42	1.72	1.72	1.72	1.72	1.72	1.85
diols	18	1.07	1.12	0.66	0.66	1.88	1.37	1.02
diacids	12	0.77	2.00	1.43	1.43	1.49	2.37	1.38
polyols	9	14.53	0.87	1.16	1.16	7.51	1.70	3.96
func. diacids	2	2.49	2.32	1.70	1.70	0.75	3.18	1.77
others*	23	nan	2.02	2.04	2.29	1.81	nan	1.66

Model representation of SOA ageing

Only the first steps in α-pinene oxidation are treated explicitly in BOREAM. To limit the size of the overall mechanism, most secondary products are lumped into so-called generic species characterized by a vapour pressure class and one explicit chemical function. Although generic species constitute only a small fraction of freshly formed SOA from α-pinene, this fraction increases over time and becomes dominant in aged SOA. To reduce the uncertainty associated to the lumping of numerous species into these generic compounds, the mechanism was extended with the help of an automatic equation generator program. More precisely, several additional generations of products were treated explicitly. The total number of chemical reactions increased from 22000 to 91000 and the number of species from 3300 to 10500, reaching the current limits of the chemical solver (KPP-2.1).

The extension of BOREAM is found to reduce the fraction of generic SOA species from ∼50-90% to 10-30%. In the experiment with the strongest ageing (Pfaffenberger et al., 2013), this fraction was reduced to ∼50%. SOA yields were found to be only moderately affected by the extension, with relative variations of at most 25% (usually

less), indicating that the generic chemistry implemented in BOREAM does not cause large deviations in SOA yields.

The BOREAM model was evaluated against recent SOA ageing experiments, focusing on the impact of photolysis and OH-oxidation. Henry and Donahue (2012) concluded to a strong SOA decline due to photolysis in their Exp. 2 (Figure 12, green). Using standard photorates, BOREAM calculates instead a modest SOA increase (red). Increasing those photorates, or only those of organic species, leads to even stronger SOA increases due to higher OH-levels. Only a 100-fold increase in photorates leads to a comparable SOA decrease, after an initial rise (purple). This indicates serious underestimation of absorption cross sections and/or quantum yields of the multi-functional SOA constituents.
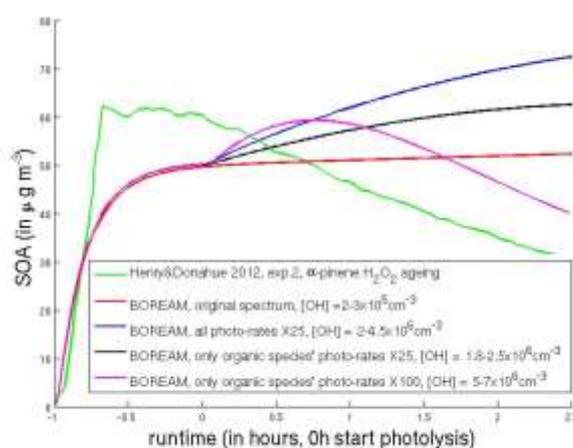

Figure 12: Experiment 2 from Henry and Donahue (2012), simulated with BOREAM.

BOREAM overestimates SOA levels by about 75% in simulations of the long-term low-NOx OH ageing experiments of Eddingsaas et al. (2012a), although the temporal evolution of SOA appears to be correct. The dominant SOA constituents in those experiments are hydroxy dihydroperoxides. In other ageing experiments (Tritscher et al., 2011; Salo et al., 2011; Pfaffenberger et al., 2013), the simulated SOA levels were also overestimated, by a factor of 2 to 10. For Pfaffenberger et al. (2013), BOREAM overestimates the reported O to C ratios by 0.1 to 0.25, and H to C ratios by 0.15 to 0.4. Wall losses are a large source of uncertainty, but cannot explain these discrepancies. Alcohol, ketone, hydroperoxide, nitrate and peroxyacyl nitrate (PAN) are the most abundant functional groups in the simulations, whereas carboxylic acids are dominant in SOA ageing studies (Eddingsaas et al., 2012b), presumably due to difficulties identifying less stable compounds such as hydroperoxides and PAN.

Model investigation of pathways to specific observed SOA compounds
We tested several proposed pathways to SOA tracers in BOREAM. The pathways proposed by Yasmeen et al. (2012) for producing 8- and 10-hydroxy pinonic acid were

not considered as they involve very unlikely isomerisation steps, but alternative pathways through OH-abstraction in pinonic acid are included in BOREAM. Several pathways were tested for terpenylic and diaterpenylic acid. Regarding MBTCA, the direct pathway proposed by Müller et al. (2012) was implemented, although it has very unlikely steps. Additionally, we modelled the oxidation of cyclobutyl methyl ketone to succinic acid (Praplan et al., 2012), which is similar to MBTCA formation. The formation of hydroperoxides observed by Eddingsaas et al. (2012a,b) was investigated. Finally, BOREAM was extended to α-pinene, based on recent theoretical work (Nguyen et al., 2009, Vereecken and Peeters, 2012).

As seen in TABLE V, the oxidation of pinonic acid as implemented in BOREAM leads to only ppt levels of 8- and 10-hydroxy pinonic acid, norpinic acid and diaterpenylic acid. Model pathways towards terpenylic, diaterpenylic acid acetate (Claeys et al., 2009) and MBTCA were found to be negligible in the studied experiment, as the multigeneration chemistry needed generally takes longer than the time scale of the experiment, and passes several unfavourable reaction branchings.

TABLE V. Calculated product concentrations in experiment E0802 in Yasmeen et al. (2012).

Name	BOREAM (ppt)	name	BOREAM (ppt)
8-Hydroxypinonic acid	29	Terpenylic acid	0.003
10-Hydroxy pinonic acid	2.2	Diaterpenylic acid acetate	< 0.001
Diaterpenylic acid	53	MBTCA (conventional chemistry)	< 0.001
Norpinic acid	11	MBTCA (pinonic acid direct pathway, Müller et al. 2012)	2.8

High observed MBTCA yields were found in both high-NO$_x$ (Szmigielski et al., 2007, Eddingsaas et al., 2012b) and low-NO$_x$ conditions (Yasmeen et al., 2012, Eddingsaas, 2012b). Müller et al. (2012) observed a yield of the order of 1% MBTCA in low-NO$_x$ pinonic acid oxidation. In Praplan et al. (2012), succinic acid is produced in a similar reaction from cyclobutyl methyl ketone. Simulations with BOREAM show that conventional reaction pathways underestimate succinic acid formation by 2-3 orders of magnitude at low-NO$_x$. A possible alternative pathway involving a shift of an aldehyde H in a peroxy radical could generate succinic peracid in significant amounts, but it does not operate at high-NOx. Similar pathways for MBTCA from pinonic acid are negligible (see TABLE V). Even the pathway of Müller et al. (2012) leads to only ppt-levels of MBTCA. Therefore the production of important acidic tracer species such as MBTCA and terpenylic acid remains unexplained from a mechanistic point of view.

Better agreement was obtained for first generation products observed in experiments by Eddingsaas et al. (2012a). The observed pinonaldehyde under low-NO$_x$

implies a novel pathway for the reaction of specific β-hydroxy peroxy radicals with HO_2 leading to alkoxy radicals and OH. Including this pathway in BOREAM with a 50% channel ratio leads to a reasonable agreement with observations (Figure 13).
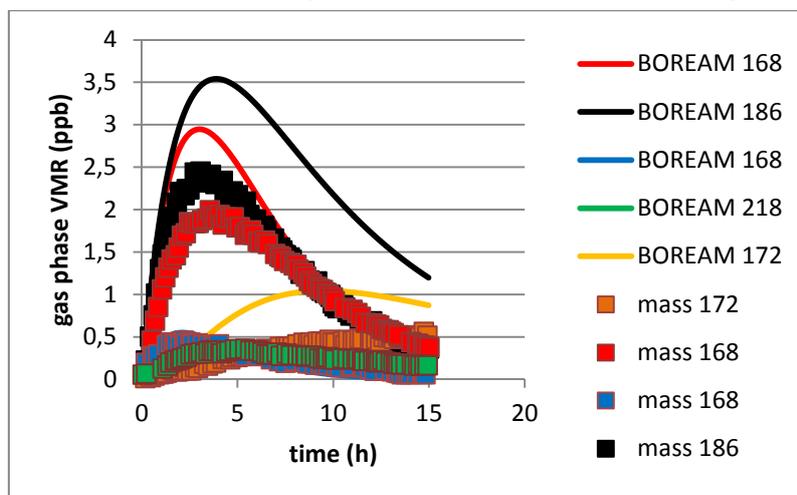

Figure 13: BOREAM simulation of an **α-pinene** low-NO$_x$ experiment of Eddingsaas et al. (2012a). m168 (red): pinonaldehyde, m186: hydroxy hydroperoxides, m218: hydroxy dihydroperoxides, m172: hydroperoxide product of pinonaldehyde oxidation, m168 (blue): hydroperoxide from the H-abstraction channel of **α-pinene**.

WP3. Laboratory studies

Chemical formation pathways leading to isoprene SOA tracers

Isoprene SOA chemistry is tightly linked to gas-phase photo-oxidation processes, which yield a number of volatile gas-phase products, including methacrolein, methyl vinyl ketone, methyl furan, C_5-alkene diols, C_5-epoxydiols, and C_5-hydroxyhydroperoxides as first-generation products. Different mechanistic pathways, involving gas- and particle-phase reactions, have been suggested to explain the formation of the 2-methyltetrols through photo-oxidation of isoprene under low-NO_x conditions in the presence or absence of acidic or neutral ammonium sulfate seed aerosol (Claeys et al., 2004a, 2004b; Böge et al., 2006; Kleindienst et al., 2009; Paulot et al., 2009b; Surratt et al., 2010). Key intermediates in the pathway reported by Claeys et al. (2004a) and later elaborated by Böge et al. (2006) and Kleindienst et al. (2009) are the C_5-alkene diols, whereas those in the pathway reported by Paulot et al. (2009b) are the C_5-epoxydiols. As to the first pathway, it has been shown by Böge et al. (2006) that the C_5-alkene diol, 1,2-dihydroxy-2-methyl-3-butene, serves as a precursor for the 2-methyltetrols. Here, we have further evaluated whether isomeric C_5-alkene diols, which have first been detected upon photo-oxidation of isoprene in the absence of NO and are known to be formed in the ambient atmosphere, can serve as precursors for the 2-methyltetrols, C_5-alkene triols, and 2-methylglyceric acid under low-NO_x conditions.

Preparation and characterisation of C_5-alkene diols: Three different positional isomers of the C_5-alkene diols were synthesised according to published procedures and included: 1,2-dihydroxy-2-methyl-3-butene (diol 1), 1,2-dihydroxy-3-methyl-3-butene (diol 2) and 1,4-dihydroxy-2-methyl-2-butene (diol 3) (Ruppert and Becker, 2000; Hodgson et al., 2001). An overview is given in Figure 14.

Smog chamber experiments: Chamber experiments were conducted at TROPOS, using the chamber described by Iinuma et al. (2009). The experiments were mainly photo-oxidation experiments under dry conditions using H_2O_2 as oxidant, except for one ozonolysis experiment at a relative humidity (RH) of 30%, and were carried out in the absence of NO_x and using $(NH_4)_2SO_4$ seed particles. In total, 12 chamber experiments were performed: 4 with isoprene, 2 with diol 1, 4 with diol 2, and 2 with diol 3. The initial hydrocarbon concentration was about 100 ppb. SOA samples were collected on Teflon filters and were worked up following procedures used in previous work (Pashynska et al., 2002).

GC/MS analysis: Selected filters were analysed for polar compounds by GC/MS with prior trimethylsilylation using a method adapted from Pashynska et al. (2002). The

identity of the compounds was confirmed by comparing the EI mass spectra with literature data (Claeys et al., 2004a, 2004b ; Wang et al., 2005).
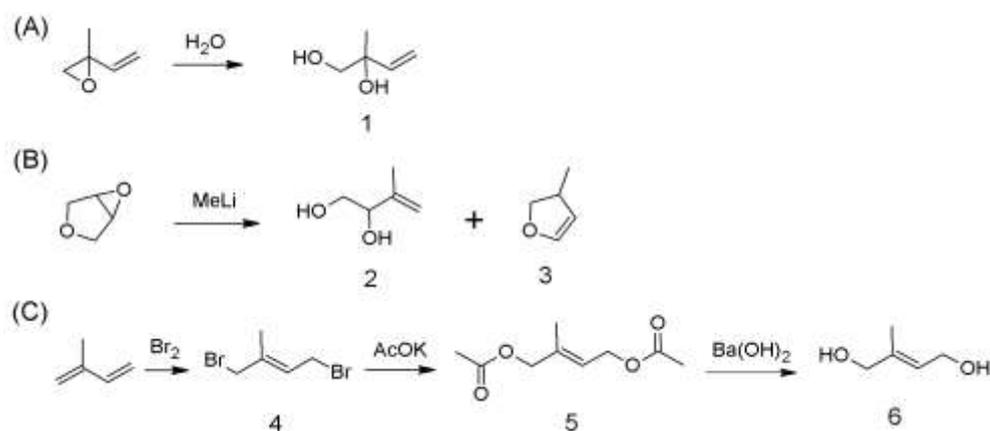

Figure 14. Overview of the synthetic procedures leading to (A) 1,2-dihydroxy-2-methyl-3-butene (1; diol 1), (B) 1,2-dihydroxy-3-methyl-3-butene (2; diol 2), and (C) 1,4-dihydroxy-2-methyl-2-butene (cis + trans) (6; diol 3).

Figure 15 shows extracted ion chromatograms (EICs) (m/z 219 + 231) obtained for ambient $PM_{2.5}$ aerosol collected from K-puszta, Hungary, and selected SOA samples from the chamber (without added NO) in the presence of neutral ammonium sulfate seed aerosol. The 2-methyltetrols (i.e. 2-methylthreitol and 2-methylerythritol) are detected as abundant marker compounds in the photo-oxidation of isoprene and the isomeric C_5-alkene diols, whereas the C_5-alkene triols are only detected in ambient $PM_{2.5}$ aerosol and in the SOA samples from the chamber irradiation of isoprene with ozone or H_2O_2. It thus appears that under the chamber conditions the C_5-alkene diols serve as gas-phase intermediates for the 2-methyltetrols but not for the C_5-alkene triols. In addition, 2-methylgyceric acid is also produced at low relative abundance from diols 1 and 3.

The threo/erythro ratio of the 2-methyltetrol diastereoisomers is different for the isoprene and C_5-alkene diol experiments, with the highest one for diol 1 (0.7) and the lowest one for diol 3 (0.3), indicating that diol 1 favours the formation of 2-methylthreitol, whereas diol 3 favuors that of 2-methylerythritol. Interestingly, the average threo: erythro ratio of the 2-methyltetrols in the three C_5-alkene diol experiments (0.44) falls between those for isoprene/O_3 (0.40) and isoprene/OH (0.57). The 2-methyltetrols contribute with more than 50% to the total mass of the identified SOA tracers for the isoprene experiments (i.e. 67% for isoprene/OH and 52% for isoprene/O_3) and their contributions were even higher for the C_5-alkene diol experiments (i.e. 80% for diol 1, 92% for diol 2, and 83% for diol 3).
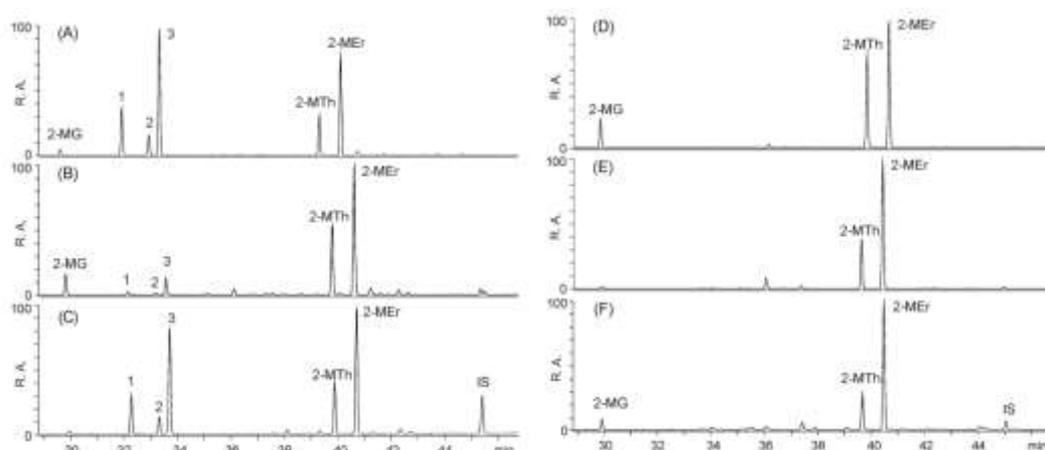
Figure 15. GC/MS extracted ion chromatograms (m/z 219 + 231) obtained for SOA from ambient aerosol sample collected in K-puszta, Hungary (A), the photooxidation of isoprene with OH, (B), isoprene with ozone, (C), and 1,2-dihydroxy-2-methyl-2-butene, (D), 1,2-dihydroxy-3-methyl-3-butene, (E), and 1,4-dihydroxy-2-methyl-2-butene (cis + trans), (F) with OH. Abbreviations: 2-MG: 2-methylglyceric acid; 1: cis-2-methyl-1,3,4-trihydroxy-1-butene; 2: 3-methyl-2,3,4-trihydroxy-1-butene; 3: trans-2-methyl-1,3,4-trihydroxy-1-butene; 2-MTh: 2-methylthreitol; 2-MEr: 2-methylerythritol; R.A., relative abundance; IS: internal standard.

In addition to the 2-methyltetrols and 2-methylglyceric acid, the SOA from the experiments of isoprene and the C_5-alkene diols with H_2O_2 contained other oxygenated organic compounds, i.e., diastereoisomeric (threo and erythro) C_5-acids and -diacids, which were identified based on the detailed interpretation of the EI-MS data of their trimethylsilyl derivatives. As these compounds could also be detected in ambient aerosols from K-puszta, Hungary, they are of atmospheric relevance. The C_5-acids and -diacids represent about 10% of the total mass of the identified SOA tracers in the irradiation of isoprene with OH, and about 3% in the case of irradiation with diols 1 and 2. Their formation from diol 3 is negligible. The C_5-diacids were detected for the first time in natural aerosols from the Amazonian rain forest and were tentatively (but wrongly) assigned to threo- and erythro-2,3-dihydroxyglutaric acids (Claeys et al., 2004a). In the present work their structures were revised as threo- and erythro-2,3-dihydroxy-2-methylbutanedioic acid. Considering the fact that the C_5-mono- and -diacids retain the isoprene skeleton and can be formed upon irradiation of isoprene and the isoprene-derived diols 1 and 2, it can be concluded that they are higher-generation photo-oxidation products of isoprene and may serve as markers for isoprene SOA.

The question arises whether the applied chamber conditions reflect those encountered under ambient conditions, as will be discussed in this and the following paragraphs. Kleindienst et al. (2009) proposed a gas-phase mechanism for the formation of the 2-methyltetrols from isoprene through C_5-alkene diols and peroxide radicals involving trihydroxyperoxy radicals which might react with HO_2 to form C_5-

trihydroxyhydroperoxides and partition to the particle phase [Figure 16(A)]. In the present study, however, no evidence could be found for the formation of C_5-trihydroxyhydroperoxides; if such hydroperoxide products would have been formed and would be stable under our conditions, we would expect the formation of oxo derivatives as thermal degradation products of the trimethylsilylated hydroperoxides upon GC/MS analysis. The photo-oxidation experiments with isoprene suggest that the 2-methyltetrols are directly generated from intermediate C_5-alkene diols under the chamber conditions, likely as a result of RO_2 + RO_2 reactions on the generated C_5-trihydroxyperoxy radicals. Isomeric C_5-epoxydiols with a MW of 118 have been reported by Paulot et al. (2009b) and proposed as gas-phase intermediates in the formation of the 2-methyltetrols and the C_5-alkene triols. A subsequent study by Surratt et al. (2010) confirmed that C_5-epoxydiols indeed serve as the intermediate gas-phase precursors for the 2-methyltetrols and C_5-alkene triols in the particle phase [Figure 16(B)], as well as for C_5-epoxydiol dimers and organosulfates. Our efforts to detect C_5-epoxydiols in the gas phase upon photo-oxidation of isoprene by a trapping experiment in acidified methanol failed; a possible explanation is that under our experimental conditions they are not formed as major gas-phase intermediates. An indication that they are produced as minor gas-phase intermediates serving as precursors for the 2-methyltetrols is that the C_5-alkene triols, which have been shown to be formed from C_5-epoxydiols, are only generated at a rather low relative abundance [Figure 15(B)].

It thus appears that our experimental conditions do not favor the formation of C_5-epoxydiols but lead to the formation of C_5-alkene diols, likely as a result of RO_2 + RO_2 reactions on the corresponding hydroperoxy radicals [Figure 16(A)]. The observations, however, that the C_5-alkene diols have been detected in the ambient atmosphere and can readily be converted to 2-methyltetrols suggest that the route through C_5-alkene diol gas-phase intermediates could be a possible minor route leading to the 2-methyltetrols. On the basis of the threo/erythro abundance ratio of the 2-methyltetrols, it is not possible to determine to which extent this route is followed; assuming that the isomeric C_5-alkene diols are produced in comparable amounts as shown by Kleindienst et al. (2009) the expected threo/erythro ratio is 0.44, very close to the ratio of 0.45 observed for ambient fine aerosol (Figure 15). It is noted that the isoprene mixing ratios applied in our study (94 ppb) are lower than the lowest mixing ratios that were applied in the studies of Ruppert and Becker (2000) (i.e. 1.86 ppm) and Kleindienst et al. (2009) (i.e. 8.7 ppm) for which C_5-alkene diols
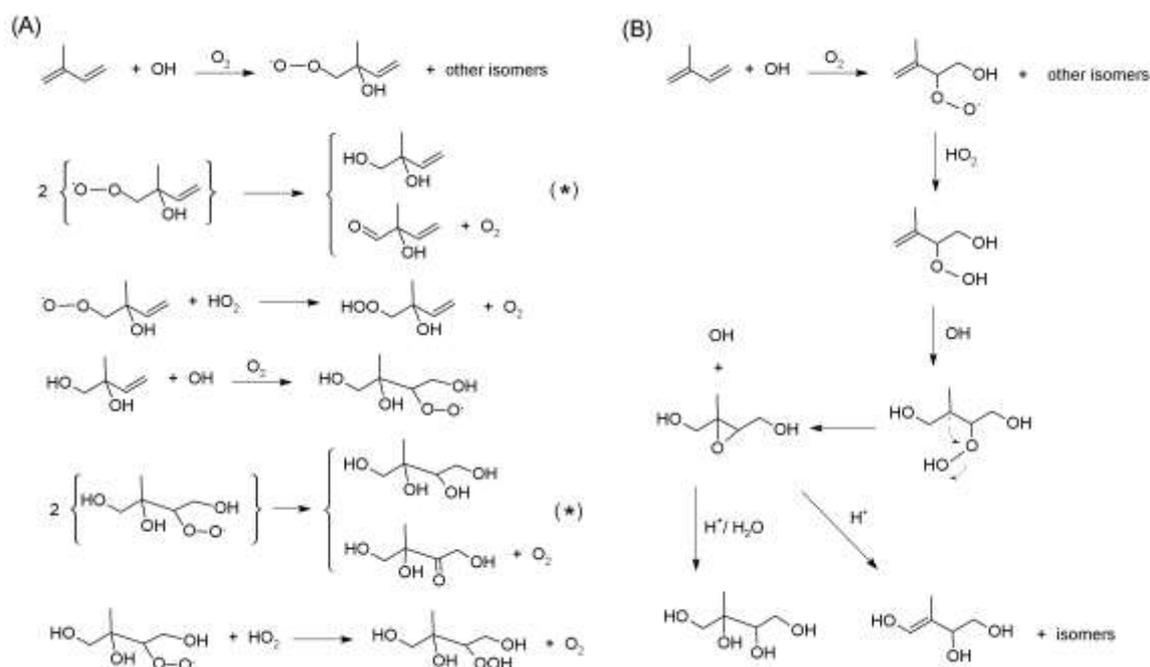
Figure 16. Pathways reported for the formation of the 2-methyltetrols through photooxidation of isoprene: (A) pathway involving C_5-alkene diols as gas-phase intermediates, and (B) pathway involving C_5-epoxydiols as gas-phase intermediates. The reactions marked with * are relevant to the current study.

were detected, but somewhat higher than those of Paulot et al. (2009b) (20.9 ppb) and Surratt et al. (2010) (40 ppb) for which C_5-epoxydiols and C_5-alkene triols, respectively, were reported. A notable difference, however, between the experimental conditions in the studies of Ruppert and Becker (2000), Kleindienst et al. (2009) and our study and the studies of Paulot et al. (2009b) and Surratt et al. (2010) is the way in which the H_2O_2 was introduced into the chamber; while H_2O_2 was continuously introduced in the first two studies and ours, a known mass of H_2O_2 was introduced in the beginning of the experiment (first 15-20 min) in the last two studies, likely giving rise to significant HO_2 radical levels by the OH + H_2O_2 reaction, which is favored at the slow chamber photolysis rate of H_2O_2. It is worth noting that the product distribution of isoprene SOA marker compounds obtained in the photolysis reaction of ozone [Figure 15(C)] under more atmospherically relevant conditions in the presence of water vapor (RH 30%) is comparable to that obtained for ambient aerosol [Figure 15(A)]; more specifically, the 2-methyltetrols and C_5-alkene triols show comparable relative abundances. A possible explanation is that photolysis of ozone in the presence of water vapor suppresses RO_2 + RO_2 reactions, but instead favors RO_2 + HO_2 reactions, thereby facilitating C_5-epoxydiol and subsequent 2-methyltetrol + C_5-alkene triol formation [Figure 16(B)].

As to the formation of 2-methylglyceric acid through photo-oxidation of isoprene, it has been shown that this marker compound is mainly formed in chamber experiments

under high-NO_x conditions (Surratt et al., 2006) and that it involves methacroyl-peroxynitrate and its subsequent oxidation product 2-methyloxirane-carboxylic acid as gas-phase intermediates (Surratt et al., 2010; Lin et al., 2013). The results show that 2-methylglyceric acid is formed as a minor compound through photo-oxidation of isoprene at low-NO_x conditions, and can also be produced from the C_5-alkene diols 1 and 3. It thus appears that there is a minor low-NO_x pathway operating in the formation of 2-methylgyceric acid. A possible pathway leading to the formation of 2-methylglyceric acid from diol 1 involving the photolysis of 2-hydroperoxy-1,3,4-trihydroxy-3-methylbutane is presented in Figure 17.
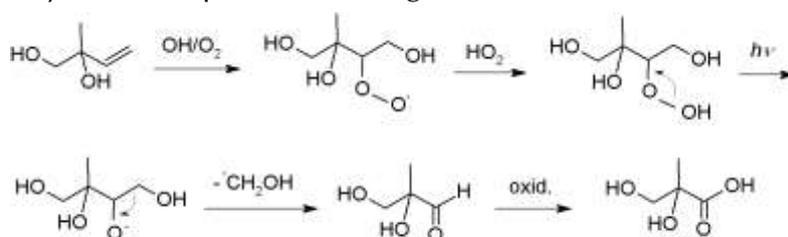

Figure 17. Proposed pathway for the formation of 2-methylglyceric acid via the C_5-alkene diol 1,2-dihydroxy-2-methyl-3-butene (diol 1) under low-NO_x conditions.

Additional insights have been obtained on pathways leading to the formation of isoprene SOA marker compounds and the discrepant results reported in the literature for the underlying formation mechanisms, more specifically, with regard to the formation of the 2-methyltetrols which can either be explained by acid-catalyzed hydrolysis of C_5-epoxydiols or further photo-oxidation of C_5-alkene diols. It is shown that isomeric C_5-alkene diols serve as precursors for the 2-methyltetrols, i.e. 2-methylthreitol and 2-methylerythritol, under low-NO_x conditions, and rule out their involvement in the formation of the C_5-alkene triols. In addition, it is demonstrated that isoprene and C_5-alkene diols result in C_5-mono- and -diacids, which have retained the isoprene skeleton and as such may serve as suitable isoprene SOA markers. Furthermore, evidence is presented for a minor low-NO_x pathway leading to 2-methylglyceric acid, which may be relevant to ambient conditions. Efforts to detect C_5-epoxydiols in the gas phase upon photo-oxidation of isoprene were not successful, likely because of the prevalence of RO_2 + RO_2 reactions on the first-order C_5-hydroxyhydroperoxy radicals leading to the formation of C_5-alkene diols.

Chemical characterisation and time evolution of α-pinene SOA tracers upon ageing
In this study, the focus is on the chemical characterisation of major products that are formed upon formation of **α-pinene** ozonolysis SOA and subsequent ageing through OH-initiated reactions in the absence of NO_x. The targeted SOA products include known as well as unknown compounds, and are denoted as markers. Differences in

their relative abundances are used as this parameter gives information about their evolution during the ageing process. The MS data obtained for selected unknown compounds is interpreted in detail and tentative structures for them are proposed taking into account that they are formed through photo-oxidation/ozonolysis of α-pinene and likely have retained the dimethylbutane ring.

Smog chamber experiments: Chamber experiments were conducted in the CESAM chamber (French acronym for Experimental Multiphasic Atmospheric Simulation Chamber) at the University of Paris-Est at Créteil. The CESAM chamber is designed to allow research in multiphase atmospheric (photo-)chemistry which involves both gas-phase and condensed-phase processes including aerosol and cloud chemistry and has been described in detail elsewhere (Wang et al., 2011). Two photooxidation experiments were performed; the initial starting conditions for the experiments are given in TABLE VI. The experiments were carried out under dry conditions (i.e. at a RH below 1%), and at room temperature and atmospheric pressure, in the absence of seed aerosol. SOA collection was done using 47-mm glass fibre filters (Glass Microfibre filters GF/F Whatman).

TABLE VI: Summary of the experimental conditions.

Exp number	$[O_3]_0$ (ppb)	$[\alpha\text{-pinene}]_0$ (ppb)	$[\text{SOA mass}]_{max}$ (μg.m^{-3})	SOA Yield	Fresh SOA sampled (μg)	Aged SOA sampled (μg)	Ageing time (min)
E0202	1300	254	441	0.31	10.7	10.7	158
E0208	1400	252	367	0.26	13.4	11.9	219

LC/MS analysis: The filters were extracted with methanol and the extracts were analysed by LC/MS in the negative ion electrospray ionization [(–)ESI] mode using conditions reported in Yasmeen et al. (2011). The identity of known compounds was confirmed by comparing the mass spectra with literature data (Szmigielski et al., 2007; Yasmeen et al., 2010, 2011), whereas for unknown compounds tentative structures were proposed based on detailed interpretation of MS data.

As the results were quite similar for the two experiments but the effects of the irradiation more pronounced for the second one owing to the longer irradiation time (230 min *vs.* 160 min), the results will only be presented for the second experiment (E0208). Results from this experiment are provided in Figures 18 and 19. The peak assignments in the EICs of Figure 19, corresponding to known and tentatively assigned products, are as follows:

- *m/z* 157: 12.0 min, terebic acid; 14.4/14.2 min, dinorpinic acid; 24.4/24.3 min: unknown
- *m/z* 171: 13.4/13.2 min: terpenylic acid; 15.9/15.7 min: norpinic acid
- *m/z* 183: 17.9/17.8 min: pinonic acid
- *m/z* 185: 17.0/16.7 min: pinic acid
- *m/z* 189 : 11.7/11.5 min: diaterpenylic acid
- *m/z* 199: 14.8/14.7 min: 10-hydroxypinonic acid; 15.5/15.4 min: 8-hydroxypinonic acid; 19.7/19.5 min: unknown
- *m/z* 203: 18.7/18.5 min: 3-methyl-1,2,3-butanetricarboxylic acid (MBTCA)
- *m/z* 231: 12.6/12.4 min: unknown; 13.4 min: terpenylic acid (acetate adduct); 16.6/16.5 min: diaterpenylic acid acetate
- *m/z* 357: 20.2/20.0 min: diester of diaterpenylic acid/pinic acid
- *m/z* 367: 21.1/21.0 min: diester of diaterpenylic acid/10-hydroxypinonic acid

Known tracers for α-pinene SOA ageing that were identified include norpinic acid, 10-hydroxypinonic acid, diaterpenylic acid acetate, and di-esters formed by esterification of pinic acid with terpenylic acid or 10-hydroxypinonic acid. Novel tracers for α-pinene SOA ageing that were tentatively identified include dinorpinic acid and 8-hydroxypinonic acid. Mechanistic pathways leading to the various products are proposed in Figure 20.
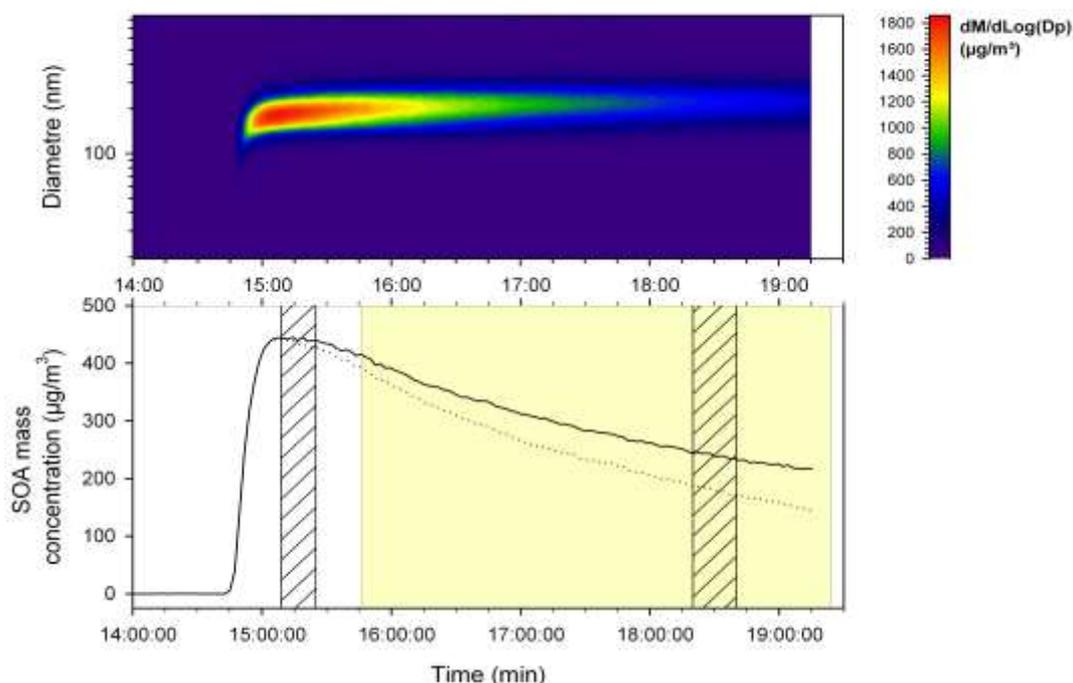

Figure 18. Mass concentration-time curve for the E0208 experiment. Size distribution in mass as a function of time (upper panel). Mass concentration as a function of time derived from a scanning mobility particle sizer (SMPS) assuming a density of 1 g mL^{-1} (bottom panel). Data corrected from dilution due to sampling are given by the bold line whereas the dashed line

corresponds to non-corrected data. The hatched areas represent the sampling periods, whereas the yellow area represents the irradiation period.

The novel tracers for α-pinene SOA ageing can be explained through different types of chemical reactions, including:

- OH-initiated hydroxylation of pinonic acid; examples of this process are the formation of 8- and 10-hydroxypinonic acid [Figure 20(A)];

- OH-initiated hydroxylation/fragmentation of pinic acid; examples of this process are the formation of norpinic acid and dinorpinic acid [Figure 20(B)]; and

- hydrolysis of lactone-containing terpenoic acids; an example of this process is the formation of diaterpenylic acid through hydrolysis of terpenylic acid [Figure 20(C)].
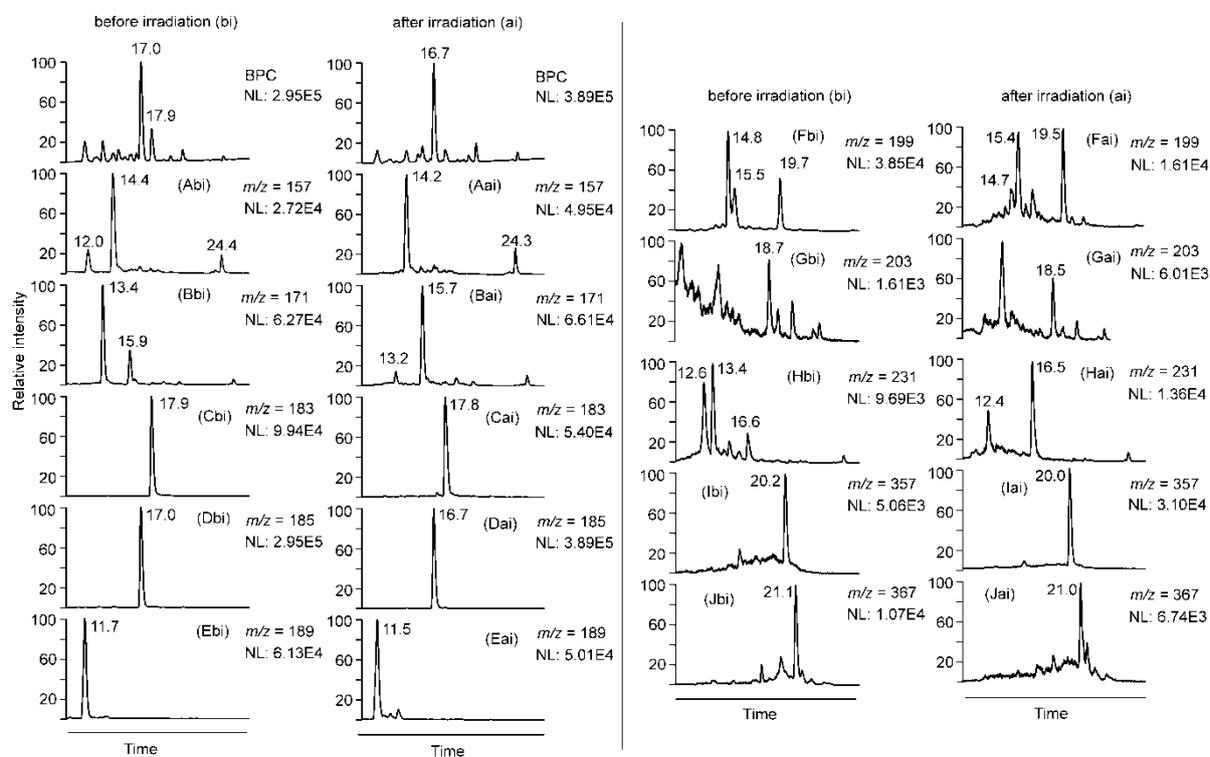

Figure 19. Selected LC/MS [base peak chromatograms (BPCs) and extracted ion chromatograms (EICs)] for experiment E0208. The retention times of all relevant chromatographic peaks are indicated in the EICs; for assignments, see the text. Abbreviation: NL, normalisation level.
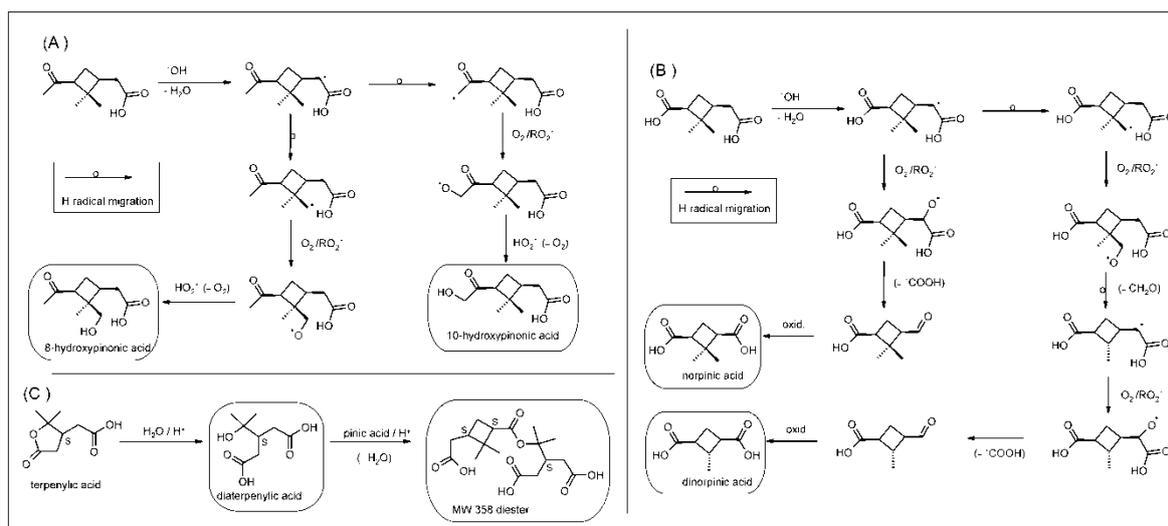
Figure 20. Proposed formation mechanisms: (a) 8- and 10-hydroxypinonic acid; (b) norpinic and dinorpinic acids; and (c) diaterpenylic acid and the MW 358 diester.

Several potential tracers for **α-pinene** SOA ageing have been tentatively identified using detailed interpretation of LC/(–)ESI-MS data. Their formation has been explained by OH-initiated hydroxylation and fragmentation, and hydrolysis. SOA ageing can thus be regarded as a complex process involving different types of chemical reactions resulting in an array of products with different MWs and polarities.

Chemical characterisation of a MW 188 terpenylic acid-related oxidation product

A comprehensive mass spectrometric analysis was performed on a MW 188 **α-pinene** SOA marker ($C_8H_{12}O_5$), which is often observed in ambient aerosol samples in high abundance and was proposed as an additional suitable marker for aged biogenic SOA (Gómez-González et al., 2012). Based on MS data, indicating the presence of a carboxylic and a hydroxyl group, and its relatively low retention time in reversed-phase LC, this unknown MW 188 compound represents a very hydrophilic compound. Its formation was reported both from laboratory **α-pinene** ozonolysis and OH radical-initiated oxidations (Claeys et al., 2009; Yasmeen et al., 2011), but was generally observed in substantially lower abundance than other known **α-pinene** SOA markers in chamber-generated samples. Two structures have been proposed for the unknown MW 188 compound, i.e. a C_8-monohydroxycarboxylic acid structure (2-hydroxyterpenylic acid) (Claeys et al., 2009) and a C_8-hydroxydicarboxylic acid structure (hydroxynorpinic acid) (Yasmeen et al., 2011). The MW 188 compound could not be detected by GC/MS with prior trimethylsilylation in previous studies, showing a similar behavior as other lactone-containing terpenoic acids, i.e., terebic and terpenylic acid. A possible analogous structure, 2-hydroxyterpenylic acid, was proposed by Claeys et al. (2009), mainly based on its non-covalent dimer formation properties similar to terpenylic acid,

but no further evidence for this structural proposal could be provided for various reasons, including the difficulty to produce the compound from laboratory α-pinene oxidations, the occurrence of several isobaric isomers, and the lack of an authentic reference compound. The MW 188 compound was recently described to form also from campholenic aldehyde ozonolysis (Kahnt et al., 2014a) and based on the agreement of MS data with those from ambient filter samples, campholenic aldehyde ozonolysis (CAO) SOA was chosen in the present investigation to further characterise the MW 188 compound.

Chamber aerosol samples: Samples from campholenic aldehyde ozonolysis were obtained as described by Kahnt et al. (2014a). Time-resolved α-pinene/NOₓ/air irradiation experiments were performed in the EPA chamber in the batch mode as described in detail in Jaoui et al. (2005). The precursor was injected with a mixing ratio of 5 ppmC in the 14.5 m³ smog chamber that was operated at 28% RH, with an initial NO mixing ratio of 508 ppb. For the photooxidation study 4 light banks were used and the experiment was carried out in the presence of 1 $\mu g\ m^{-3}$ $(NH_4)_2SO_4$ seed particles.

Atmospheric aerosol samples: Pooled filter samples, which were collected during a summer field campaign from K-puszta, Hungary, in 2006 were used. Details on the measurement campaign can be found in Maenhaut et al. (2008). The pooled filter samples were prepared as described in Kahnt et al. (2014a).

Sample preparation: The samples were extracted with methanol and part of the methanol extracts were derivatised with ethereal diazomethane for GC/MS and LC/MS analysis.

Chemical analysis: LC/MS analysis was carried out using a Surveyor Plus system (pump and autosampler) (Thermo Scientific, San Jose, CA, USA) connected to an Atlantis T3 column (2.1 x 150 nm, 3 μm particle size, Waters, Milford, MA, USA), providing polar retention for the MW 188 compounds under investigation. The mobile phase consisted of (A) 50 mM ammonium formate buffer with pH 3 and (B) methanol. Details of the LC gradient can be found in Kahnt et al. (2014a).

GC/MS analysis was performed using a TRACE GC2000 gas chromatograph and a Polaris Q ion trap mass spectrometer fitted with an external electron ionization source (Thermo Scientific). A deactivated silica pre-column (2 m x 0.25 mm i.d.) and a CP Sil 8CB low-bleed capillary column (95% dimethyl-, 5% phenylpolysiloxane, 0.25 μm film thickness, 30 m x 0.25 mm i.d.) (Chrompack, Middelburg, The Netherlands) were employed. Details about the experimental conditions can be found in Kahnt et al. (2014b).

Quantum chemical calculations: Theoretical calculations on 2-hydroxyterpenylic acid were performed using the Gaussian 03 suite of programs (Frisch et al., 2004) in combination with the RELAX program, which is part of the BRABO suite of programs

(Van Alsenoy and Peeters, 1993) applying the density functional theory. The calculations were performed for the gas phase as well in continuum to derive information about solvation effects. After chemical structure optimization dipole moments were derived for 2-hydroxyterpenylic acid in the gas phase, as well as in water and methanol using epsilon-values of 78.4 and 32.6, respectively.

Structural characterisation of the MW 188 compounds as 2-hydroxyterpenylic acid diastereoisomers:

Figure 21 presents selected LC/MS data (EICs) for m/z 187 corresponding to the deprotonated molecule of the targeted analytes eluting at 16.4 and 17.2 min and MS data (m/z 187 MS^2 and m/z 187 $\rightarrow m/z$ 125 MS^3 product ion spectra) present in CAO SOA and ambient fine aerosol from K-puszta. It is worth noting that CAO SOA clearly shows two MW 188 compounds in a ratio of about 1:5, of which the second-eluting isomer (17.2 min) is also present at relative small abundance in the ambient sample. The product ion spectra from the (–)ESI-MS^n analysis for the compound eluting at 16.4 min agreed well with reported spectra in the literature. This MW 188 compound was proposed earlier as 2-hydroxyterpenylic acid (Claeys et al., 2009), however, no diastereoisomeric assignment was made in this earlier study. The m/z 187 MS^2 product ion spectrum [Figure 21(C, D)] is dominated by m/z 125, which corresponds to the combined loss of a molecule water and CO_2 (62 u) and is in agreement with a hydroxycarboxylic acid structure (Figure 22). Further fragmentation of m/z 125 leads to ions at m/z 107, 97 and 81 [Figure 21(E, F)], which can also be explained with the proposed structure. It can be noted that the MS data obtained for the MW 188 compound eluting at 17.2 min [Figure 21(G-I)] are very similar to those of the first-eluting isomer [Figure 21(C-F)] and mainly differ by the relative abundances of their product ions, which is consistent with diastereoisomeric forms of 2-hydroxyterpenylic acid.

In order to obtain additional structural information, the targeted MW 188 compounds were also analysed with LC/ESI-MS in the positive ion mode with and without methylation and the MS data were compared with those of available standard compounds, i.e. terebic and terpenylic acid. The m/z 187 MS^2 data supported the proposed 2-hydroxyterpenylic acid structure. In addition, the methylated samples were subjected to GC/EI-MS analysis, which revealed two peaks for methylated 2-hydroxyterpenylic acid diastereoisomers in the case of the CAO SOA sample, with one of them matching a peak present in the K-puszta sample.
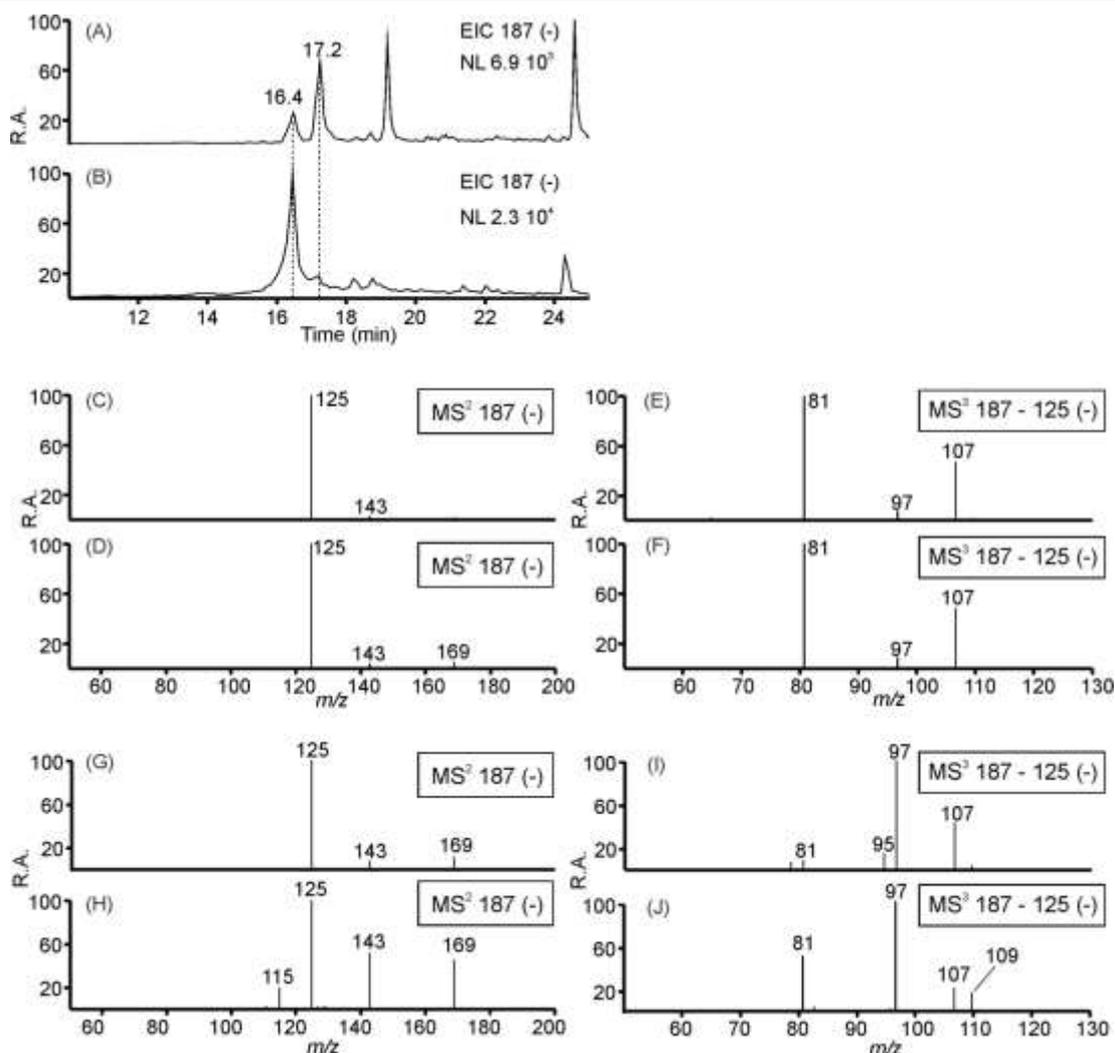
Figure 21. Selected LC/(–)ESI-MS data for MW 188 compounds present in campholenic aldehyde ozonolysis SOA (A) and K-puszta fine aerosol (B) showing the m/z 187 extracted ion chromatograms (EICs). (C) and (D) show m/z 187 MS^2 data, (E) and (F) m/z 187 →m/z 125 MS^3 data for the compound eluting at 16.4 min in CAO and the ambient SOA sample, respectively, and (G) and (H) corresponding m/z 187 MS^2 data, and (I) and (J) m/z 187 →m/z 125 MS^3 data for the compound eluting at 17.2 min. Abbreviation: NL, normalisation level.
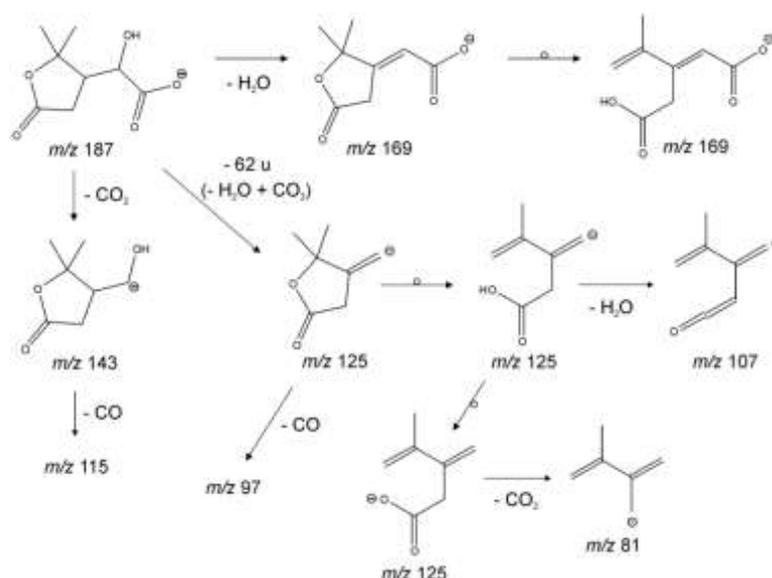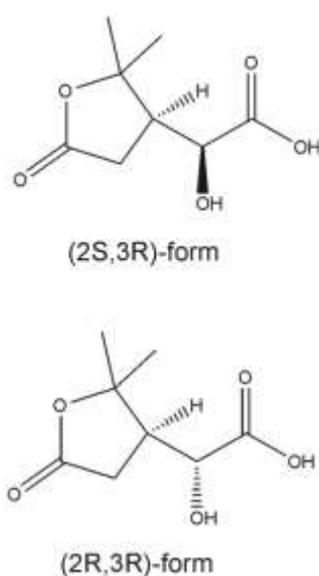
Figure 22. Fragmentation pathways for 2-hydroxyterpenylic acid.

Assignment of 2-hydroxyterpenylic acid diastereoisomers:

Considering that 2-hydroxyterpenylic acid is formed from the oxidation of (-)α-pinene which has a 1S,5S configuration for its two chiral C-atoms, the stereochemistry in the resulting C-3 position of the oxidation product is fixed. Also for terpenylic acid the chiral C-3 atom has a S configuration. However, the introduction of an OH-group at the neighbouring position in 2-hydroxyterpenylic acid, changes the order of priorities according to the Cahn-Ingold-Prelog nomenclature (Moss, 1996), resulting in a 3R configuration for 2-hydroxyterpenylic acid. The stereochemistry for the other chiral C-2 atom can be either S or R. Based on theoretical considerations the major diastereoisomer in ambient fine aerosol [Figure 21(B)] was assigned to the 2R,3R diastereoisomer as it is more polar in comparison to the (2S,3R) 2-hydroxyterpenylic acid (Figure 23). Derived dipole moments for the R,R-form were 5.5, 7.2 and 7.3 Debye (D) in the gas phase, methanol and water, respectively. In comparison to the S,R-form, which had dipole moments of 4.2, 5.1 and 5.1 D in the gas phase, methanol and water, respectively, a much higher polarity was hence observed for the (2R,3R) 2-hydroxyterpenylic acid, explaining its earlier retention time in reversed-phase LC.

(2S,3R)-form

(2R,3R)-form

Figure 23. Structures of the major (bottom) and minor (top) 2-hydroxyterpenylic acid diastereosiomers observed in ambient fine aerosol.

Temporal evolution of the major 2-hydroxyterpenylic acid 2R,3R diastereoisomer:

The temporal evolution of the targeted MW 188 compound, which elutes at 16.4 min and is attributed to the 2-hydroxyterpenylic acid 2R,3R diastereoisomer (Figure 23), and of other known oxidation products was examined in an **α-pinene** photo-oxidation experiment, together with the SOA mass formation as a function of irradiation time. It was found that the concentrations of all the studied oxidation products increased until a maximum was observed for most of the markers at 5 hours of irradiation. The most abundant compound was diaterpenylic acid acetate (m/z 231), followed by terpenylic acid (m/z 171), cis-pinic acid (m/z 185), cis-pinonic acid (m/z 183), MBTCA (m/z 203), terebic acid (m/z 157) and the targeted MW 188 compound at the maximum. A further significant formation was only observed for MBTCA, a known ageing compound (Szmigielski et al., 2007), whereas for terebic acid and the MW 188 compound only a marginal increase was detected until the chamber experiment was stopped after 7 hours. All the other oxidation products decreased after 5 hours of irradiation, although an on-going SOA mass formation was observed, pointing to particle-phase reactions that lead to additional aerosol growth. However, based on the observed product evolution, the 2-hydroxyterpenylic acid 2R,3R diastereoisomer cannot be assigned to an ageing marker from this laboratory experiment. Compared to the formation of terpenylic acid, that of 2-hydroxyterpenylic acid involves one additional oxidation step; hence, it is logical to propose that 2-hydroxyterpenylic acid is a higher-generation product of the α-pinene oxidation cascade.

An α-pinene SOA marker with MW 188 that is abundantly present in ambient fine aerosol from vegetated sites has been structurally assigned to the 2-hydroxyterpenylic acid 2R,3R diastereosiomer. The other less abundant isomer could be attributed to the 2-hydroxyterpenylic acid 2S,3R diastereoisomer. Based on the results of a time-resolved α-pinene photo-oxidation experiment it cannot be concluded that the 2-hydroxyterpenylic acid 2R,3R diastereoisomer is as MBTCA a suitable marker for aged α-pinene SOA as previously suggested, but rather should be regarded as a higher-generation product of the α-pinene oxidation cascade.

Chemical characterisation of sulfated SOA tracers from isoprene and unsaturated C5 and C6 aldehydes

In this project, the focus was on the structural characterisation of polar OSs from isoprene, the C5 unsaturated aldehyde 2-*E*-pentenal, and the C6 unsaturated aldehydes 3-*Z*-hexenal and 2-*E*-hexenal, which show relative abundances in ambient fine aerosol that are comparable to those of the major isoprene SOA-related OSs, i.e. the sulfates esters of the 2-methyltetrols. As to isoprene, the emphasis was on the characterisation of

additional isoprene SOA-related OSs, which have not been covered in earlier work or require a revision of their structure.

Chamber aerosol samples: SOA from 2-*E*-pentenal, 2-*E*-hexenal and 3-*Z*-hexenal was generated in the 14.5 m^3 stainless-steel EPA chamber with 40 μm Teflon-coated walls (Kleindienst et al., 2007). The temperature, aerosol size distribution, and relative humidity, as well as the O_3, nitric oxide (NO) and NO_x concentrations were continuously measured. OH radicals were generated from the NO_x-mediated photochemical chain reactions. Different seed aerosols were used to create different acidity levels in the chamber, either sulfuric acid alone or a mixture of sulfuric acid and ammonium sulfate (1/1; w/w). Experiments were conducted in the dynamic mode (i.e., continuously stirred tank reactor) with a residence time of approximately 4 hr. NO was continuously added from a high-pressure cylinder to the reaction chamber through a mixing manifold. The SOA precursors were introduced by air flow through the neat liquid in a temperature-controlled bath. The steady-state nature of the chamber operation allows for filter sampling for extended periods, providing sufficient aerosol mass for determining the composition of the resultant SOA. Once steady-state conditions were attained (24 h), samples for determining the composition of the SOA were collected on Teflon-impregnated glass fiber filters (Pallflex Fiberfilm, Pall Corporation, Port Washington, NY, USA).

Atmospheric aerosol samples: Pooled filter samples, which were collected during a summer field campaign from K-puszta, Hungary, in 2006 were used. Details on the measurement campaign can be found in Maenhaut et al. (2008). The pooled filter samples were prepared as described in Shalamzari et al. (2013).

Organic synthesis: Organosulfates of 3,4-dihydroxy-2-butanone used for the characterisation of an isoprene SOA-related OS with MW 184 were prepared according to Figure 24.
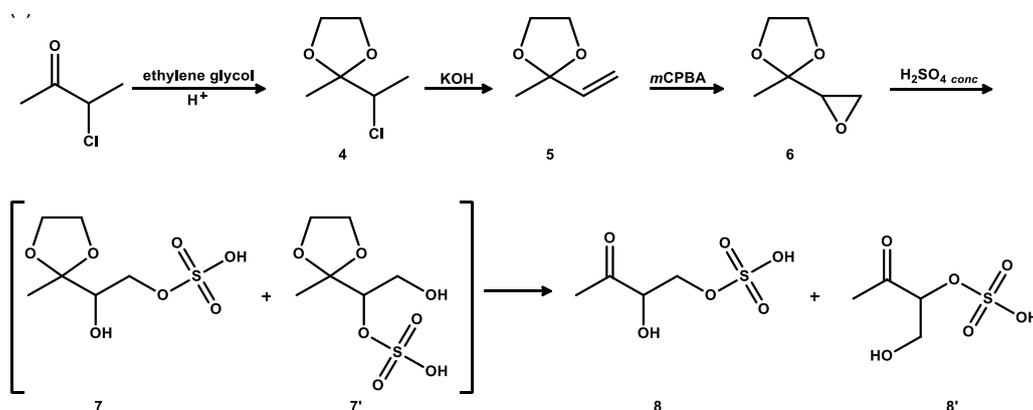

Figure 24. Synthetic procedure leading to organosulfates of 3,4-dihydroxy-2-butanone.

Sample workup: Chamber-generated SOA and ambient filter samples were extracted with methanol. Extracts from isoprene SOA and ambient aerosol were reacted with 2,4-dinitrophenylhydrazine (DNPH) to derivatise the keto group.

Chemical analysis: LC/MS analysis was carried out using a Surveyor Plus system (pump and autosampler) (Thermo Scientific, San Jose, CA, USA) connected to an Atlantis T3 column (2.1 x 150 nm, 3 μm particle size, Waters), providing polar retention for organosulfates. The mobile phase consisted of (A) 50 mM ammonium formate buffer with pH 3 and (B) methanol. In selected cases, use was made of ion-pairing LC employing an Hypersil C18 Gold column (3 μm; 2.1 x 150 mm) (Thermo Scientific, PA, USA) and dibutylammonium acetate as ion-pairing reagent, following a procedure reported in Wang et al. (2013). Details of the applied LC gradients can be found in Shalamzari et al. (2013, 2014). High-resolution MS measurements were performed on an Orbitrap mass spectrometer.

Isoprene SOA-related OSs:

Figure 25 shows selected LC/MS data obtained for K-puszta fine aerosol, including a base peak chromatogram (BPC) and extraction ion chromatograms (EICs) at *m/z* 215, 199, 183, 169 and 155, corresponding to OSs that are related to isoprene SOA. The most abundant polar OSs are the *m/z* 215 compounds (RT 2.58 min), which are well-known compounds and correspond to isomeric 2-methyltetrol OSs. It can be seen from the EIC data that the other targeted OSs at *m/z* 199, 183, 169 and 155 are also rather abundant, with an abundance for the major ones at each *m/z* value higher than 10% of that of the *m/z* 215 compounds. Of these, the major *m/z* 199, 169 and 155 compounds were already examined in previous work and could be assigned to/confirmed as sulfate esters of 2-methylgyceric acid, glycolic, and lactic acid.

The *m/z* 183 OS was found to correspond to an unknown OS and therefore its chemical structure was elucidated. Detailed interpretation of LC/(–)ESI-MS data, including MS[2] and MS[3] ion trap data and MS[2] accurate mass data of the underivatised compound and its DNPH-derivative, and synthesis of reference compounds, led to its assignment as the sulfate ester of 3,4-dihydroxy-2-butanone with the sulfate group located at the C-3 position (compound 8' in Figure 24). This novel OS can be related to methyl vinyl ketone, which, together with methacrolein, is a major gas-phase oxidation product of isoprene (Pierotti et al., 1990). Recent research demonstrated that this MW 184 OS can be explained by sulfation of methyl vinyl ketone in the particle phase through reaction with the sulfate radical anion (Schindelka et al., 2013). An overview of the organosulfates related to gas-phase oxidation products of isoprene (i.e. C_5-epoxydiol, methacrolein, methyl vinyl ketone, glyoxal and methyl glyoxal) is presented in Figure 26.
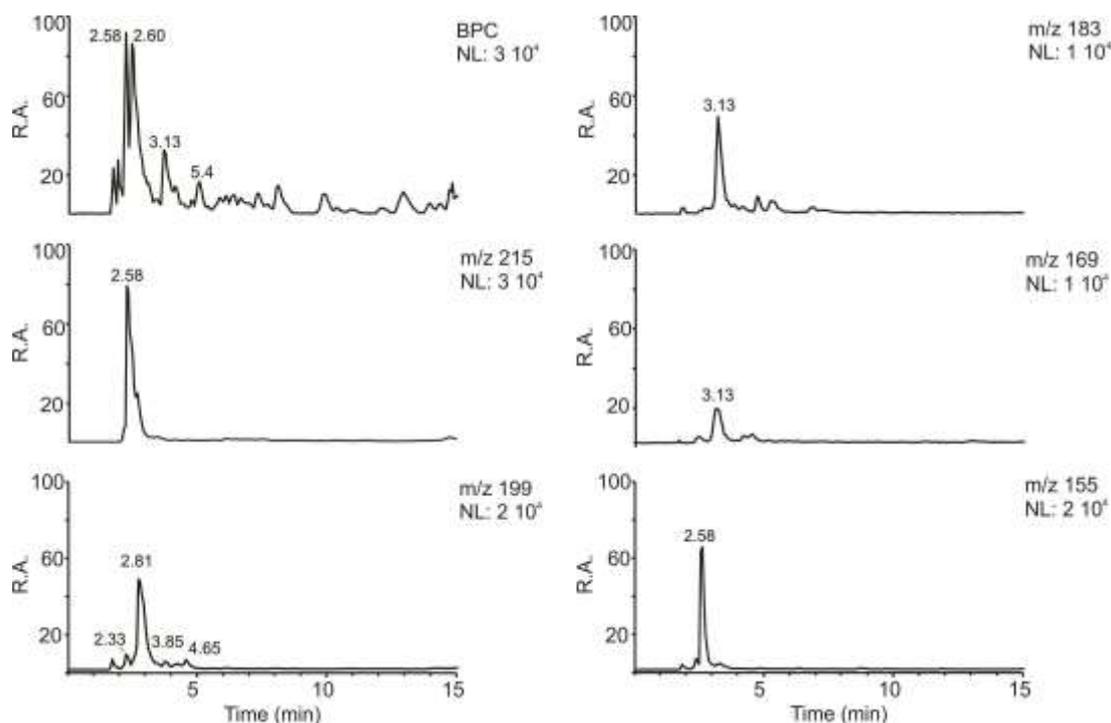
Figure 25. Selected LC/MS chromatographic data [base peak chromatogram (BPC) and extracted ion chromatograms (EICs)] obtained for K-puszta PM$_{2.5}$ aerosol. Abbreviation: NL, normalisation level.

3-Z-hexenal SOA-related OSs:

Two MW 226 organosulfates that are specific to 3-Z-hexenal and have a substantial abundance in ambient fine aerosol were structurally elucidated using detailed interpretation of MS data as isomeric sulfate esters of 3,4-dihydroxyhex-5-enoic acid with the sulfate group located at the C-3 or C-4 position (Figure 27). The formation of the MW 226 OSs is tentatively explained through photooxidation of 3-Z-hexenal in the gas phase resulting in an alkoxy radical, followed by a rearrangement, and subsequent sulfation of the epoxy group in the particle phase (Figure 28).

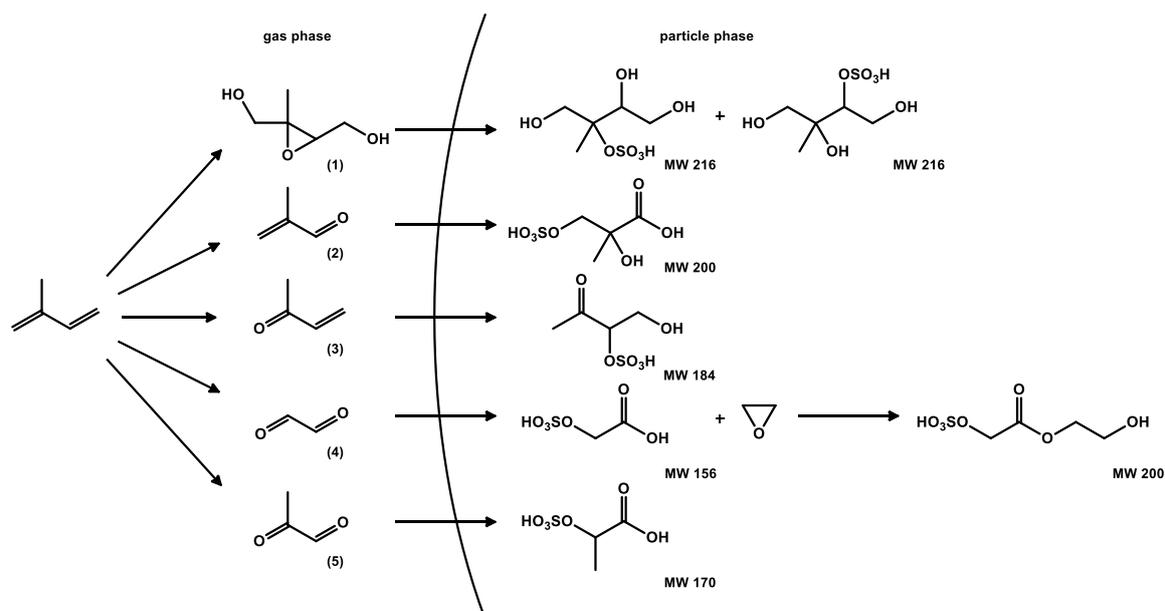Figure 26. Overview of the organosulfates related to the following gas-phase oxidation products of isoprene: (1) C$_5$-epoxydiol; (2) methacrolein; (3) methyl vinyl ketone; (4) glyoxal; and (5) methyl glyoxal.
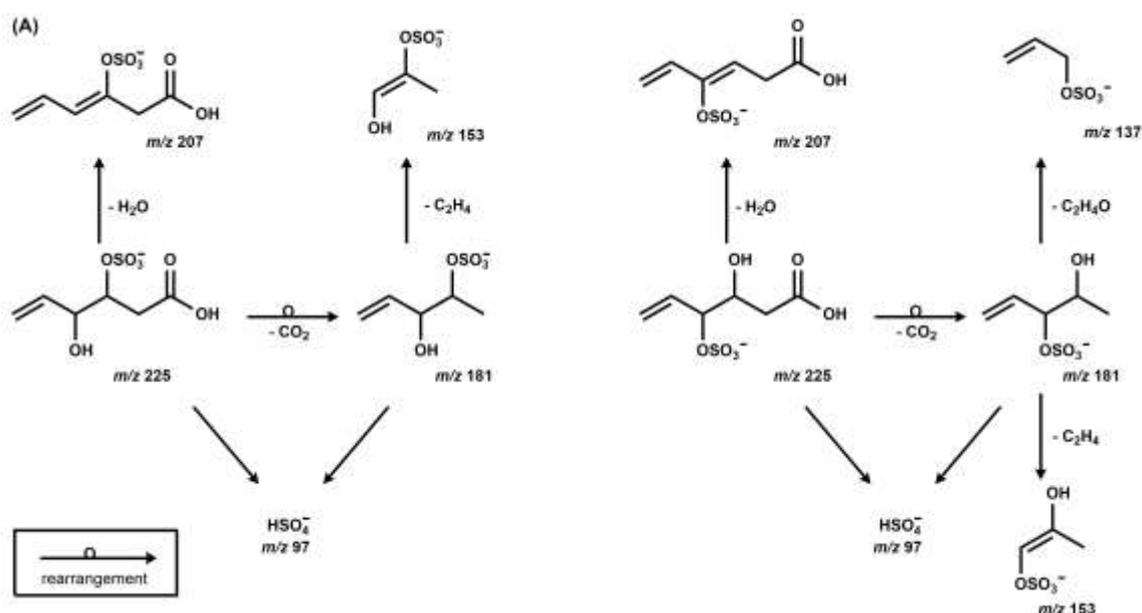

Figure 27. Fragmentation routes for deprotonated MW 226 compounds, related to 3- Z-hexenal SOA, which are assigned to sulfate esters of 3,4-dihydroxyhex-5-enoic acid with the sulfate group at C-3 (left) and C-4 (right).
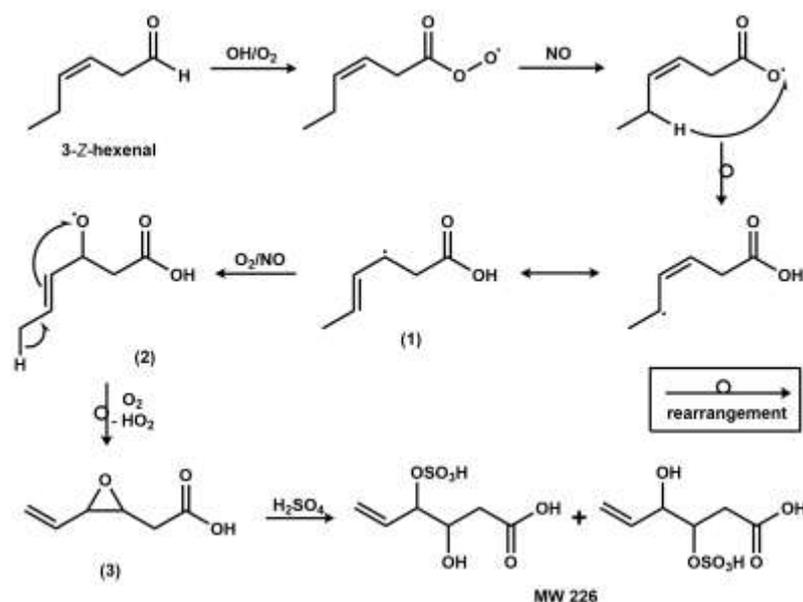
Figure 28. Proposed formation pathway for the MW 226 OSs from 3-Z-hexenal.

2-E-pentenal, 2-E-hexenal and 3-Z-hexenal SOA-related OSs:

A series of OSs with MWs 230, 214 and 170 were found to be formed from the C_5 unsaturated aldehyde 2-E-pentenal, which were also detected in SOA from 2-E-hexenal and 3-Z-hexenal and were observed at substantial concentrations in ambient fine aerosol. As 2-E-pentenal is a photolysis product of 3-Z-hexenal (O' Connor er al., 2006) the detection of 2-E-pentenal-related OSs appears reasonable. Selected LC/MS chromatographic data obtained for K-puszta fine aerosol are shown in Figure 29.

Figure 29. Selected LC/MS chromatographic data using regular RP-LC obtained for ambient fine aerosol, including a base peak chromatogram (BPC) and extracted ion chromatogram (EICs) at *m/z* 215, 169, 213 and 229, corresponding to the deprotonated forms of OSs related to isoprene (*m/z* 215) and OSs related to 2-E-pentenal (*m/z* 229, 213, and 169).
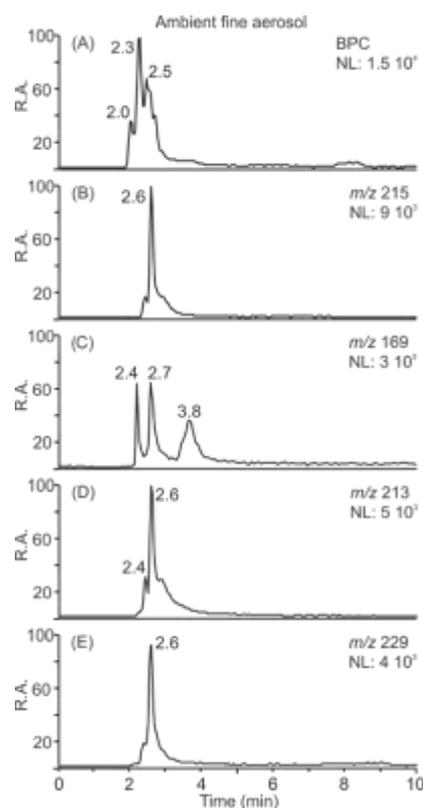
The MW 230 OSs were structurally assigned to stereoisomeric forms of the sulfate ester of 2,3,4-trihydroxypentanoic acid, with the sulfate group located at the C-3 position (Figure 30). A possible formation pathway leading to isomeric MW 230 organosulfates is proposed in Figure 31. Reaction (1) involves abstraction of a hydrogen atom by the OH radical, resulting in a C_5-radical which has two resonance forms. In a following reaction,

the C$_5$-radical with the radical located at C-2 can react with O$_2$ and the OH$_2$ radical (or a RO$_2$• radical), resulting in a C$_5$-hydroperoxide [reactions (2) and (3)]. The next reaction (4) involves a rearrangement of the C$_5$-hydroperoxide into a C$_5$-epoxyhydroxide. To our knowledge, such a rearrangement reaction has not been reported so far in the formation of SOA from BVOCs; however, it is well known that hydroperoxides resulting from the enzymatic oxidation of unsaturated fatty acids such as linoleic acid through the action of lipoxygenase are instable and undergo an acid-catalysed non-enzymatic rearrangement into epoxyhydroxy derivatives (Gardner et al., 1994). It is proposed that a similar acid-catalysed rearrangement may occur in the case of the C$_5$-hydroperoxide and that this reaction takes place in the particle phase. Subsequent oxidation [reaction (5)] and sulfation of the epoxy group [reaction (6)] in the particle phase results in stereoisomeric OSs of 2,3,4-trihydroxypentanoic acid with the sulfate group located at the C-3 position.

Figure 30. Fragmentation routes for the deprotonated MW 230 compound, related to 2-E-pentenal SOA and assigned to an organosulfate of 2,3,4-trihydroxypentanoic acid with the sulfate group located at the C-3 position.

Figure 31. Proposed formation pathways leading to MW 230 organosulfates related to 2-*E*-pentenal, which are assigned to organosulfates of 2,3,4-trihydroxypentanoic acid with the sulfate group located at the C-3 position.

The MW 214 OSs could be assigned to isomers of 2,3-dihydroxypentanoic acid with the sulfate group located at the C-2 or C-3 positions, whereas the MW 170 OSs were found to be decarboxylation products of the MW 214 compounds (Figure 32). A possible formation pathway leading to the MW 214 organosulfates is proposed in Figure 33. The pathway involves epoxidation of the double bond of 2-*E*-pentenal with ozone, oxidation of the aldehyde to a carboxylic acid group, and reaction of the epoxy group with sulfuric acid in the particle phase.
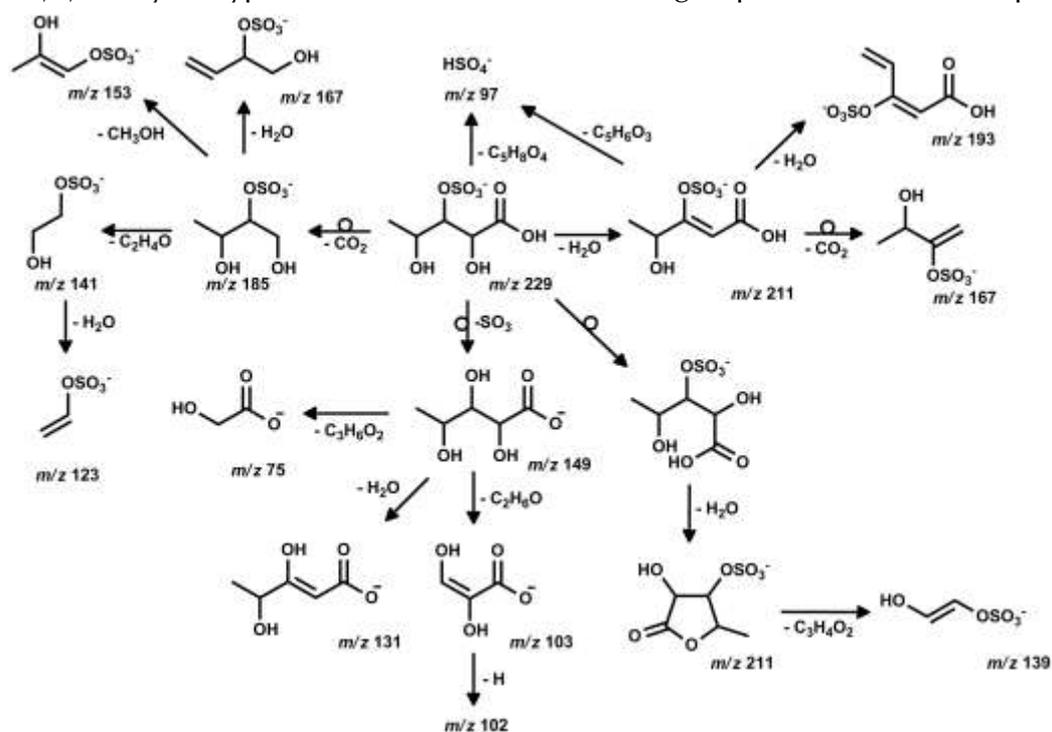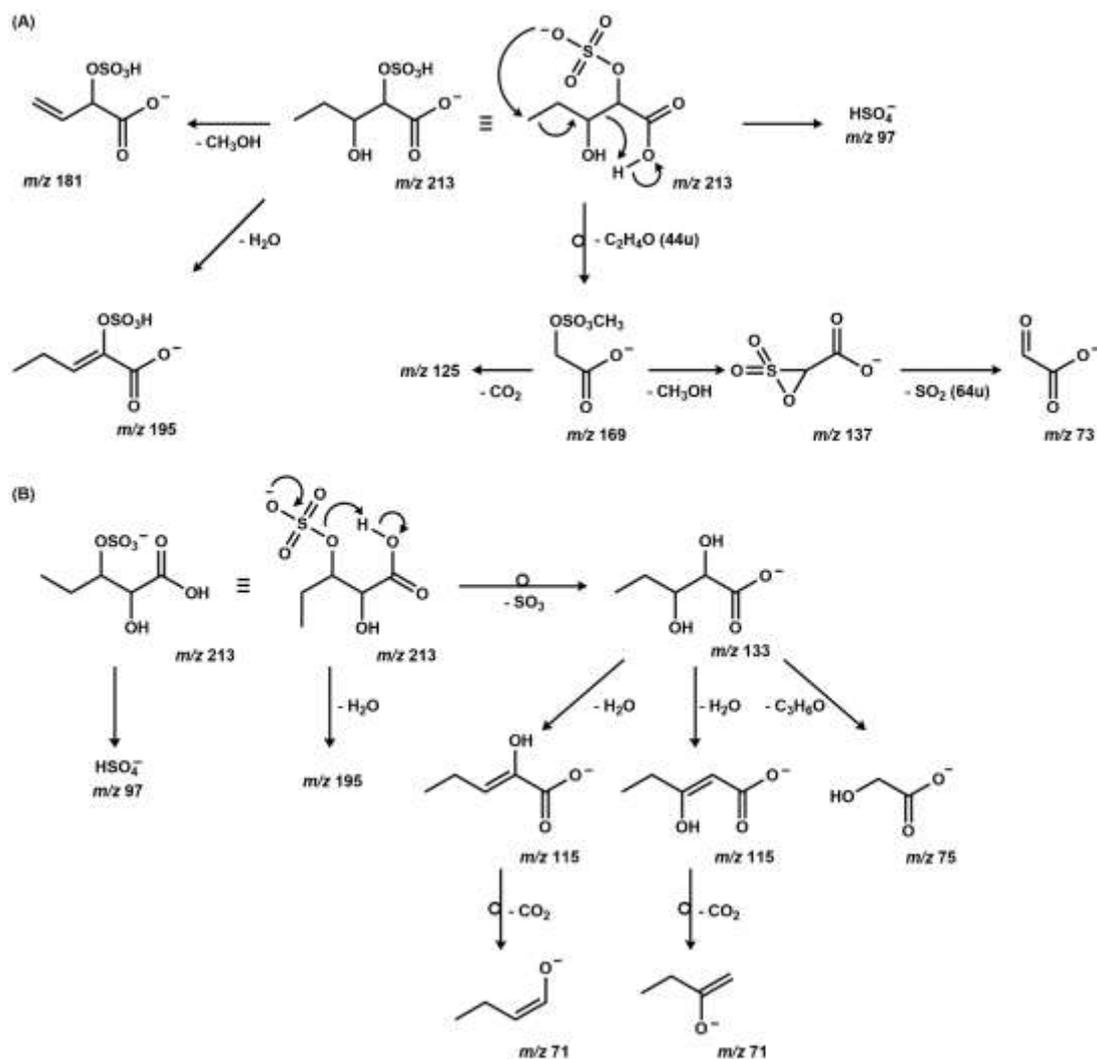
Figure 32. Proposed fragmentation routes for the MW 214 compounds, related to 2-E-pentenal SOA and assigned to organosulfates of 2,3-dihydroxypentanoic acid with the sulfate group located at the C-2 or C-3 positions, on the basis of detailed interpretation of MS^2, MS^3, MS^4, and accurate mass data.
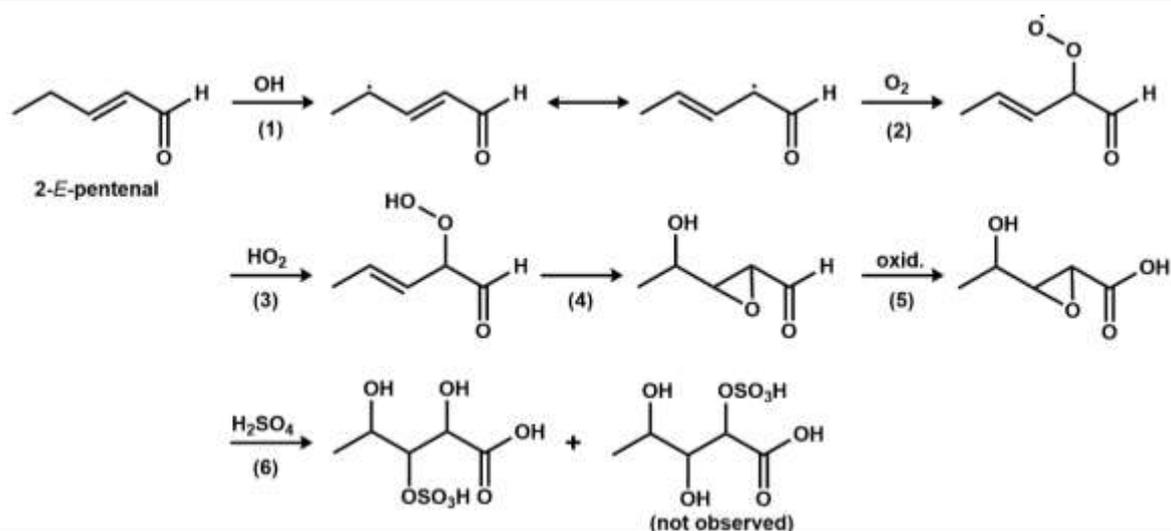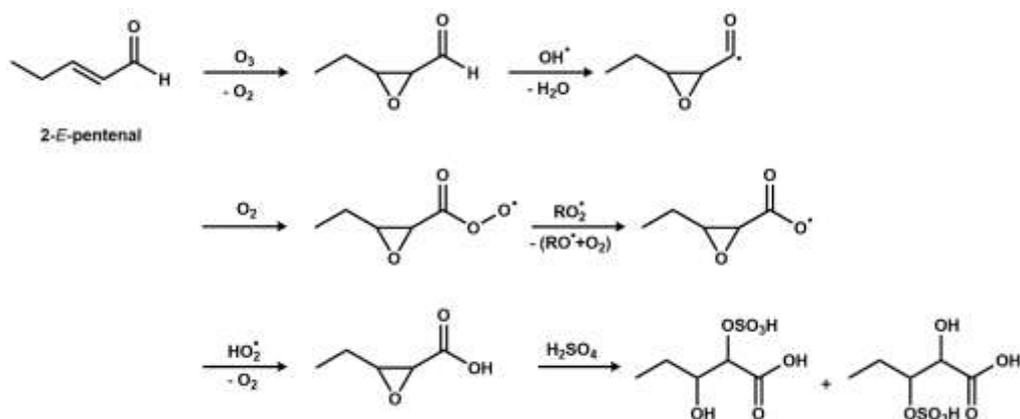

Figure 33. Formation pathway leading to MW 214 compounds related to 2-E-pentenal, assigned to organosulfates of 2,3-dihydroxypentanoic acid.

Detailed interpretation of LC/MS data, including MS^2, MS^3, MS^4 and accurate mass data, and synthesis of reference compounds, led to the structural characterisation of polar organosulfates that are present in ambient fine aerosol and are related to SOA from isoprene and green leaf volatiles, i.e. the C_5 unsaturated aldehyde 2-*E*-pentenal and the C_6 unsaturated aldehydes 3-*Z*-hexenal and 2-*E*-hexenal. Novel sources for polar organosulfates have been identified as methyl vinyl ketone, a major gas-phase oxidation product of isoprene, and 2-*E*-pentenal, a photolysis product of the green leaf volatiles 3-*Z*-hexenal. Possible formation pathways involving sulfation of an epoxy-containing intermediate have been suggested.

Development of analytical methodology based on LC/ESI-MS for quantifying the contributions of individual BVOCs to the OA

For this task, analytical methodology using LC/(−)ESI-MS based on ion-pairing chromatography was evaluated for the determination of polar organosulfates such as the isoprene SOA tracers, the 2-methyltetrol sulfates. The developed method was apllied to the separation of polar organosulfates from 2-*E*-pentenal, 2-*E*-hexenal and 3-*Z*-hexenal (Task 3.3).

An Hypersil C18 Gold column (150 x 2.1 mm; 3 µm) (Thermo Scientific) was used. Dibutylammonium acetate (DBAA) was employed as ion-pairing (IP) reagent. The mobile phases consisted of 50 mM DBAA in water (A), acetonitrile (B), and water (C). The applied 70 min gradient elution program was as follows: the concentration of eluent A was kept at 10% during the whole 70 min program; the concentration of water (C) was kept at 3% for 10 min, then increased to 87% in 15 min, kept at 87% for 25 min, then decreased to 3% in 10 min, and kept at 3% for 10 min. A mixture of four commercially available compounds including three organosulfonates as surrogate compounds, i.e. methanesulfonate, ethanesulfonate, 2-propanesulfonate, and D-galactose 6-sulfate, was employed to develop the ion-pairing LC/MS method.

In a first series of experiments, only IP reagent was used in the mobile phase and methanol was compared with acetonitrile as mobile phase (B). Satisfactory retention times for the test compounds were obtained with acetonitrile but were too long with methanol. However, using this system peak broadening was observed for galactose sulfate. In a second series of experiments, IP reagent was added to the injection mixture, which resulted in satisfactory peak shapes for the four test compounds [Figure 34(A)]. Adding the IP reagent directly to the reconstitution solution has been reported to be successful in the ion-pairing LC/MS analysis of an organophosphate drug metabolite (Zhao et al., 2013). We further evaluated whether satisfactory peak shapes could still be achieved upon omitting the IP reagent from the mobile phase. However, this approach

turned out to lead to co-elution of the three sulfonic acids, although with satisfactory peak shape, and a poor peak shape for galactose sulfate. Hence, further work was performed with IP reagent being present both in the mobile phase and the reconstitution solution. To evaluate the sensitivity of the ion-pairing LC/MS method, standards at 7 concentrations spanning the range 0.002 ng – 1.5 ng mL^{-1} were prepared and an aliquot of 5 µL was injected. The test compounds could be detected with a S/N ratio of about 10 for an amount injected on column of 3.7 ng, 0.04 ng, 0.03 ng, and 0.02 ng, for methanesulfonate, ethanesulfonate, 2-propanesulfonate, and D-galactose 6-sulfate, respectively, demonstrating the sensitivity of the method.

Figure 34(A) shows selected LC/MS data obtained for a standard mixture (corresponding to 8.3 ng, 10.3 ng, 20.5 ng and 10 ng injected on column for methanesulfonate, ethanesulfonate, 2-propanesulfonate, and D-galactose 6-sulfate, respectively), including a BPC and EICs at m/z 191, 109, 123, and 259, corresponding to an adduct ion of methanesulfonate (i.e. $CH_3SO_3H:CH_3SO_3^-$), ethanesulfonate, 2-propanesulfonate, and D-galactose 6-sulfate, respectively. It can be seen that ethanesulfonate (m/z 109) is also detected, owing to the formation of an adduct ion with sodium acetate (82 Da) which is present in the system (acetate is the anionic part of the IP reagent). In a following step, the method was applied to an ambient aerosol sample, i.e. an extract of K-puszta fine aerosol containing polar organosulfates, which was investigated in detail in a previous study (Shalamzari et al., 2013).

Figure 34 presents the comparison of selected LC/MS data for K-puszta fine aerosol obtained with the developed ion-pairing method (B) and the method using the T3 column (C). BPCs and EICs at m/z 195, 215, 199, and 183 corresponding to sulfate and abundant OSs that are related to isoprene SOA are shown. It can be seen that the ion-pairing method provides better retention for the targeted OSs (i.e. OSs of 2-methyltetrols (m/z 215), 1,2-dihydrobutan-3-one (m/z 183), and 2-methylglyceric acid (m/z 199)) compared to the method based on the T3 column, where the 2-methyltetrol OSs are only partially separated from sulfate and 2-methylglyceric acid OS. Sulfate (RT 9.99 min) elutes as a broad tailing peak after the OSs of the 2-methyltetrols (m/z 215) (RTs 4.26 and 4.87 min), which are baseline-separated, and a 1,2-dihydroxy-3-butanone OS containing the sulfate group at the 1-position (m/z 183) (RT 5.51 min). Furthermore, a better chromatographic separation of m/z 199 OSs could be achieved compared to the T3 method with the major compound, 2-methylglyceric acid OS containing the sulfate group at the terminal position (RT 13.15 min) being separated from other isobaric m/z 199 compounds.
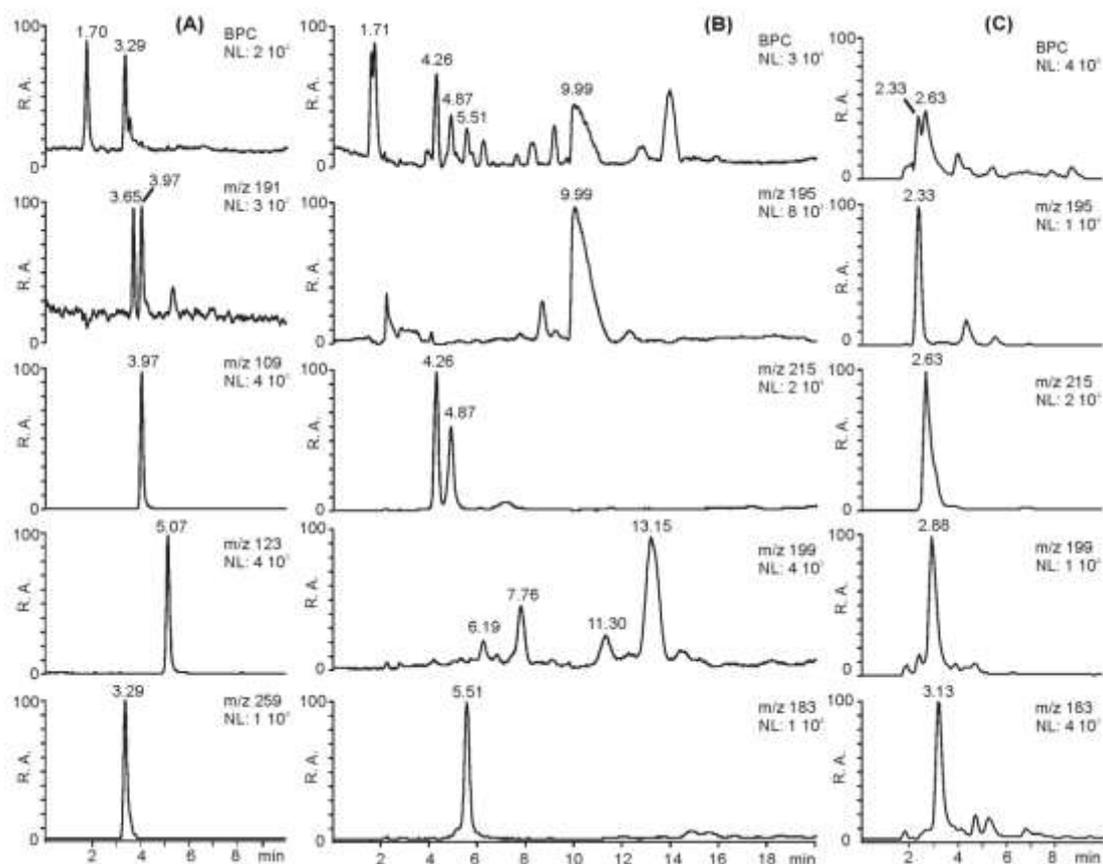
Figure 34. Selected LC/($-$)ESI-MS data [i.e. base peak chromatograms (BPCs) and extracted ion chromatograms (EICs)] for (A) a test mixture containing methanesulfonate (8.3 ng) (m/z 191), ethanesulfonate (10.3 ng) (m/z 109), 2-propylsulfonate (20.5 ng) (m/z 123), and D-galactose 6-sulfate (10 ng) (m/z 259) analysed with the developed ion-pairing method; (B) K-puszta fine aerosol containing sulfate (m/z 195) and sulfate esters of 2-methyltetrols (m/z 215), 2-methylglyceric acid (m/z 199), and 1,2-dihydroxy-3-butanone (m/z 183) analysed with the same ion-pairing method as for (A); and (C) the same K-puszta fine aerosol analysed with a method previously reported using a C18 T3 column (Shalamzari et al., 2013).

Experimental determination of the rate coefficient of the reaction of OH with hydroxyacetone, CH₃C(O)CH₂OH

Hydroxyacetone is an oxidation product of isoprene. Its oxidation by OH forms mainly methylglyoxal, an SOA-precursor (Liu et al., 2012). However, whereas five groups reported rate coefficient values k(290 - 300 K) of $(2.5 - 3.5) \times 10^{-12}$ cm^3 s^{-1} and one group a positive T-dependence (Baasandorj et al. 2009), Dillon et al. (2006) measured k(298 K) of 6.1×10^{-12} cm^3 s^{-1}, with a negative T-dependence.

We measured this rate constant using Pulsed Laser Photodissociation - Laser Induced Fluorescence, PLP-LIF. The OH radicals were generated pulse-wise by 248 nm excimer laser photolysis of H₂O₂ at pulse energies of only ~1 mJ/pulse, to keep photodissociation of HYAC and hence interfering product-radical reactions negligible.

Time-resolved [OH] decays at large excess HYAC were monitored by LIF at 282 nm, and this for a wide range of HYAC concentrations. The HYAC concentrations were determined from accurately measured gas-mixture flows with known HYAC partial pressure. The OH-decays in these conditions are perfectly exponential, showing no sign of OH-regeneration. The bimolecular rate coefficient is derived from the slope of the first-order decay rates versus [HYAC]. Temperature range is 290 - 500 K.

We measured the rate coefficient at pressures of 50 Torr He finding $k(298 \text{ K})$ = $(5.8\pm0.4)\times10^{-12}$ cm^3 s^{-1}, with a slight negative T-dependence over 290 - 380 K in agreement with Dillon et al. (2006), but reverting to a positive T-dependence for T = 410 - 500 K. We reconciled our and Dillon's results with the much lower k(T) values and positive T-dependence for the entire T-range found by of Basaandorj et al. (2009) at pressures of 2 - 5 Torr He, by showing that the k(T) exhibits pressure-dependence below 20 Torr. We ascribe this to the reaction proceeding through a pre-reactive complex and a submerged transition state, as we confirmed theoretically. The theoretical work also shows that the reaction proceeds by abstraction of the α-hydroxy-H, leading to methylglyoxal. This work was published (Vu et al., 2013).

WP4. Global modelling of organic aerosols

Parameterisation of SOA formation due to terpenoid compounds

In our previous work, a parameterisation for SOA formation was developed, based on BOREAM calculations (Ceulemans et al., 2011). This parameterisation reproduces the quasi-steady-state equilibrium SOA concentrations simulated with continuous α-pinene emissions as well as ventilation/deposition losses. It accounts for water uptake and NO_x dependence. SOA ageing processes included in BOREAM are implicitly taken into account, and lead to higher SOA yields than in previous parameterisations based on laboratory data. Those processes include not only the gas-phase oxidation of condensable compounds, but also the particle-phase photolysis of SOA compounds.

However, the parameterisation failed to reproduce the temporal dependence of SOA formation, primarily because it did not account for the SOA sinks due to photochemical transformation of condensable species into more volatile compounds. A revised parameterisation has been therefore developed. It accounts for this photochemical loss through the photolysis of the lumped condensable compounds. The photolysis rates, yields and partitioning coefficients of the condensable species are adjusted based on BOREAM calculations (Ceulemans et al., 2012).

Global impact of BVOC emissions on organic aerosol distribution

The IMAGES CTM includes emissions of Primary Organic Aerosol (POA) and an SOA module including partitioning of semi-volatile organics from isoprene, terpenes, and aromatics, as well as irreversible uptake of dicarbonyls by aerosols and clouds. The model results were compared to many other global aerosol models in the framework of the AEROCOM intercomparison (Tsigaridis et al., 2014). However, comparisons with in situ measurements revealed that, as in the case of many other models, the simulated OC concentrations are (i) largely underestimated over polluted areas, and (ii) overestimated over biogenically-influenced regions. In order to better match the observations, an additional OA source was included, equal to 3-5 times the anthropogenic POA source, and the SOA production due to monoterpene oxidation in low-NO_x conditions was reduced by a factor of 5. Previous analyses (Spracklen et al., 2011; Heald et al., 2011) have pointed to the existence of a large OA source over anthropogenically-influenced regions, of the order of 100 Tg yr^{-1}. Its precise nature is unclear, but SOA likely makes up for a large fraction. The additional source included in the model amounts to 68 Tg yr^{-1}; the global SOA source amounts to 53 Tg yr^{-1}. The IMAGES simulations were evaluated against ground-based and airborne organic carbon (OC) measurements. The comparison with ground-based measurements is summarized in TABLE VII.

TABLE VII. Averaged OC (μg m^{-3}) measured at ground stations and simulated using either the unadjusted (U) or adjusted (A) model. *n* is the number of stations.

	n	**obs.**	model (U)	model (A)
U.S. (IMPROVE network)	164	**1.1**	0.7	1.1
Europe (EMEP)	33	**3.1**	0.7	2.5
Europe (exc. EMEP)	29	**2.9**	0.8	2.4
China/Korea	20	**6.7**	1.6	5.2
India/Nepal	11	**7.9**	2.6	8.9
Africa & S. America	15	**8.0**	4.5	5.2

The model bias is strongly reduced by the OA source adjustment. The model often overestimates the observations at tropical sites during the wet season, confirming that the biosphere is only a moderate source of organic aerosol in absence of a strong anthropogenic influence. The seasonal variation of OC is fairly well reproduced over polluted areas (Figure 35). Over the S-E U.S., the overestimated seasonal amplitude suggests an overestimated role of biogenic SOA. For more details on this comparison, see Stavrakou et al. (2013).
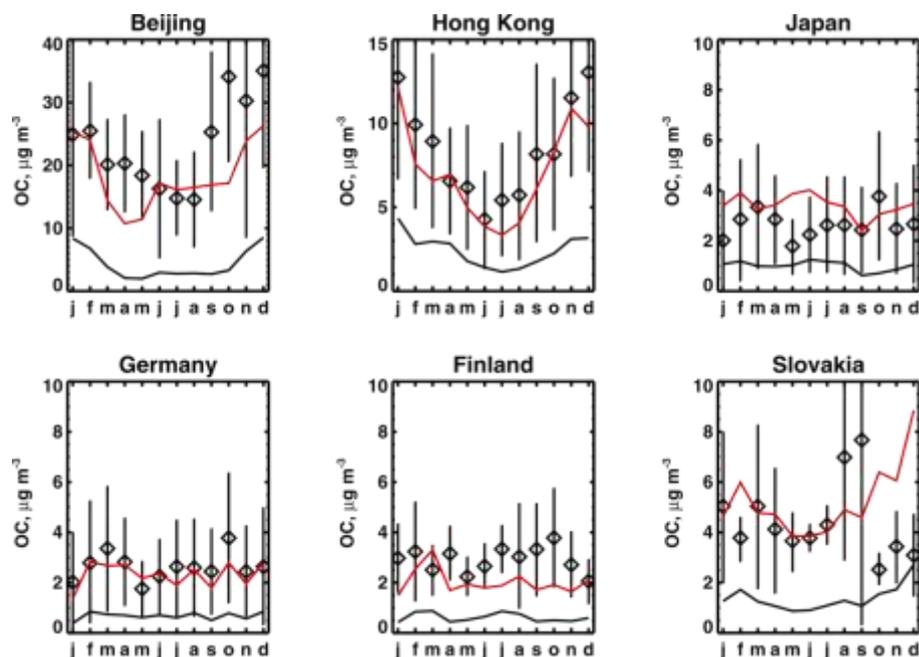

Figure 35. Seasonal variation of OC (μg m^{-3}) at different sites (Bahadur et al., 2009), and comparison with modelled values using unadjusted (black) or adjusted OA sources (red).

3. POLICY SUPPORT

Our project addresses two major environmental issues: air pollution and the role of the biosphere in climate change.

It is now well admitted that climate change is happening and affects the composition of the atmosphere and the abundance of climate agents such as methane, tropospheric ozone and secondary organic aerosol. The climate forcing of those agents is not well quantified, e.g. due to a poor understanding of aerosol composition. The better assessment made possible by our results should contribute to a better understanding and quantification of climate-chemistry feedbacks.

The adverse effects of air pollution are receiving increased attention. It is estimated that air pollution claims the lives of over 3 million people globally, due to short-term respiratory and cardiac effects as well as long-term cancer and other metabolic and cellular effects, according to the Global Burden of Diseases study published in The Lancet in 2012. In Europe, despite emission regulations, air pollution is believed to cut human lives by about eight months, according to the European Environmental Agency. Fine particulate matter is considered the most serious air pollution risk in Europe, followed by ozone, especially in Mediterranean countries where sunlight is abundant. Both tropospheric ozone and organic aerosols (the single largest component of fine particulate matter over continents) are to a large extent formed in the air as the result of reactions involving biogenic organic compounds and anthropogenic pollutants. The main result of BIOSOA, i.e. the improved characterisation and quantification of the role of biogenic hydrocarbons should provide useful support to policies aiming at the mitigation of air pollution.

Although not directly related to BIOSOA, partner P3 has performed research requested by the Flemish Environment Agency within the frame of the European Life+ATMOSYS project. PM10 samples taken by VMM at different locations in Flanders were analysed. It was found that wood burning in Flanders contributes, on average, with about 10% to the PM10 mass in winter. Flanders struggles to comply with the EU regulation that allows exceeding the daily PM10 limit value of 50 $\mu g/m^3$ at maximum on 35 days per year at any location. Since most of those exceedances occur in winter, cutting down on wood burning in winter would definitely help. It was estimated that the number of exceedance days would be cut in half in the absence of wood burning. This information was provided to the Flemish minister of the environment Joke Schauvliege and it is certainly of use for decision making.

4. DISSEMINATION AND VALORISATION

Dissemination has been mostly done through publications in international journals and presentations at international conferences. Articles were published in peer-reviewed journals with high impact factor and/or broad distribution, e.g. Nature Geoscience, Atmospheric Chemistry and Physics, Journal of Geophysical Research, and Environmental Science and Technology, and also leading journals on physical chemistry, analytical chemistry and/or instrumental techniques and methods. Presentations were given at international conferences, such as organised by the European Network for Atmospheric Composition Change (ACCENT), by the programme EuroVOL of the European Science Foundation, and by the projects iLEAPS, SOLAS and IGAC of the International Geosphere-Biosphere Programme, and furthermore at the International Conferences on Gas Kinetics, the Atmospheric Chemical Mechanisms (ACM) meetings, the Spring Meeting of the American Chemical Society (ACS), the prestigious Telluride Conference, the European and International Aerosol Conferences, the General Assembly of the European Geosciences Union (EGU), and the Fall Meeting of the American Geophysical Union (AGU). Several of those presentations (Telluride, ACM, AGU,...) were solicited.

The research results were also presented at workshops and reports aiming at the transfer of knowledge to policy advisers and the general public. The research results were also disseminated through a comprehensive review article dealing with the identification of organic compounds (Nozière et al., 2015) for publication in a special issue of Chemical Reviews on « Chemistry and Climate ». At the national level, the dissemination was done through Follow-up Committee meetings and through articles in magazines and newspapers, which report on scientific research and especially on research that is relevant to man and the Earth system. A press release was issued at IASB/BIRA and Belspo: « New satellite observations reveal a link between forests and rain acidity ». This press release prompted the publication of short articles in the Belgian (Le Soir, Het Laatste Niews) and international (New Scientist) press.

In addition, the project results were used for university teaching and education. Students have performed research within the frame of this project, enabling them to complete master and doctoral degrees and to gain expertise on environmental issues, atmospheric aerosols, biogenic volatile organic compounds and their impact on climate and health.

5. REFERENCES

Arey J., S. Aschmann, E. Kwok & R. Atkinson (2001) J. Phys. Chem. A, 105, 1020-1027.

Asatryan R., G. da Silva & J. W. Bozzelli (2010) J. Phys. Chem. A, 114, 8302-8311.

Bahadur R., G. Habib & L. M. Russell (2004) Atmos. Environ., 43, 2499-2512.

Barnes I., K. H. Becker & T. Zhu (1993) J. Atmos. Chem., 17, 353-373.

Baasandorj M., S. Griffith, S. Dusanter & P. S. Stevens (2009) J. Phys. Chem. A, 113, 10495-10502.

Böge O., Y. Miao, A. Plewka & H. Herrmann (2006) Atmos. Environ., 40, 2501-2509.

Boyd A. A., P.-M. Flaud, N. Daugey & R. Lesclaux (2003) J. Phys. Chem. A, 107, 818-821.

Booth A. M., M. H. Barley, D. O. Topping, G. McFiggans, A. Garforth & C. J. Percival (2010) Atmos. Chem. Phys., 10, 4879-4892.

Butkovskaya N. I., A. Kukui & G. Le Bras (2012) J. Phys. Chem. A, 116, 5972-5980.

Carlton A. G., B. J. Turpin, K. E. Altieri, S. Seitzinger, A. Reff, J.-J. Lim & B. Ervens (2007) Atmos. Environ., 41, 7588-7602.

Ceulemans K. , S. Compernolle & J.-F. Müller (2011) Atmos. Chem. Phys. Discuss, 11, 23421-23468.

Ceulemans K., S. Compernolle, J. Peeters & J.-F. Müller (2010) Atmospheric Environment, 44, 5434-5442.

Ceulemans K., S. Compernolle & J.-F. Müller (2012) Atmos. Chem. Phys., 12, 5343-5366.

Claeys M., B. Graham, G. Vas, W. Wang, R. Vermeylen, V. Pashynska, J. Cafmeyer, P. Guyon, M. O. Andreae, P. Artaxo & W. Maenhaut (2004a) Science, 303, 1173-1176.

Claeys M., W. Wang, A. C. Ion, I. Kourtchev, A. Gelencsér & W. Maenhaut (2004b) Atmos. Environ., 38, 4093-4098.

Claeys M., Y. Iinuma, R. Smigielski, J. D. Surratt, F. Blockhuys, C. Van Alsenoye, O. Böge, B. Sierau, Y. Gómez-González, R. Vermeylen, P. Van der Veken, M. Shahgholi, A. W. H. Chan, H. Herrmann, J. H. Seinfeld & W. Maenhaut (2009) Environ. Sci. Technol., 43, 6976-6982.

Compernolle S., K. Ceulemans & J.-F. Müller (2011a) Atmos. Chem. Phys., 11, 8385-8394.

Compernolle S., K. Ceulemans & J.-F. Müller (2011b) Atmos. Chem. Phys., 11, 9431-9450.

Crounse J. D., F. Paulot, H. G. Kjaergaard & P. O. Wennberg (2011) Phys. Chem. Chem. Phys., 13, 13607-13613.

Crounse J. D., F. Paulot, H. G. Kjaergaard & P. O. Wennberg (2012) Correction and addition to PCCP paper above.

Crounse, J. D., A. Teng & P. Wennberg (2014) oral presentation at Atmospheric Chemical Mechanisms (ACM) meeting, Davis, California, Dec. 2014.

da Silva G., C. Graham, Z.-F. Wang (2010) Environ. Sci. Technol., 44, 250-256.

Dibble T. S. (2002) J. Phys. Chem. A, 106, 6643-6650.

Dillon T. J., A. Horowitz, D. Hölscher, J. N. Crowley, L. Vereecken & J. Peeters (2006) Phys. Chem. Chem. Phys., 8, 236-246.

Eddingsaas N. C., C. L. Loza, L. D. Lee, J. H. Seinfeld, & P. O. Wennberg (2012a) Atmos. Chem. Phys., 12, 6489-6504.

Eddingsaas N. C., C. L. Loza, L. D. Lee, M. Chan, K. A. Schilling, P. S. Chhabra, J. H. Seinfeld & P. O. Wennberg (2012b) Atmos. Chem. Phys., 12, 7413-7427.

Facchini M. C., M. Mircea, S. Fuzzi & R. J. Charlson (1999) Nature, 401, 257-259.

Fantechi G., L. Vereecken & J. Peeters (2002) Phys. Chem. Chem. Phys., 4, 5795-5805.

Flocke F., E. Atlas, S. Madronich, S. M. Schuffler, K. Aikin, J. J. Margitan, & T. P. Bui (1998) Geophys. Res. Lett., 25, 1891-1894.

Frisch M. J., G. W. Trucks, H. B. Schlegel, G. E. Scuseria, M. A. Robb, J. R. Cheeseman, J. R., J. A. Montgomery, Jr, T. Vreven, K. N. Kudin & J. C. Burant, Gaussian, Inc.: Wallingford CT, 2004.

Fu T.-M., D. J. Jacob, F. Wittrock, J. P. Burrows, M. Vrekoussis & D. K. Henze (2008) J. Geophys. Res., 113, D15303.

Fuchs H., A. Hofzumahaus, F. Rohrer, T. Brauers, H.-P. Dorn, R. Häseler, F. Holland, M. Kaminski, X. Li, K. Lu, S. Nehr, R. Tillmann, R. Wegener & A. Wahner (2013) Nat. Geosci., 6, 1023-1026.

Gardner H. W., E. C. Nelson, L. W. Tjarks & R. E. England (1984) Chem. Phys. Lipids, 35, 87–101.

Ghosh B., A. Bugarin, B. T. Connell & S. W. North (2010) J. Phys. Chem. A, 114, 2553-2560.

Gómez-González Y., W. Wang, R. Vermeylen, X. Chi, J. Neirynck, I. A. Janssens, W. Maenhaut, & M. Claeys (2012) Atmos. Chem. Phys., 12, 125-138.

Greenwald E. E., S. W. North, Y. Georgievskii & S.J. Klippenstein (2007) J. Phys. Chem. A, 111, 5582-5592.

Hallquist J. C., J. C. Wenger, U. Baltensperger, Y. Rudich, D. Simpson, M. Claeys, J. Dommen, N. M. Donahue, C. George, A. H. Goldstein, J. F. Hamilton, H. Herrmann, T. Hoffmann, Y. Iinuma, M. Jang, M. E. Jenkin, J. L. Jimenez, A. Kiendler-Scharr, W. Maenhaut, G. McFiggans, Th. F. Mentel, A. Monod, A. S. H. Prévôt, J. H. Seinfeld, J. D. Surratt, R. Smigielski & J. Wildt (2009) Atmos. Chem. Phys., 9, 5155-5236.

Hasson H. S., G. S. Tyndall & J. J. Orlando (2004) J. Phys. Chem. A, 108, 5979-5989.

Heald C. L., H. Coe, J. L. Jimenez, R. J. Weber, B. Bahreini, A. M. Middlebrook, L. M. Russell, M. Jolleys, T.-M. Fu, J. D. Allan, K. N. Bower, G. Capes, J. Crosier, W. T.

Morgan, N. H. Robinson, P. I. Williams, M. J. Cubison, P. F. DeCarlo & E. J. Dunlea (2011) Atmos. Chem. Phys., 11, 12673-12696.

Henry K. M. & N. M. Donahue (2012) J. Phys. Chem. A, 116, 5932-5940.

Hermans I., J.-F. Müller, T. L. Nguyen, P. Jacobs & J. Peeters (2005) J. Phys. Chem. A, 109, 4303-4311.

Hodgson D. M., M. A. H. Stent & F. X. Wilson (2001) Org. Lett., 3, 3401-3403.

Hofzumahaus A., F. Rohrer, K. Lu, B. Bohn, T. Brauers, C.-C. Chang, H. Fuchs, F. Hollond, L. Kita, Y. Kondo, X. Li, S. Lou, M. Shao, L. Zeng, A. Wahner & Y. Zhang (2009) Science, 324, 1702-1704.

Hofzumahaus A., I. Acir, M. Bachner, B. Bohn, T. Brauers, S. Broch, J.-P. Dorn, H. Fuchs, S. Gomm, R. Häseler, F. Holland, J. Jäger, M. Kaminski, X. Li, S. Lou, K. Lu, S. Nehr, F. Rohrer, R. Tillmann, R. Wegener & A. Wahner (2014) oral presentation at Atmospheric Chemical Mechanisms (ACM) meeting, Davis, California, Dec. 2014.

Holopainen J. K. (2004) Trends in Plant Science, 9, 529–533.

Huisman A. J., U. K. Krieger, A. Zuend, C. Marcolli & T. Peter (2013) Atmos. Chem. Phys. Discuss., 13, 1133-1177.

Iinuma Y., O. Böge, A. Kahnt & H. Herrmann (2009) Phys. Chem. Chem. Phys., 36, 7985-7997.

Iinuma Y., O. Böge, M. Keywood, T. Gnauk & H. Herrmann (2009) Environ. Sci. Technol., 43, 280-285.

IUPAC Subcommittee for Gas Kinetic Data Evaluation: HOx + isoprene datasheet: http://iupac.pole-ether.fr/datasheets/pdf/HOx_VOC8_HO_CH2C(CH3)CHCH2(isoprene).pdf

Jaoui M., T. E. Kleindienst, M. Lewandowski, J. H. Offenberg & E. O. Edney (2005) Environ. Sci. Technol., 39, 5661-5673.

Jenkin M. E., A. A. Boyd & R. Lesclaux (1998) J. Atmos. Chem., 29, 267-298.

Jimenez J. L., M. R. Canagaratna, N. M. Donahue, A. S. H. Prévôt, A. Zhang, J. H. Kroll, P. F. DeCarlo, J. D. Allan, H. Coe, N. L. Ng, A. C. Aiken, K. S. Docherty, I. M. Ulbrich, A. P. Grieshop, A. L. Robinson, J. Duplissy, J. D. Smith, K. R. Wilson, V. A. Lanz, C. Hueglin, Y. L. Sun, J. Tian, A. Laaksonen, T. Raatikainen, J. Rautiainen, P. Waattovaara, M. Ehn, M. Kulmala, J. M. Tomlinson, D. R. Collons, M. J. Cubison, E. J. Dunlea, J. A. Huffman, T. B. Onasch, M. R. Alfarra, P. I. Williams, K. Bower, Y. Kondo, J. Schneider, F. Drewnick, S. Borrmann, S. Weimer, K. Demerjian, D. Salcedo, L. Cottrell, R. Griffin, A. Takami, T. Miyoshi, S. Hatakeyama, A. Shimono, J. Y. Sun, Y. M. Zhang, K. Dzepina, J. R. Kimmel, D. Sueper, J. T. Jayne, S. C. Herndon, A. M. Trimborn, L. R. Williams, E. C. Wood, A. M. Middlebrook, C. E. Kolb, U. Baltensperger & D. R. Worsnop (2009) Science, 326, 1525-1529.

Kahnt A., Y. Iinuma, A. Mutzel, O. Böge, M. Claeys & H. Herrmann (2014a) Atmos. Chem. Phys., 14, 719-736.

Kahnt A., Y. Iinuma, F. Blockhuys, A. Mutzel, R. Vermeylen, T. E. Kleindienst, M. Jaoui, J. H. Offenberg, M. Lewandowski, O. Böge, H. Herrmann, W. Maenhaut & M. Claeys (2014b) Environ. Sci. Technol., 48, 4901-4908.

Kleindienst T. E., M. Jaoui, M. Lewandowski, J. H. Offenberg, C. W. Lewis, P. V. Bhave & E. O. Edney (2007) Atmos. Environ., 41, 8288-8300.

Kleindienst T. E., M. Lewandowski, J. H. Offenberg, M. Jaoui & E. O. Edney (2009) Atmos. Chem. Phys., 9, 6541-6558.

Kroll J. H. & J. H. Seinfeld (2008) Atmos. Environ., 42, 3593-3624.

Kroll J. H., N. M. Donahue, J. L. Jimenez, S. H. Kessler, M. R. Canagaratna, K. R. Wilson, K. E. Altieri, L. R. Mazzoleni, A. S. Wozniak, H. Bluhm, E. R. Mysak, J. D. Smith, C. E. Kolb & D. R. Worsnop (2011) Nature Chem., 3, 133-139.

Kwan A. J., A. W. H. Chan, N. Ng, H. G. Kjaergaard, J. H. Seinfeld & P. O. Wennberg (2012) Atmos. Chem. Phys., 12, 7499-7515.

Lee L., A. P. Teng, P. O. Wennberg, J. D. Crounse & R. C. Cohen (2014) J. Phys. Chem., 118,, 1622-1637.

Lei W. & R. Zhang (2001) J. Phys. Chem. A 2001, 105, 3808.

Lelieveld J., T. M. Butler, J. N. Crowley, T. J. Dillon, H. Fischer, L. Ganzeveld, H. Harder, M. G. Lawrence, M. Martinez, D. Taraborrelli & J. Williams (2008) Nature, 452, 737-740.

Leu G.-H., C.-L. Huang, S.-H. Lee, Y.-C. Lee & I.-C. Chen (1998) J. Chem. Phys., 109, 9340-9350.

Lim H.-J., et al., Environ. Sci. Technol., 39, 4441-4446, 2005.

Lim Y. B., et al., Atmos. Chem. Phys., 10, 10521-20539, 2010.

Lim Y. B., Y. Tan & B. J. Turpin (2013) Atmos. Chem. Phys., 13, 8651-8667.

Lin Y.-H., H. Zhang, H. O. T. Pye, Z. Zhang, W. J. Marth, S. Park, M. Arashiro, T. Cui, S. H. Budisulistiorini, K. G. Sexton, W. Vizuete, Y. Xie, D. J. Luecken, I. R. Piletic, E. O. Edney, L. J. Bartoloti, A. Gold & J. D. Surratt (2013) Proc. Natl. Acad. Sci. U.S.A., 110, 6718-6723.

Liu J., L. W. Horowitz, S. Fan, A. G. Carlton & H. Levy II (2012), J. Geophys. Res., 117, D15303.

Liu Y. J., I. Herdlinger-Blatt, K. A. McKinney & S. T. Martin (2013), Atmos. Chem. Phys. 13, 5715-5730.

Loeffler K. W., C. A. Koehler, N. M. Paul, & D. O. De Haan (2006) Environ. Sci. Technol., 40, 6318-6323.

Kleindienst T. E., M. Lewandowski, J. H. Offenberg, M. Jaoui& E. O. Edney (2009) Atmos. Chem. Phys., 9, 6541-6558.

Maenhaut W., N. Raes, X. Chi, J. Cafmeyer & W. Wang (2008) X-Ray Spectrom., 37, 193-197.

Méreau R., M. T. Rayez, J. C. Rayez, F. Caralp & R. Lesclaux (2001) Phys. Chem. Chem. Phys., 3, 4712-4717.

Messaadia L., G. El Dib, A. Ferhati, E. Roth & A. Chakir (2012) Chem. Phys. Lett., 529, 16-22.

Moss G. P., Pure Appl. Chem., 68, 2193-2222, 1996.

Müller J.-F., J. Peeters & T. Stavrakou (2014) Atmos. Chem. Phys., 14, 2497-2508.

Müller L., M.-C. Reinnig, K. H. Naumann, H. Saathoff, T. F. Mentel, N. M. Donahue & T. Hoffmann (2012) Atmos. Chem. Phys., 12, 1483-1496.

Nannoolal Y., J. Rarey & D. Ramjugernath (2008) Fluid Phase Equilib., 269, 117-133.

Neeb P. (2000) J. Atmos. Chem., 35, 295-315.

Nguyen T. L., J. Peeters & L. Vereecken (2009) Phys. Chem. Chem. Phys., 11, 5643-5656.

Nguyen T. L., L. Vereecken & J. Peeters (2010) Chem. Phys. Chem., 11, 3996-4001.

Nguyen, S. V., and J. Peeters (2015) J. Phys. Chem. A., web-published ASAP, DOI:10.1021/jp512057t, 2015.

Novelli A., K. Hens, C. Tatum Ernest, D. Kubistin, E. Regelin, T. Elste, C. Plass-Dülmer, M. Martinez, J. Lelieveld, and H. Harder (2014) Atmos. Meas. Tech. Discuss., 7, 819-858.

Nozière B., M. Kalberer, M. Claeys, J. Allan, B. D'Anna, S. Decesari, E. Finessi, M. Glasius, I. Grgic, J. F. Hamilton, T. Hoffmann, Y. Iinuma, M. Jaoui, A. Kahnt, C. J. Kampf, I. Kourtchev, W. Maenhaut, N. Marsden, S. Saarikoski, J. Schnelle-Kreis, J. D. Surratt, S. Szidat, R. Szmigielski & A. Wisthaler (2015) Chem. Rev., in press, doi: 10.1021/cr5003485.

Odum J. R., T. Hoffmann, F. Bowman, D. Collins, R. C. Flagan, & J. H. Seinfeld (1996) Environ. Sci. Technol., 30, 2580-2585.

O'Connor M. P., J. C. Wenger, A. Mellouki, K. Wirtz & A. Muñoz (2006) Phys. Chem. Chem. Phys., 8, 5236-5246.

O'Meara, S., A. M. Booth, M. H. Barley, D. Topping & G. McFiggans (2014) Phys. Chem. Chem. Phys., 16, 19453-19469.

Orlando J. J. & Tyndall, G. S. (2012) Chem. Soc. Rev., 41, 6294-6317.

Palmer P. I., D. S. Abbot, T.-M. Fu, D. J. Jacob, K. Chance, T. P. Kurosu, A. Guenther, C. Wiedinmyer, J. C. Stanton, M. J. Pilling, S. N. Pressley, B. Lamb & A. L. Sumner (2006) J. Geophys. Res., 111, D12315.

Pankow J. F. & W. E. Asher (2008) Atmos. Chem. Phys., 8, 2773-2796.

Park J., C. G. Jongsma, R. Zhang & S. W. North (2004) J. Phys. Chem. A, 108, 10688-10697.

Pashynska V., R. Vermeylen, G. Vas, W. Maenhaut & M. Claeys (2002) J. Mass Spectrom., 37, 1249-1257.

Paulot F., J. D. Crounse, H. G. Kjaergaard, J. H. Kroll, J. H. Seinfeld & P. O. Wennberg (2009a) Atmos. Chem. Phys., 9, 1479-1501.

Paulot F., J. D. Crounse, H. G. Kjaergaard, A. Kürten, J. M. St. Clair, J. H. Seinfeld & P. O. Wennberg (2009b) Science, 325, 730-733.

Paulot F., D. Wunch, J. D. Crounse, G. C. Toon, D. B. Millet, P. F. DeCarlo, C. Vigouroux, N. M. Deutscher, G. González Abad, J. Notholt, T. Warneke, J. W. Hanningan, C. Warneke, J. A. de Gouw, E. J. Dunlea, M. De Mazière, D. W. T. Griffith, P. Bernath J. L. Jimenez & P. O. Wennberg (2011) Atmos. Chem. Phys., 11, 1989-2013.

Peeters J., W. Boullart & J. Van Hoeymissen (1994) Proceedings of Eurotrac Symposium'94, 110-114, ed. P. M. Borrell, SPB Academic Publishers, The Hague.

Peeters J., L. Vereecken & G. Fantechi (2001) Phys. Chem. Chem. Phys., 3, 5489-5504.

Peeters J., G. Fantechi & L. Vereecken (2004) J. Atmos. Chem., 48, 59-80.

Peeters J., W. Boullart, V. Pultau, S. Vandenberk & L. Vereecken (2007) J. Phys. Chem. A, 111, 1618-1631.

Peeters J., T. L. Nguyen & L. Vereecken (2009) Phys. Chem. Chem. Phys., 11, 5935-5939.

Peeters J. & J.-F. Müller (2010), Phys. Chem. Chem. Phys., 12, 14227-14235.

Peeters J. & T. L. Nguyen (2012) J. Phys. Chem. A, 116, 6134-6141.

Peeters J., J.-F. Müller, T. Stavrakou & V. S. Nguyen (2014) J. Phys. Chem. A, 118, 8625-8643.

Pierotti D., S. C. Wofsy, D. J. Jacob & R. A. Rasmussen (1990) J. Geophys. Res., 95, 1871-1881.

Pilling M. J. (2013) J. Phys. Chem. A, 117, 3697-3717.

Pfaffenberger L., P. Barmet, J. G. Slowik, A. P. Praplan, J. Dommen, A. S. H. Prévôt & U. Baltensperger (2013) Atmos. Chem. Phys., 13, 6493-6506.

Praplan A. P., P. Barmet, J. Dommen & U. Baltensperger (2012) Atmos. Chem. Phys., 12, 10749-10758.

Razavi A., F. Karagulian, L. Clarisse, D. Hurtmans, P. Coheur, C. Clerbaux, J.-F. Müller & T. Stavrakou (2011) Atmos. Chem. Phys., 11, 857-872.

Ren X., J. R. Olson, J. H. Crawford, W. H. Brune, J. Mao, R. B. Long, Z. Chen, G. Chen, M. A. Avery, G. W. Sachse, J. D. Barrick, G. S. Diskin, L. G. Huey, A. Fried, R. C. Cohen, B. Heikes, P. O. Wennberg, H. B. Singh, D. R. Blake & R. E. Shetter (2008) J. Geophys. Res., 113, D05310.

Ruppert R. & K. H. Becker (2000) Atmos. Environ. 34, 1529-1542.

Rudzinski K. J., L. Gmachowski & I. Kuznietsova (2009) Atmos. Chem. Phys., 9, 2129-2140.

Salo K., M. Hallquist, A. M. Jonsson, H. Saathoff, K.-H. Naumann, C. Spindler, R. Tillmann, H. Fuchs, B. Bohn, F. Rubach, Th. F. Mentel, L. Müller, M. Reinnig, T. Hoffmann & N. M. Donahue (2011) Atmos. Chem. Phys., 11, 11055-11067.

Sander, R. (2014) Atmos. Chem. Phys. Discuss., 14, 29615-30521.

Saunders S. M., M. E. Jenkin, R. G. Derwent & M. J. Pilling (2003) Atmos. Chem. Phys., 3, 161-180.

Scala A., S. Allmann, R. Mirabella, M. Haring & R. Schuurink (2013) Int. J. Mol. Sci., 14, 17781-17811, 2013.

Schindelka J., Y. Iinuma, D. Hoffmann & H. Herrmann (2013) Faraday Discuss., 165, 237-259.

Shalamzari M. S., O. Ryabtsova, A. Kahnt, R. Vermeylen, M.-F. Hérent, J. Quetin-Leclercq, P. Van der Veken, W. Maenahut & M. Claeys (2013) Rapid Commun. Mass Spectrom., 27, 784-794.

Shalamzari M. S., A. Kahnt, R. Vermeylen, T. E. Kleindienst, M. Lewandowski, F. Cuyckens, W. Maenhaut & M. Claeys (2014) Environ. Sci. Technol., 48, 12671-12678.

Spracklen D. V., J. L. Jimenez, K. S. Carslaw, D. R. Worsnop, M. J. Evans, G. W. Mann, Q. Zhang, M. R. Canagaratna, J. Allan, H. Coe, G. McFiggans, A. Rap & P. Forster (2011) Atmos. Chem. Phys., 11, 12109-12136.

Stavrakou T., J.-F. Müller, I. De Smedt, M. Van Roozendael, G. R. van der Werf, L. Giglio & A. Guenther (2009a) Atmos. Chem. Phys., 9, 3663-3679.

Stavrakou T., J.-F. Müller, I. De Smedt, M. Van Roozendael, M. Kanakidou, M. Vrekoussis, F. Wittrock, A. Richter & J. P. Burrows (2009b) Atmos. Chem. Phys., 9, 8431-8446.

Stavrakou T., J.-F. Müller, I. De Smedt, M. Van Roozendael, G. R. van der Werf, L. Giglio & A. Guenther (2009c), Atmos. Chem. Phys., 9, 1037-1060.

Stavrakou T., J. Peeters & J.-F. Müller (2010) Atmos. Chem. Phys., 10, 9863-9878.

Stavrakou T., J.-F. Müller, J. Peeters, A. Razavi, L. Clarisse, C. Clerbaux, P.-F. Coheur, D. Hurtmans, M. De Mazière, C. Vigouroux, N. M. Deutscher, D. W. T. Griffith, N. Jones & C. Paton-Walsh (2012) Nature Geosci., 5, 26-30.

Stavrakou T., J.-F. Müller, K. F. Boersma, R. J. van der A, J. Kurokawa, T. Ohara & Q. Zhang (2013) Atmos. Chem. Phys., 13, 9057-9082.

Suarez-Bertoa R., B. Picquet-Varrault, W. Tamas, E. Pangui & J.-F. Doussin (2012) Environ. Sci. Technol., 46, 12502-12509.

Surratt J. D., Y. Gómez-González, A. W. H. Chan, R. Vermeylen, M. Shahgholi, T. E. Kleindienst, E. O. Edney, J. H. Offenberg, M. Lewandowski, M. Jaoui, W. Maenhaut, M. Claeys, R. C. Flagan & J. H. Kleindienst (2006) J. Phys. Chem. A, 110, 9665-9690.

Surratt J. D., J. H. Kroll, T. E. Kleindienst, E. O. Edney, M. Claeys, A. Sorooshian, N. L. Ng, J. Offenberg, M. Lewandowski, M. Jaoui, R. C. Flagan & J. H. Seinfeld (2007) Environ. Sci. Technol., 41, 517-527.

Surratt J. D., A. W. H. Chan, N. C. Eddingsaas, M. Chan, C. L. Loza, A. J. Kwan, S. P. Hersey, R. C. Flagan, P. O. Wennberg & J. H. Seinfeld (2010) Proc. Natl. Acad. Sci. USA, 107, 6640-6645.

Szmigielski R., J. D. Surratt, Y. Gómez-González, P. Van der Veken, I. Kourtchev, R. Vermeylen, F. Blockhuys, M. Jaoui, T. E. Kleindienst, M. Lewandowski, J. H. Offenberg, E. O. Edney, J. H. Seinfeld, W. Maenhaut & M. Claeys (2007) Geophys. Res. Lett., 34, doi:10.1029/2007GL031338.

Tan Y., A. G. Carlton, S. P. Seitzinger, & B. J. Turpin (2010) Atmos. Environ., 44, 5218-5226.

Taraborrelli D., M. G. Lawrence, J. N. Crowley, T.J. Dillon, S. Gromov, C. B. M. Grosz, L. Vereecken & J. Lelieveld (2012) Nature Geosci., 5, 190-193.

Tritscher T., J. Dommen, P. F. DeCarlo, M. Gysel, P. B. Barmet, A. P. Praplan, E. Weingartner, A. S. H. Prévôt, I. Riipinen, N. M. Donahue & U. Baltensperger (2011) Atmos. Chem. Phys., 11, 11477-11496.

Tsigaridis K., N. Daskalakis, M. Kanakidou, P. J. Adams, P. Artaxo, R. Bahadur, Y. Balkanski, S. E. Bauers, N. Belloin, A. Benedetti, T. Bergman, T. K. Berntsen, J. P. Beukes, H. Bian, K. S. Carslaw, M. Chin, G. Curci, T. Diehl, R. C. Easter, S. J. Ghan, S. L. Gong, A. Hodzic, C. R. Hoyle, T. Iversen, S. Jathar, J. L. Jimenez, J. W. Kaiser, A. Kirkevåg, D. Koch, H. Kokkola, Y. H. Lee, G. Lin, X. Liu, G. Luo, X. Ma, G. W. Mann, N. Mihalopoulos, J.-J. Morcrette, J.-.F Müller, G. Myhre, S. Myriokefalitakis, N. L. Ng, D. O'Donnell, J. E. Penner, L. Pozzoli, K. J. Pringle, L. M. Russell, M. Schultz, J. Sciare, Ø. Seland, D. T. Shindell, S. Sillman, R. B. Skeie, D. Spracklen, T. Stavrakou, S. D. Steenrod, T. Takemura, P. Tiitta, S. Tilmes, H. Tost, T. van Noije, P. G. van Zyl, K. von Salzen, F. Yu, Z. Wang, Z. Wang, R. A. Zaveri, H. Zhang, K. Zhang, Q. Zhang & X. Zhang (2014) Atmos. Chem. Phys., 14, 10845-10895.

Van Alsenoy C. & A. Peeters (1993) J. Mol. Struct. (THEOCHEM), 105, 19-34.

Vereecken L. & J. Peeters (2003) J. Chem. Phys., 119, 5159-5170.

Vereecken L., T. L. Nguyen, I. Hermans & J. Peeters (2004) Chem. Phys. Lett., 393, 432-436.

Vereecken L., J.-F. Müller & J. Peeters (2007) Phys. Chem. Chem. Phys., 9, 5241-5248.

Vereecken L. & J. Peeters (2009) Phys. Chem. Chem. Phys., 11, 9062-9074.

Vereecken L. & J. Peeters (2010) Phys. Chem. Chem. Phys., 12, 12608-12620.

Vereecken L. & J. Peeters (2012), Phys. Chem. Chem. Phys., 14, 3802-3815.

Vu N. D., V. Khamaganov, V. S. Nguyen, S. A. Carl & J. Peeters (2013) J. Phys. Chem., 117, 12208-12215.

Wang J., J.-F. Doussin, S. Perrier, E. Perraudin, Y. Katrib, E. Pangui & B. Picquet-Varrault (2011) Atmos. Meas. Tech., 4, 2465- 2494.

Wang W., I. Kourtchev, B. Graham, J. Cafmeyer, W. Maenhaut & M. Claeys (2005) Rapid Commun. Mass Spectrom., 19, 1343-1351.

Wang W., M. S. Shalamzari, W. Maenhaut & M. Claeys (2013) Rapid Commun. Mass Spectrom., 27, 1585-1589.

Wolfe G. M., J. D. Crounse, J. D. Parrish, J. M. St. Clair, M. R. Beaver, F. Paulot, T. P. Yoon, P. O. Wennberg & F. N. Keutsch (2012) Phys. Chem. Chem. Phys., 14, 7276-7286.

Yasmeen F., R. Vermeylen, R. Szmigielski, Y. Iinuma, O. Böge, H. Herrmann, W. Maenhaut & M. Claeys (2010) Atmos. Chem. Phys., 10, 9383-9392.

Yasmeen F., R. Szmigielski, R. Vermeylen, Y. Gómez-González, J. D. Surratt, A. W. H. Chan, J. H. Seinfeld, W. Maenhaut & M. Claeys (2011) J. Mass Spectrom., 46, 425-442.

Yasmeen F., R. Vermeylen, N. Maurin, E. Perraudin, J.-F. Doussin & M. Claeys (2012) Environ. Chem., 9, 236-246.

Yoon M. C., Y. S. Choi & S.K. Kim (1999) Chem. Phys. Lett., 300, 207-212.

Zhang F. & TS Dibble (2011) Phys. Chem. Chem. Phys., 13, 17969 - 17977.

Zhao Y., G. Liu, Y. Liu, L. Yuan, D. Hawthorne, J. X. Shen, M. Guha & A. Aubry (2013) Rapid Commun. Mass Spectrom., 27, 481- 488.

Zuend A., C. Marcolli, A. M. Booth, D. M. Lienhard, V. Soonsin, U. K. Krieger, D. O. Topping, G. McFiggans, T. Peter & J. H. Seinfeld (2011) Atmos. Chem. Phys., 11, 9155-9206.

Zuend, A. & J. H. Seinfeld (2012) Atmos. Chem. Phys., 12, 3857-3882.

6. PUBLICATIONS

6.1 Peer-reviewed

Ceulemans, K., S. Compernolle, and J.-F. Müller, Parameterising secondary organic aerosol from a-pinene using a detailed oxidation and aerosol formation model. Atmos. Chem. Phys., 12, 5343-5366, 2012.
[Ceulemans_ACP2012.pdf]

Claeys, M., R. Vermeylen, F. Yasmeen, Y. Gómez-González, X. Chi, W. Maenhaut, T. Mészáros, and I. Salma: Chemical characterisation of humic-like substances from urban, rural and tropical biomass burning environments using liquid chromatography with UV/VIS photodiode array detection and electrospray ionisation mass spectrometry, Environ. Chem., 9(3), 273-284, 2012.
[PUBLI5_claeys_ec2012.pdf] [PUBLI6_claeys_ec2012_SOM.pdf]

Compernolle, S., K. Ceulemans, and J.-F. Müller, Technical Note: Estimating fusion properties for polyacids, Atmos. Chem. Phys., 11, 7535-7553, 2011.
[Compernolle_ACP2011a.pdf]

Compernolle, S., K. Ceulemans, and J.-F. Müller, EVAPORATION: a new vapour pressure estimation method for organic molecules including non-additivity and intramolecular interactions, Atmos. Chem. Phys., 11, 9431-9450, 2011.
[Compernolle_ACP2011b.pdf]

Compernolle, S., and J.-F. Müller, Henry's law constants of diacids and hydroxypolyacids: recommended values, Atmos. Chem. Phys., 14, 2699-2712, 2014.
[Compernolle_ACP2014.pdf]

Compernolle, S., and J.-F. Müller, Henry's law constant of polyols, Atmos. Chem. Phys., 14, 12815-12837, 2014.
[Compernolle_polyols_ACP2014.pdf]

Gómez-González, Y., W. Wang, R. Vermeylen, X. Chi, J. Neirynck, I. A. Janssens, W. Maenhaut, and M. Claeys: Chemical characterisation of atmospheric aerosols during a 2007 summer field campaign at Brasschaat, Belgium: sources and source processes of biogenic secondary organic aerosol, Atmos. Chem. Phys., 12, 125-138, 2012.
[PUBLI2_gomez_acp2012.pdf]   [PUBLI3_gomez_acp2012_supplement.pdf]

Kahnt, A., Y. Iinuma, A. Mutzel, O. Böge, M. Claeys, H. Herrmann: Campholenic aldehyde ozonolysis: a mechanism leading to specific biogenic secondary organic aerosol constituents, Atmos. Chem. Phys. 2014, 14, 719–736.
[kahnt_ACP2014.pdf] [kahnt_ACP2014.supplement.pdf]

Kahnt, A., T. Iinuma, F. Blockhuys, A. Mutzel, R. Vermeylen, T. E. Kleindienst, M. Jaoui, J. H. Offenberg, MM. Lewandowski, O. Böge, H. Herrmann, W. Maenhaut, and M. Claeys, 2-Hydroxyterpenylic acid : An oxygenated marker compound for alpha-pinene Secondary Organic Aerosol in ambient fine aerosol, Environ. Sci. Technol, 48, 4901-4908, 2014.
[Kahnt_EST2014.pdf] [Kahnt_EST2014_supplement.pdf]

Müller, J.-F., J. Peeters and T. Stavrakou, Fast photolysis of carbonyl nitrates from isoprene, Atmos. Chem. Phys., 14, 2497-2508, 2014.
[Muller_photolysis_ACP2014.pdf]

Nguyen, S. V., and J. Peeters, Fast (E)-(Z) isomerization mechanisms of substituted allyloxy radicals in isoprene oxidation, J. Phys. Chem., web-published Feb. 6, 2015.
[Nguyen_JPC2015.pdf]

Nozière B., M. Kalberer, M. Claeys, J. Allan, B. D'Anna, S. Decesari, E. Finessi, M. Glasius, I. Grgic, J. F. Hamilton, T. Hoffmann, Y. Iinuma, M. Jaoui, A. Kahnt, C. J. Kampf, I. Kourtchev, W. Maenhaut, N. Marsden, S. Saarikoski, J. Schnelle-Kreis, J. D. Surratt, S. Szidat, R. Szmigielski & A. Wisthaler, The molecular identification of organic compounds in the atmosphere: State of the art and challenges, Chem. Rev., in press, doi: 10.1021/cr5003485, 2015.

Peeters, J., and T. L. Nguyen, Unusually Fast 1,6-H Shifts of Enolic Hydrogens in Peroxy Radicals: Formation of the First-Generation C2 and C3 Carbonyls in the Oxidation of Isoprene", J. Phys. Chem. A, 116, 6134-6141, 2012.
[Peeters_JPC2012.pdf]

Peeters, J., J.-F. Müller, T. Stavrakou, and S. V. Nguyen, Hydroxyl radical recycling in isoprene oxidation driven by hydrogen bonding and hydrogen tunneling : the upgraded LIM1 mechanism, J. Phys. Chem. A, 1180, 8625-8643, 2014.
[Peeters_JPC2014.pdf] [Peeters_JPC2014_suppl.pdf]

Shalamzari, M. S., O. Ryabtsova, A. Kahnt, R. Vermeylen, M.-F. Hérent, J. Quetin-Leclercq, P. Van der Veken, W. Maenhaut, M. Claeys: Mass spectrometric characterization of organosulfates related to secondary organic aerosol from isoprene, Rapid Commun. Mass Spectrom., 27, 784-794, 2013.
[shalamzari_RCM2013.pdf] [shalamzari_RCM2013_supplement.pdf]

Shalamzari, M. S., A. Kahnt, R. Vermeylen, T. E. Kleindienst, M. Lewandowski, F. Cuykens, W. Maenhaut, and M. Claeys, Characterization of polar organosulfates in Secondary Organic Aerosol from the green leaf volatile 3-Z-hexenal, Environ. Sci. Technol., 48, 12671-12678, 2014.
[Shalamzari_EST2014.pdf]

Stavrakou, T., J.-F. Müller, J. Peeters, A. Razavi, L. Clarisse, C. Clerbaux, P.-F. Coheur, D. Hurtmans, M. De Mazière, C. Vigouroux, N. M. Deutscher, D. W. T. Griffith, N. Jones, C. Paton-Walsh, Satellite evidence for a large source of formic acid from boreal and tropical forests, Nature Geosci., 5, 26-30, doi:10.1038/ngeo1354, 2012.
[Stavrakou_NGEO2012.pdf] [Stavrakou_NGEO2012-supplement.pdf]

Stavrakou, T., J.-F. Müller, K. F. Boersma, R. J. van der A, J. Kurokawa, T. Ohara, and Q. Zhang, Key chemical NOx sink uncertainties and how they influence top-down emissions of nitrogen oxides, Atmos. Chem. Phys., 13, 9057-9082, 2013.
[Stavrakou_NOx_ACP2013.pdf] [Stavrakou_NOx_ACP2013_supplement.pdf]

Stavrakou, T., J.-F. Müller, M. Bauwens, I. De Smedt, M. Van Roozendael, A. Guenther, M. Wild, and X. Xia, Isoprene emissions over Asia 1797-2012: impact of climate and land use changes, Atmos. Chem. Phys., 14, 4587-4605, 2014.
[Stavrakou_Asia_ACP2014.pdf]

Tsigaridis, K., N. Daskalakis, M. Kanakidou, P.J. Adams, P. Artaxo, R. Bahadur, Y. Balkanski, S.E. Bauer, N. Bellouin, A. Benedetti, T. Bergman, T.K. Berntsen, J.P. Beukes, H. Bian, K.S. Carslaw, M. Chin, G. Curci, T. Diehl, R.C. Easter, S.J. Ghan, S.L. Gong, A. Hodzic, C.R. Hoyle, T. Iversen, S. Jathar, J.L. Jimenez, J.W. Kaiser, A. Kirkevåg, D. Koch, H. Kokkola, Y.H. Lee, G. Lin, X. Liu, G. Luo, X. Ma, G.W. Mann, N. Mihalopoulos, J.-J. Morcrette, J.-F. Müller, G. Myhre, S. Myriokefalitakis, S. Ng, D. O'Donnell, J.E. Penner, L. Pozzoli, K.J. Pringle, L.M. Russell, M. Schulz, J. Sciare, Ø. Seland, D.T. Shindell, S. Sillman, R.B. Skeie, D. Spracklen, T. Stavrakou, S.D. Steenrod, T. Takemura, P. Tiitta, S. Tilmes, H. Tost, T. van Noije, P.G. van Zyl, K. von Salzen, F. Yu, Z. Wang, Z. Wang, R.A. Zaveri, H. Zhang, K. Zhang, Q. Zhang, and X. Zhang, 2014: The AeroCom evaluation and intercomparison of organic aerosol in global models. Atmos. Chem. Phys., 14, 10845-10895, doi:10.5194/acp-14-10845-2014.
[Tsigaridis_ACP2014.pdf]

Vereecken, L, and J. Peeters, Theoretical study of the OH-initiated gas-phase oxidation mechanism of β-pinene (C10H16): First generation products, Phys. Chem. Chem. Phys., 14, 3802-3815, 2012.
[Vereecken_PCCP2012.pdf]

Vu, N. D., V. Khamaganov, S. V. Nguyen, S. A. Carl, and J. Peeters, Absolute rate coefficient of the gas-phase reaction between hydroxyl radical (OH) and hydroxyacetone: Investigating the effects of temperature and pressure, J. Phys. Chem. A, 117, 12208-12215, DOI:10.1021/jp407701z, 2013.
[Vu_JPC2013.pdf]

Wang, W., M. S. Shalamzari, W. Maenhaut, M. Claeys: Ion-pairing liquid chromatography/ negative ion mass spectrometry for improved analysis of polar isoprene-related organosulfates, Rapid Commun. Mass Spectrom., 2013, 27, 1585-1589.
[wang_RCM2013.pdf]

Wang, W., Y. Iinuma, A. Kahnt, O. Ryabtsova, A. Mutzel, R. Vermeylen, P. Van der Veken, W. Maenhaut, H. Herrmann, M. Claeys: Formation of secondary organic aerosol marker compounds from the photooxidation of isoprene and isoprene-derived alkene diols under low-NOx conditions, Faraday Discuss., 165, 261-272, 2013.
[wang_FD2013.pdf] [wang_FD2013.supplement.pdf]

Yasmeen, F., R. Vermeylen, N. Maurin, E. Perraudin, J.-F. Doussin, and M. Claeys: Characterisation of tracers for ageing of α-pinene secondary organic aerosol using liquid chromatography/negative ion electrospray ionisation mass spectrometry, manuscript Environ. Chem., 9(3), 236-246, 2012.
[PUBLI4_yasmeen_ec2012.pdf]

6.2 Other

Ceulemans, K., Organic aerosol from the oxidation of biogenic organic compounds: a modelling study, PhD Thesis, University of Antwerp, 2014.
[Ceulemans_PhD2014.pdf]

Claeys, M., R. Szmigielski, R. Vermeylen, W. Wang, M. S. Shalamzari, W. Maenhaut: Tracers for biogenic secondary organic aerosol from α-pinene and related monoterpenes: An overview, in: I. Barnes and K.J. Rudzinski (eds.), Disposal of Dangerous Chemicals in Urban Areas and Mega Cities, NATO Science for Peace and Security Series C: Environmental Security, DOI 10.1007/978-94-007-5034-0_18, Springer Science + Business Media, Dordrecht 2013, Chapter 18, pp. 227-238.
[claeys_NATOproc2013.pdf]

Compernolle, S., K. Ceulemans, J.-F. Müller, J. Peeters, S. V. Nguyen, M. Claeys, Les composés organiques dans l'atmosphère /Organische stiffen in de atmosfeer, Science Connection, 46, 31-33, 2015.
[Compernolle_SC_FR_2015.pdf] [Compernolle_SC_NL_2015.pdf]

Kahnt A., Semivolatile compounds from atmospheric oxidation, PhD Thesis, University of Leipzig, Germany, 2012.
[Kahnt_PhD2012.pdf]

Stavrakou, T., J.-F. Müller, J. Peeters, L. Clarisse, C. Clerbaux, P.-F. Coheur, D. Hurtmans, M. De Mazière, C. Vigouroux, Hebben wouden een invloed op zuurtegraad

van regen ? / Les plantes influencent-elles l'acidité des pluies? Science Connection, 37, 26-29, 2012.
[Stavrakou_SC_FR_2012.pdf] [Stavrakou_SC_NL_2012.pdf]

Vu, N. D., Kinetics of the elementary gas-phase reactions between hydroxyl radical and some (substituted) alcohols, PhD Thesis, University of Leuven, June 2014.